SKI Report 95:70

Research

Crack Characterisation for In-service Inspection Planning

Peter Ekström
Jan Wåle

November 1995

ISSN 1104–1374
ISRN SKI-R-95/70-SE

SKI

SKI Report 95:70

Crack Characterisation for In-service Inspection Planning

Peter Ekström
ABB Atom AB, S-721 63 VÄSTERÅS

Jan Wåle
SAQ Inspection Ltd, Box 49306, S-100 29 STOCKHOLM

November 1995

Abstract

During in-service inspection by non destructive testing the reliability is highly dependent on how the equipment is adjusted to the specific object and to the anticipated crack features. The crack feature and morphology vary widely between different cracking mechanisms and between material types, in which the cracks appear. The major objective of this study was to characterise a number of morphology parameters for common crack mechanism/structure material combinations. Critical morphology parameters are crack orientation, shape, width, surface roughness and branching. The crack parameters were evaluated from failure analyses reported from the nuclear and non-nuclear industry. In addition, a literature review was carried out on crack parameter reports and on failure analysis reports, which were further evaluated.

The evaluated crack parameters were plotted and statistically processed in data groups with respect to crack mechanism and material type. The fatigue crack mechanisms were classified as mechanical, thermal or corrosion fatigue and the stress corrosion crack mechanisms as intergranular, transgranular or interdendritic stress corrosion cracking. Furthermore, some common weld defects were characterised for comparison. The materials were divided into three broad groups, namely, ferritic low alloy steels, stainless steels and nickel base alloys.

The results indicate significant differences between crack parameters when comparing data from different crack mechanism/material type combinations. Typical parameter values and scatter were derived for several crack mechanism/material data groups, where the amount of compiled data was sufficient for statistical significance.

Sammanfattning

Vid oförstörande provning är provningens tillförlitlighet beroende av hur provningssystemet anpassas till det objekt som skall provas och till de förväntade defekternas morfologiska egenskaper. Dessa egenskaper varierar avsevärt mellan olika sprickmekanismer och mellan de materialtyper där sprickorna uppträder. Målet med denna studie har varit att kartlägga ett antal parametrar som beskriver de morfologiska egenskaperna hos de vanligaste sprickmekanism/materialkombinationerna. Kritiska parametrar är sprickorientering, form, bredd, ytfinhet och förgreningsgrad. Dessa parametrar har hämtats direkt från skaderapporter eller uppmätts från foton över trvärsnitt på sprickor som redovisas i rapporterna. Utvärderade sprickor är skador som inträffat inom kärnteknisk och inom konventionell industri. Dessutom har en litteraturstudie genomförts med syfte att sammanställa data från liknande parameterstudier och därutöver samla in resultat från skadeutredningar för egen utvärdering.

De uppmätta parametrarna har behandlats statistiskt och grafiskt i grupper indelade efter sprickmekanism och materialtyp. För utmattningssprickor särskiljs mekanisk, termisk och korrosionsutmattning. För spänningskorrosionssprickor särskiljs interkristallin, transkristallin och interdendritisk spänningskorrosion. Dessutom har några av de vanligaste svetsfelen utvärderats för jämförelse med sprickorna. Materialen har delats in i tre stora grupper, nämligen ferritiska låglegerade stål, rostfria stål och nickelbaslegeringar.

Resultaten indikerar att signifikanta skillnader för utvärderade sprickparametrar föreligger när olika sprickmekanism/materialgrupp-kombinationer jämförs. Typiska värden och spridning för de utvärderade parametrarna har bestämts för alla de datagrupper där ett tillräckligt underlag förelegat.

Table of contents

1 Introduction

Reliable inspections of nuclear components throughout all manufacturing stages and later during their service life, play a significant role in preventing structural failures. Reliable inspections also plays an important role in plant life management and component residual life assessment of nuclear power plants as they get older. The effectiveness of these inspections can, however, be affected by many different aspects, such as the objective of the inspections, timing of the inspections, acceptance criteria to be used as well as the capability and reliability of non destructive testing (NDT) systems that are applied.

The capability and reliability of NDT systems depends upon a wide range of factors, such as the nature of structure under examination, the types of defects being sought and the choice of NDT technique to be employed. Other aspects are the reliability of inspection equipment, the ergonomics of the use of the equipment in power plants, and the performance of the NDT personnel, including physiological and psychological factors. All these factors must consequently be taken into account during the NDT system development stage, as well as, during the subsequent validation and qualification stage.

The optimisation of the NDT equipment and NDT procedure with respect to the component that shall be inspected and to the type of defects being sought is, however, fundamental. While, the optimisation to the component and its geometry, material structure and surface structure, normally is relatively straightforward when the fabrication specification is known, the optimisation with respect to the defects being sought can be problematic. The main reason for this is that quantitative data not always are available as to which crack characteristics depend on underlying degradation mechanisms.

In 1994 the Swedish Nuclear Power Inspectorate (SKI) initiated a project for assembling crack characteristics based on systematic studies of cracks that have been observed in different plants (nuclear and non-nuclear) in order to determine typical as well as more extreme values of e.g. orientation, width and surface roughness.

The results of the project are presented in this report, which has been given the form of a data handbook that can be used by NDT engineers working with development and qualification of NDT systems. The major part of the report is a record of the evaluated crack parameters. Thus, the authors want to emphasise that the intention has been to supply a handbook of compiled data, not to write a textbook.

Although, this report is based on a fairly large number of identified cracking incidents it is recognised that further studies are needed in order to increase the data base, and thereby getting more confidence in the use of different crack characteristic data for NDT development and qualification purposes. It is therefore hoped that the report will facilitate discussions on further such projects for compilation of crack characteristics.

2 Objective

The major objective of this study was to characterise a number of morphology parameters for the most common crack mechanism/material group combinations. Typical parameter values and scatter were determined, as well as relevant extreme values. Furthermore, general descriptions of characteristic features of the different crack mechanisms are derived.

3 Crack evaluation methods

Crack parameter data was collected and evaluated from a large number of failure analysis reports. The records comprised failures from both nuclear and non-nuclear industry. Furthermore, a comprehensive literature review has been carried out as a complement to the failure report study. In this section a detailed description is given of the recorded morphology parameters. The limitations of using failure analysis reports for this purpose are discussed, as well.

3.1 Recorded morphology parameters

The basis for this work was failure analysis reports from failure investigations over the last 10-15 years. A template was designed in order to make the recording of the morphology parameters as rational as possible. The collected parameters were then stored in a computer data-base for easy handling and evaluation. The template used for the recording of the morphology parameters is given in Appendix 1.

The recorded parameters were divided into two groups, general data and crack morphology data. General data are data such as crack mechanism, crack location, type of material, references etc. Crack morphology data are data such as crack length, crack depth, angel of the crack in relation to the surface, crack tip radius etc. For all parameters a limited number of expressions were defined. This was made in order to simplify both the recording of parameters and the evaluation of typical characteristics for different types of

cracks. A brief description of the parameters and some of the used expressions are given in the following two sub sections.

3.1.1 General data

The recorded parameters are:

Identification: The system or component and power plant where the crack was found.

Reference: Reference to the failure report

Mechanism: Failure mechanism, IGSCC, IDSCC, TGSCC mechanical fatigue etc.

Crack location: For example in a pipe bend, close to a weld, in a fitting etc.

Material grade: Standard designation of the material

Material group: The material grades were divided into material groups, such as, austenitic stainless steel, ferritic-austenitic stainless steel, martensitic stainless steel, carbon steel, low alloy steel and nickel base alloy.

Condition: The delivery condition of the material i.e. solution annealed, cold worked, normalised, as welded etc.

Delivery form: plate, pipe, pipe bend, fitting, forging etc.

D_y: Outside diameter of pipe or similar.

T: Wall thickness of pipe or plate.

Loading conditions: Information on the loading condition in the vicinity of the crack that can affect the crack behaviour, for example internal pressure, residual stresses, alternating thermal loads etc.

3.2.1 Crack morphology data

The recorded parameters are:

Crack dimensions: Crack length on the surface and crack depth. The crack depth/wall thickness ratio was also recorded.

Distance to...: Distance from the crack to a weld, pipe bend or similar feature affecting the crack initiation or propagation.

Through thickness angle: The angle is measured in relation to the surface. If the crack was located close to a weld, then the angle is $< 90°$ if the crack slopes towards the centre line of the weld or $> 90°$ if the crack slopes away from the weld. The definition of the through thickness angle is given in Fig. 1. If the crack was located far away from a weld then the angle is always in the range of 0-90°.

Angle in surface direction: This angle describes the direction of the crack on the surface. If the crack is far away from a weld, then 0° is in the longitudinal direction of the

pipe and 90° is perpendicular to the pipe. If the crack is close to a weld, then 0° is parallel to the weld and 90° is perpendicular to the weld, see Fig. 1.

Macroscopic shape in the through thickness direction: The expressions used are straight, winding, bend, slightly bend, bilinear, branched, heavily branched and zig-zag. The different shapes are illustrated in Fig. 2.

Macroscopic shape in surface direction: The same expressions are used as for the through thickness direction.

Number of cracks: The number of cracks in the damaged area. A numerical value in the range of 1-5 was recorded. If the number of cracks was larger than five, then >5 was recorded.

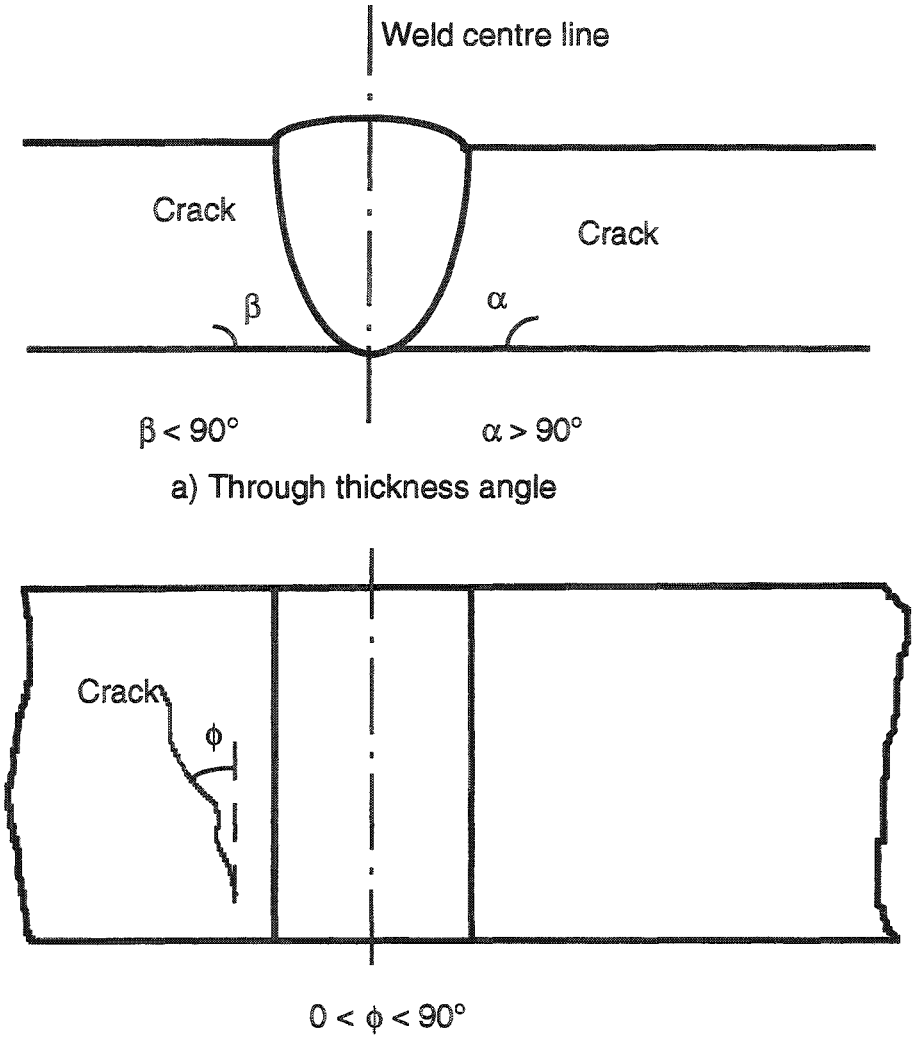

Fig. 1, Definition of angles when the cracks are located close to a weld, a) in through thickness direction and b) in surface direction.

Cobble stone pattern distance: Cobble stone pattern is very common as a surface pattern for cracking caused by thermal fatigue. A typical value of the distance between the cracks at the surface was recorded. A typical cobble stone pattern is shown in micro graph no 5 in Appendix 2.

Macroscopic branching: This parameter describe the amount of branching in the through thickness direction. Only branches longer than five grain diameters were recorded. The number of branches per mm crack length was recorded. Crack branches shorter than five grain diameters were regarded as microscopic branching.

Grain size: The grain size adjacent to the evaluated crack was recorded. The grain size was measured with the intercept method, and given as a mean grain diameter.

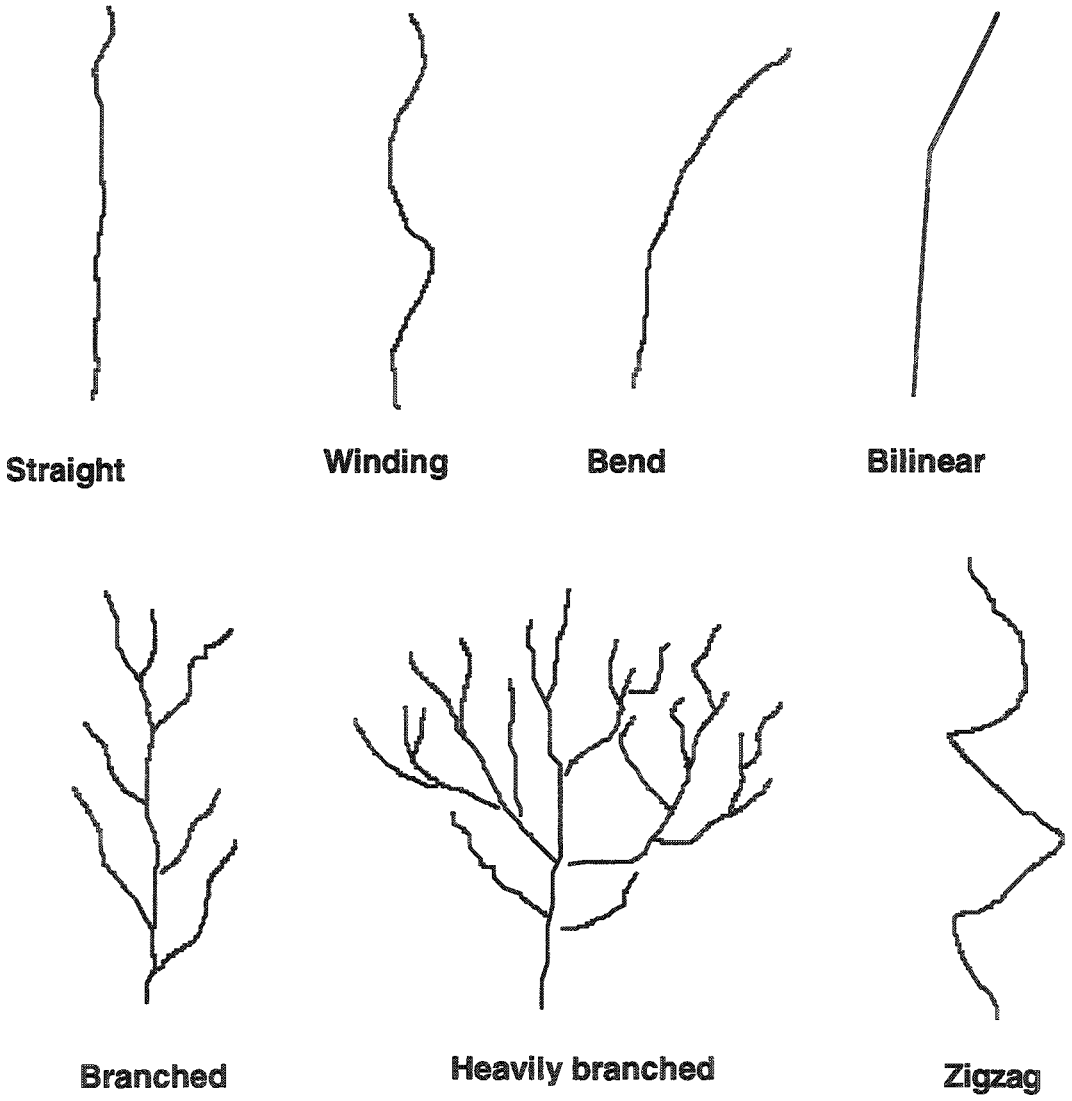

Fig. 2, Schematic illustration of different types of crack shapes.

Micro-structure: The micro-structure in terms of the shape of the grains close to the crack was recorded. The following expressions were used: equiaxed grains, column formed grains, cold worked structure, cast structure.

Crack surface roughness: The surface roughness of a crack is a difficult parameter to measure. In particular if the measurements are made on photos from failure investigation reports. Thus, an accurate and a robust methods must be used. The definition of the roughness parameter should therefore be rather simple and the required number of measurements should be low. A well known roughness parameter that is quite simple to evaluate is the "ten point height of irregularities", R_Z. The definition of R_Z is given in Fig. 3. To determine R_Z, the five highest peaks and the five lowest valleys on the crack surface, within a certain length of the crack, are measured. This makes R_Z a good parameter to use in this type of investigation. Furthermore, R_Z can easily be converted to other, more well known surface roughness parameter, such as, "the arithmetical mean deviation of the profile", R_a. The relation between R_a and R_Z is, $R_a \approx R_Z / 4$

This relation is valid for R_Z-values in the range of 12-1000 μm.

The crack surface roughness that is of interest is the roughness on a macro scale and not on a grain size level. Therefore, the measurement length L, is in the range of 1-2 mm.

Measurement length: The crack length used for the determination of R_Z, see Fig. 3, was, whenever possible, in the range of 1-2 mm.

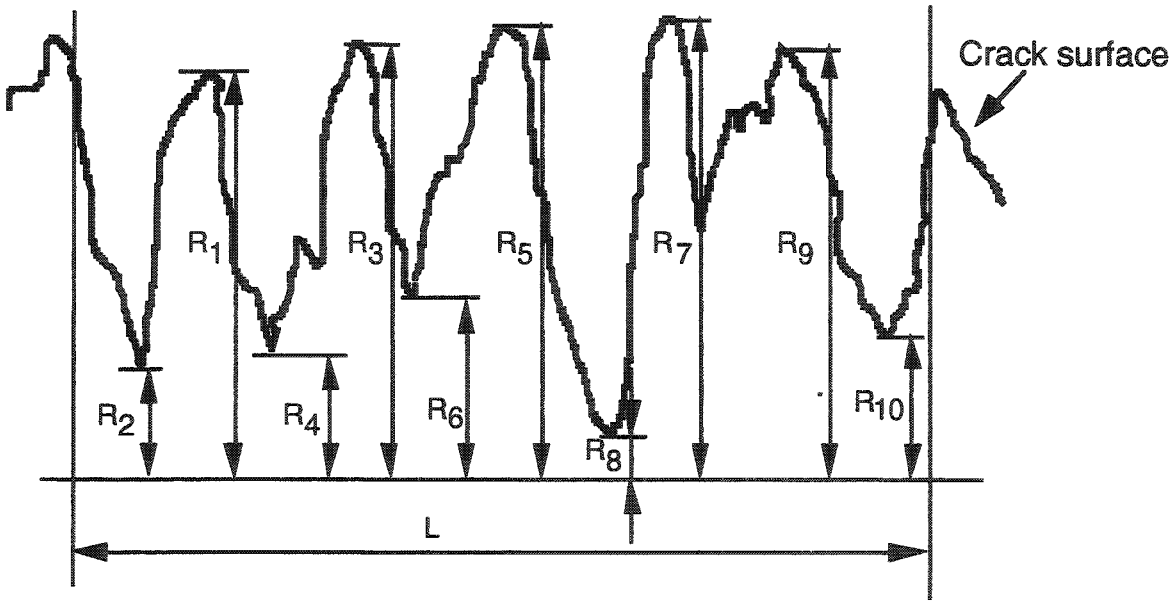

$$R_Z = \frac{(R_1+R_3+R_5+R_7+R_9) - (R_2+R_4+R_6+R_8+R_{10})}{5}$$

Fig. 3, Definition of the crack surface roughness parameter, R_Z.

Correlation length: The correlation length, λ_0, controls the rate of change of surface height with distance along the surface. To calculate λ_0 from its theoretical definition is rather complicated and involves a large number of measurements. In this work an empirical formula for the correlation length has been used, see Fig. 4.

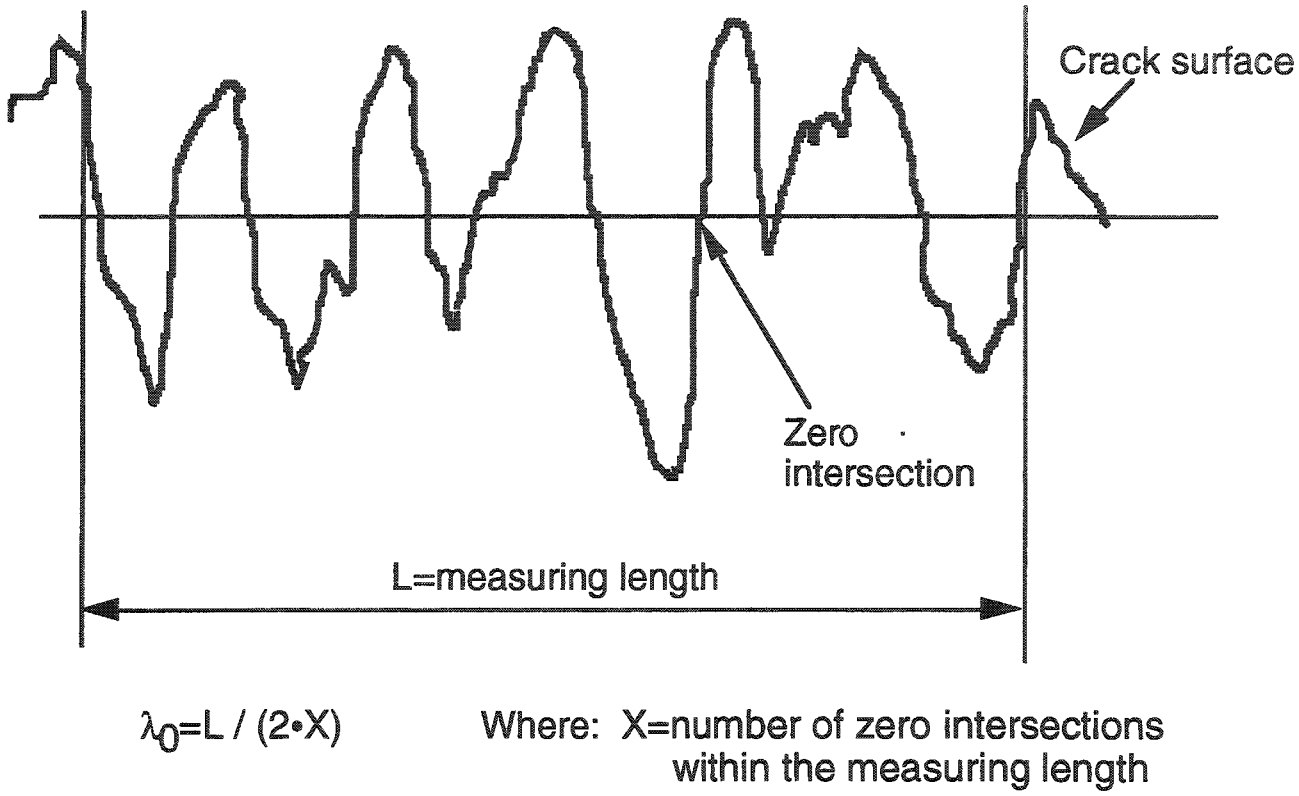

Fig. 4, Definition of correlation length, λ_0.

Crack width: The crack width was recorded at three locations for each crack, at the surface, at half the distance between the surface and the crack tip and at the crack tip.

Influence of sampling: The method of cutting out samples for failure investigations can have a great influence on the measured crack opening. An attempt was made to estimate the influence by assigning a number from one to three, where one is no influence, two is minor influence and three is a large influence on the crack opening. The lowest number represents a large sample, including the whole wall thickness, not in connection to a weld. The intermediate number represents a large sample close to a weld, or a small sample far away from welds, and finally, the highest number was assigned to small samples close to a weld.

Crack tip radius: The crack tip radius was measured and recorded for those cracks where it was meaningful to measure the crack tip radius, i.e. corrosion fatigue cracks.

Amount of oxides: The amount of oxides at the crack tip, halfway between the surface and the crack tip and at the surface was recorded. A number from one to three was used to represent the amount of oxides, where the number, in increasing order, represents, no oxide, a small amount of oxide, and a heavily oxidised crack surface, respectively.

Sketch over crack location: A simple sketch was made showing the evaluated crack shape. The sketch was then scanned into the database.

3.2.3 Limitations

The basis for this work was failure analysis reports. The purpose with such investigations is generally to identify and explain the failure mechanism, for each specific case. A detailed description of the crack shape and location is often of less importance. Therefore, the amount of useful information varies considerably between different failure reports. In none of the cases all the parameters specified in the template could be evaluated from one single failure report. This means that there is some information missing in the data base for most registered cracks. The lack of data is clearly shown in the presentation of the results in Section 4.

A crack is a three-dimensional defect. The specified parameters in this work do not cover a complete description of a three dimensional crack. The reason for this is of course lack of information in the evaluated failure reports. The information extracted in this work, over the crack characteristics, must therefore be treated in the light of these shortcomings. For example, the crack width at the surface is known to be varying along the crack length on the surface. The crack width measurements are made on micro graphs showing the crack in the through thickness direction. These photos are taken from a cross section of the sample somewhere along the crack length. Thus, the registered crack widths are dependent on were the cross sections were made along the crack length. Normally, there is no information in the failure reports on the exact location of these cross sections. The lack of information is shown as a large scatter in the registered crack width values. Large scatter in other parameters can be explained similarly.

4 Results

4.1 Survey of compiled data from evaluated cracks

In all, 194 cracks were evaluated, of which 84 are collected from nuclear industry failure reports, 71 from non-nuclear industry and 39 from nuclear industry failures reported in the literature. The crack types are divided into seven crack mechanisms and the material types into three groups. In Table 1 the number of cracks of each crack type/material group combination is shown.

In-service cracks often exhibit mixed features of two or more crack mechanisms. For example mixed features between the various fatigue mechanisms or between IGSCC and TGSCC are quite common. In Table 1, mechanical and thermal fatigue cracks are those where either mechanism is the obvious dominating crack mechanism. Corrosion fatigue comprise both pure corrosion fatigue and mixtures between corrosion fatigue and one of the other two fatigue mechanisms. When both IGSCC and TGSCC are present, the cracking was classified as IGSCC, and thus, the number of cracks designated TGSCC are mainly pure TGSCC. Weld flaws comprise all kinds of defects from welding during manufacturing.

Material groups	Mechanical fatigue	Thermal fatigue	Corrosion fatigue	IGSCC	TGSCC	IDSCC	Weld flaws	Total
Ferritic low alloy steels	**1**/6	**0**/6	**0**/20	**1**/12	**0**/4	**0**/0	**1**/6	**3**/54
Stainless steels	**2**/5	**22**/0	**1**/0	**39**/4	**19**/7	**0**/0	**5**/1	**88**/17
Nickel base alloys	**0**/0	**0**/0	**0**/0	**18**/0	**3**/0	**11**/0	**0**/0	**32**/0
Total	**3**/11	**22**/6	**1**/20	**58**/16	**22**/11	**11**/0	**6**/7	**123**/71 = 194

Table 1, Number of evaluated cracks of each crack type/material group combination divided into nuclear/non nuclear **industry.**

The reason for dividing material types into three large groups was the same as the limiting of the number of crack mechanism types, namely, to reduce the splitting of the data into too many groups. The material groups comprise material types as shown in Table 2.

Material groups		
Ferritic low alloy steels	**Stainless steels**	**Nickel base alloys**
Mild carbon steels	Austenitic stainless steels	Alloy 600
Micro-alloyed fine-grain steels	Ferritic stainless steels	Alloy 690
Low alloy high temperature steels	Ferritic/austenitic stainless steels	Alloy 182
Low alloy quenched and tempered steels	Martensitic/austenitic stainless steels	Alloy 82

Table 2, Dividing of material types into groups.

4.2 General description of crack morphology

In this section a general description of the morphology of each crack mechanism is given independent of material group. The description is based on general trends derived from the crack evaluation. Examples of typical crack features are shown by micro graphs in Appendix 2.

4.2.1 Mechanical fatigue

During cracking caused by mechanical fatigue, crack initiation and growth are controlled by external alternating service loads. The external loads often interact with internal stresses, e.g. weld residual stresses or residual stresses from cold forming. Thermal loads and corrosion attack from the surrounding environment are considered insignificant with respect to both crack initiation and growth of pure mechanical fatigue cracking.

Fatigue cracks are normally oriented perpendicular to the major stress direction. For example, in shafts subjected to axial bending loads, fatigue cracks occur in an orientation perpendicular to the axial direction, while torsion loads cause fatigue cracking in an angle 45° to the axial direction. Although, crack growth in the through thickness direction mostly is perpendicular to the surface, variations in the residual stress field adjacent to welds often cause deviations from right angle orientation. Another important factor controlling the crack orientation is geometrical stress raisers, such as under cut along welds and design related dimensional changes, see micro graphs no 1, 4 and 5 in Appendix 2.

Fatigue cracks are typically straight and unbranched, see micro graphs no 1 - 4 in Appendix 2. However, non-constant residual stress fields or redistribution of stresses during crack growth may cause curved crack paths, see micro graph no 6 in Appendix 2. The crack growth is in general transgranular and independent of most other micro-structural constituents. Crack tip morphology is predominantly unbranched and extremely sharp, see micro graph no 3 in Appendix 2. Typical crack tip radius is less than 5 μm. Mechanical fatigue usually produce narrow crack widths due to low surface roughness and the absence of corrosion products inside the crack. However, the crack width is strongly dependent on other factors, such as external and internal stresses acting perpendicular to the crack plane. The straight, micro-structural independent crack growth often results in smooth crack surfaces exhibiting low surface roughness, especially at low crack growth rates, where every step in growth produces shallow striations. A relationship between surface roughness and the stress intensity factor (K_I) have readily been shown for fatigue cracks, where surface roughness increases with an increasing stress intensity factor, [1].

4.2.2 Thermal fatigue

Thermal fatigue cracks initiate and grow as a consequence of alternating thermal loads. The loads cause tensional/compressive stresses due to gradients in thermal expansion. The micro-mechanism for crack initiation and growth by thermal loads is basically the same as for mechanical loads, but the resulting crack morphology, in some respects, deviates from that of mechanical fatigue.

A major difference between mechanical and thermal fatigue is the crack pattern on the surface of the component. Mechanical fatigue cracking normally produces a single or very few cracks, while thermal fatigue cracking, with a few exceptions, results in a large number of cracks. In addition, the crack orientation is more randomly distributed at thermal fatigue cracking compared to mechanical fatigue, due to the absence of a well defined major stress direction under thermal loads. The cracks often occur in a fabric-like pattern

known as cobble stone pattern, see micro graphs no 10 - 12 in Appendix 2. When a major stress direction exist due to geometrical conditions or at high service stresses, other than thermal, a more well oriented surface crack pattern are formed, see micro graph no 7 in Appendix 2. In the through thickness direction thermal fatigue cracks are characterised by a low tendency for crack branching and transgranular crack growth. The shape in the through thickness direction is in most cases straight, although bent and winding cracks have been observed. Thermal fatigue cracking in ferritic low alloy steels and stainless steels, at high temperatures, cause oxidation of the crack surfaces and at the crack tip. This may affect the crack width and tip radius, see micro graphs no 8 - 9 in Appendix 2.

4.2.3 Corrosion fatigue

During corrosion fatigue cracking, a corrosion attack contributes considerably to crack initiation, crack growth or both. The corrosion attack interacts with alternating mechanical or thermal loads. A large number of cracks, a large tendency for crack branching, considerable amounts of corrosion products inside the cracks and blunted crack tips are the most characteristic features of corrosion fatigue cracks, which distinguish them from other fatigue cracking mechanisms, see micro graphs no 16 - 19 in Appendix 2.

4.2.4 Intergranular stress corrosion cracking, IGSCC

Intergranular stress corrosion cracking, IGSCC, is caused by the combined effects of tensile stresses and corrosion. The origin of stresses may be external loads or internal residual stresses. Other important factors, besides the stress level and environment, are temperature, material grade and the material condition. A typical example is sensitisation of austenitic stainless steels, which produce a material condition enhancing the cracking propensity. For welded structures, which have not been post weld heat treated, residual stresses are of utmost importance for stress corrosion cracking to occur. Residual stresses and phase transformations from cold forming are other important contributors.

IGSCC in nuclear power stations was first observed in austenitic stainless steel piping in the late sixties. In Swedish BWRs, IGSCC in austenitic stainless steels has been found close to welds, in the heat affected zone (HAZ), or in cold worked pipe bends. However, IGSCC in carbon and low alloy steels has been known for more than 100 years. This type of cracking was earlier known as "caustic embrittlement" or "caustic cracking". Today, IGSCC still causes failures in structures made of ferritic low alloy steels serving in a number of more or less aggressive environments, other than caustic solutions.

Like fatigue cracking, IGSCC is controlled by external service stresses or residual stresses from welding or cold forming. Therefore, cracks oriented perpendicular to the direction of the major stresses are anticipated. On the other hand, IGSCC is considerably more dependent on the micro structure, and deviation from pure stress controlled growth is often observed. The intergranular crack path make the cracking less straight and more branched compared to fatigue cracks. The IGSCC crack tip is often sharper than of a fatigue crack, but crack branching in the vicinity of the IGSCC crack tip is more common than of fatigue cracking, see micro graphs no 29 - 30 in Appendix 2.

As in the case of pure mechanical fatigue cracking, IGSCC does not primarily produce large amounts of corrosion products inside the crack. This makes it possible for IGSCC to form extremely narrow crack widths, provided external or residual stresses does not open up the cracks. However, often secondary corrosion products are formed inside old cracks. The crack surface roughness of IGSCC is closely related to the grain size of the material in the cracked region, provided the surface roughness is measured on a grain size scale. Thus, a high surface roughness is anticipated for IGSCC in the coarse grained region of the HAZ, compared to the fine grained parent metal, or in a coarse grained austenitic stainless steel, compared to a fine grained ferritic low alloy steel. Examples of typical IGSCC in ferritic low alloy steels, austenitic stainless steels and nickel base alloys are shown in micro graphs no 20 - 32 in Appendix 2.

4.2.5 Transgranular stress corrosion cracking, TGSCC

Transgranular stress corrosion cracking, TGSCC, has a lot in common with IGSCC. As for IGSCC, important factors for TGSCC are stress, environment, temperature and material grade. The major difference is that the crack propagates through the grains and not along the grain boundaries. The crack preferentially grows along specific lattice planes in each grain, which makes the crack to change direction at every grain boundary.

TGSCC is typically heavy branched, which makes it less meaningful to consider such parameters as crack orientation or surface roughness. The crack appearance in the through thickness direction are shown in micro graphs no 34 - 38 in Appendix 2. The crack tip morphology for TGSCC is better characterised by the branching than by the crack tip radius. As for mechanical fatigue and IGSCC, the absence of corrosion products inside the cracks, TGSCC may produce narrow crack widths. Examples of typical TGSCC in ferritic low alloy steels and austenitic stainless steels are shown in micro graphs no 33 - 38 in Appendix 2.

4.2.6 Inter dendritic stress corrosion cracking, IDSCC

Inter dendritic stress corrosion cracking (IDSCC) occurs in material with a solidification structure. In this study all IDSCC are cracks found in nickel base alloy weld metal. The mechanism for IDSCC is essentially the same as for IGSCC in austenitic stainless steel. However, IDSCC cracks in weld metal often are confused with hot cracks. Both crack types are usually located at the centre of the weld, and both cracks are inter dendritic. Hot cracking is not necessarily surface penetrating, while IDSCC always is. Hot cracks are formed during an early stage of solidification of the weld metal. Thus, the crack morphology is slightly different from IDSCC. However, in some cases it is hard to distinguish between these two types of cracks.

The crack surface roughness is considerably larger for IDSCC-cracks compared to IGSCC-cracks. The reason for that is the large difference in micro structure between the weld metal and the base material. For IDSCC-cracks, there is also a difference in the surface roughness in the longitudinal direction compared to the transverse direction of the crack. The roughness is always larger in the transverse direction due to the inter dendritic propagation of the crack. In the longitudinal direction, when the crack propagates in the same direction as the the dendrites, an IDSCC-crack is rather smooth. Typical examples of IDSCC are shown in micro graphs no 39 - 41 in Appendix 2

4.2.7 Weld flaws

Weld flaws are included in the study for comparison with service induced cracking. Evaluated weld flaws are lack of fusion along the fusion line, hot cracks (solidification cracks) in the weld metal and hydrogen induced cold cracks in the heat affected zone next to the weld. Typical weld flaws are shown in micro graphs no 42 - 45.

Flaws due to lack of fusion are oriented along the fusion line and thus parallel to the weld joint surfaces. Lack of fusion between weld passes also occur. Typically, they are extremely narrow, unbranched and exhibit a low surface roughness. Both oxide filled and oxide free flaws exist, depending on whether the flaw is internal or surface penetrating.

Hot cracking is inter dendritic, and thus, typically non-straight. The most common orientation is cracking parallel to the weld direction, and the cracks are located in the weld centre. However, hot cracks may as well occur in directions parallel to the solidification direction of the weld metal.

Cold cracks grow intergranularly along prior austenite grain boundaries, preferentially in the coarse grain heat affected zone. Thus, the crack orientation is parallel to the weld joint geometry. The tendency for crack branching is low and the surface roughness is high due to the large grain size in the cracked region.

4.3 Orientation in surface and through thickness direction

The effect of the cracking mechanism on five major crack morphology parameters is given in detail in Sections 4.3 - 4.7. The results are presented in sub-sections for each cracking mechanism/material group combination, where data were obtained. The parameters evaluated are crack orientation, branching, tip morphology, width and surface roughness. With a few exceptions, cracks from nuclear and non-nuclear industry are evaluated as one group. By dividing the data in nuclear and non-nuclear failures, one or the other are dominating each group, as is evident from Table 1.

In Section 4.3 the crack orientation in the through thickness and surface direction is reported. The surface orientation is related to welds or geometrical features, as defined in Section 3.1.1. If relevant data on the crack location are available these are also included.

4.3.1 Mechanical fatigue

4.3.1.1 Ferritic low alloy steel

The number of evaluated cracks were seven. Three out of seven cracks initiate at design related stress raisers, and two at weld fusion lines. Thus, the surface orientation is controlled by geometrical features. The angle in the through thickness direction are for six of the cracks 90°. The only exception is a crack initiated in the weld fusion line, where the crack tends to follow the joint geometry in a 75° angle. No information were available on orientation in the surface direction.

4.3.1.2 Stainless steel

The number of evaluated cracks were seven. Two cracks in austenitic stainless steel are from the nuclear industry, and five from the non-nuclear industry. Of the five latter cracks, two are in austenitic stainless steel and three in martensitic-austenitic stainless steel. The two cracks from the nuclear industry are both located at the fusion line in connection to welds. The through thickness angles are 65° and 90°, respectively. Of the five cracks from the non-nuclear industry only one is located at the fusion line. The other four cracks are initiated at other geometrical stress raisers, such as fillets. The through thickness angle for all of those five cracks are in the range of 60-90°. No information are available on orientation in the surface direction.

4.3.2 Thermal fatigue

4.3.2.1 Ferritic low alloy steel

Six cracks were evaluated, all from the non-nuclear industry. The through thickness direction of all six cracks are 90°. Four of those cracks are from boiler tubes and the orientation in the surface direction is 90° to the tube axis.

4.3.2.2 Austenitic stainless steel

Twenty-two cracks in austenitic stainless steel were evaluated, all from the nuclear industry. Fifteen cracks are oriented at 85-90° in the through thickness direction. Four cracks have a through thickness direction at 70-76°, and one at 65°. There are no information available for the two remaining cracks. The surface orientation is difficult to determine due to the lack of information. However, fourteen of the cracks show a cobble stone pattern on the surface. The orientation of the pattern seems to bee controlled by the flow conditions in the pipes.

4.3.3 Corrosion fatigue

4.3.3.1 Ferritic low alloy steel

All evaluated cracks were from the non-nuclear industry. The number of evaluated corrosion fatigue cracks were 20. Ten are located at welds, of which four were oriented perpendicular and six parallel to the weld. Out of the six cracks running parallel to the weld, three are located in the coarse grain heat affected zone at a distance of 0-1 mm from the fusion line, two are inside the weld metal and one 5 mm away from the weld. The orientation in the through thickness direction is 90° for all but three cracks.

4.3.3.2 Austenitic stainless steel

Only one crack was found (nuclear industry). The crack is located close to a weld and the through thickness orientation is 90°. The surface orientation is parallel to a circumferential but weld.

4.3.4 IGSCC

4.3.4.1 Ferritic low alloy steel

All cracks but one were from the non-nuclear industry. Ten cracks show pure IGSCC and three mixed IGSCC and TGSCC features. Five of those are located at welds. Three are running along and two across the weld. Two of the cracks oriented along the weld are located close to the fusion line and one 6 mm away from the weld. For the cracks running across the weld it is not possible to determine the site of crack initiation.

Eight cracks are not located at welds but in cold formed bends of seamless boiler tubes. Crack site and orientation are strongly dependent on local heavily cold formed regions in the bends. Surface orientations between 0 and 90° to the tube axis were measured.
Out of 13 cracks 12 are oriented 90° in the through thickness direction.

4.3.4.2 Stainless steel

Out of 43 evaluated cracks four were from non-nuclear industry. 41 cracks in austenitic stainless steel and one crack each in ferritic stainless steel and precipitation hardening austenitic stainless steel. 33 cracks are located in connection to welds, four cracks are located in cold worked austenitic stainless steel pipes and six cracks are from laboratory test specimens. The dominating through thickness angle is 80-90° for all cracks, even though the scatter range is 45-130°. The surface orientation, for those cracks which are located close to a weld, is parallel to the weld. The surface orientation for other cracks is more unclear due to lack of information.

4.3.4.3 Nickel base alloys

Sixteen cracks were evaluated. Fifteen are cracks in Alloy 600. Ten of those are laboratory cracks and the remaining five service cracks from the nuclear industry. One is a laboratory crack in Alloy 800. The through thickness orientation are 90° for nine cracks, three cracks are oriented in 60° and there were no information from four cracks. The surface orientation, for the cracks where it could be evaluated, are either 90° or 0° to the pipe axis, depending on the main stress direction.

4.3.5 TGSCC

4.3.5.1 Ferritic low alloy steel

The number of evaluated pure TGSCC in ferritic low alloy steel were four. All of them are from the non-nuclear industry. The main crack orientation in the through thickness direction is measured as 75 - 90° for three cracks. One of them is located in the heat affected zone oriented along the weld.

4.3.5.2 Austenitic stainless steel

Out of totally 26 evaluated cracks 20 are from the nuclear industry and 6 from non-nuclear applications. Ten out of 26 are weld related. Of those ten, five are oriented mainly along the weld, and the distances from the fusion line are 0 - 10 mm. The orientation in the surface direction is less well defined, compared to IGSCC, because of the large number of cracks scattered in several directions, which is common for TGSCC. Several crack angles were measured in the range 0 - 90°, and in four cases as 45° for cracking at welds.

As for surface orientation the through thickness orientation is more scattered compared to IGSCC. Out of 26 cracks 13 are oriented in other angles than 90°.

4.3.5.3 Nickel base alloys

The number of evaluated cracks were three, all induced in aggressive environments at laboratory tests . The orientation in the through thickness direction of the main cracks are 90° in two cases and 60° in one. No information is available on the surface orientation.

4.3.6 IDSCC

4.3.6.1 Nickel base alloys

Thirteen cracks were evaluated, all from the nuclear industry. Two are service induced cracks and the remaining eleven are laboratory cracks from various types of test specimens. The through thickness angles are 75° and 80° for the two service induced cracks. Five of the laboratory cracks have a through thickness direction in the range of 45-90°. Six of the laboratory cracks are cracks in CT-specimens, and thus, the crack orientation is not meaningful to evaluate.

4.3.7 Weld flaws

Out of 13 evaluated weld flaws six were from the nuclear and seven from the non-nuclear industry. Three cracks were caused by lack of fusion, hot cracking and cold cracking, respectively. The other four were other types of welding defects.

All cold cracks are located close to the fusion line. Two of the cracks are located in the coarse grain HAZ, at a distance of 0.1-0.2 mm from the fusion line. The lack of fusion flaws coincide with the fusion line. The location of the hot cracks are inside the weld metal but no particular orientation was observed. The through thickness orientation of the lack of fusion flaws and cold cracks are typical for that of common weld joint geometry, i.e. 35 - 70°.

4.3.8 Literature data

Lapides [2] investigated IGSCC at circumferential welds in austenitic stainless steel piping. He claims that the crack orientation depends on pipe size, welding process and weld preparation variables. Furthermore, stresses and sensitisation pattern control the crack orientation. Provided the crack starts at the inner surface, the first 25% of the growth is perpendicular to the surface then it turns and follow the weld fusion line.

Crack orientation data on other cracking mechanisms than IGSCC was not found in the literature.

4.4 Crack shape and branching

In this section data on crack shape, number of cracks in the damaged area and crack branching are reported. The used designations for crack shape is defined in Fig. 2, Section 3. Comparisons between the data groups are shown in Table 3.

4.4.1 Mechanical fatigue

4.4.1.1 Ferritic low alloy steel

Out of seven evaluated cracks five are considered straight and two are lightly curved in the through thickness direction. Five of them also appear straight in the surface direction. In four cases only one or two cracks exist in the cracked area. In two cases more than ten cracks occur due to geometrical conditions. No crack branching was recorded for any of the seven cracks.

4.4.1.2 Austenitic stainless steel

Two cracks from the nuclear industry and five cracks from the non-nuclear industry were evaluated, see Section 4.3.1.3. The through thickness shape of the two cracks from nuclear industry are winding. Four of the other cracks are considered straight and one bent.

The shape in the surface direction for five of the cracks is straight. For the other two cracks, one each from the nuclear and the non-nuclear industry, there is no information available.

4.4.2 Thermal fatigue

4.4.2.1 Ferritic low alloy steel

Out of six evaluated cracks, all but one are straight. The exception is partly branched. In all cases but one, more than ten cracks are present in the damaged area. The average distance between the cracks were evaluated for five cases and measured as 0.4 - 1.0 mm. Except the branched crack mentioned, the five remaining cracks do not show any tendency to crack branching.

The most common surface shape in all six cases is slightly curved cracks, showing preferential propagation, typically shown in micro graph no 6 in Appendix 2. No cobble stone surface pattern was observed in any case.

4.4.2.2 Austenitic stainless steel

A typical surface pattern for thermal fatigue cracking in austenitic stainless steel components from nuclear power service is the cobble stone pattern. Out of 22 evaluated cracks 14 show a well developed cobble stone pattern. Four cracks are straight in the surface direction, without a cobble stone pattern. The shape in the through thickness direction is straight for nine cracks, bent or slightly bent for five cracks, winding for three cracks and one crack shows a zig-zag pattern. Only two cracks show a tendency for micro branching. Consequently, the cobble stone pattern results in a large number of cracks, but also straight cracks have, in most cases, more than five cracks in the damaged area. The distance between the cracks in the cobble stone pattern was in three cases 6-8 mm.

4.4.3 Corrosion fatigue

4.4.3.1 Ferritic low alloy steel

Out of 20 evaluated cracks, ten are straight in the surface direction and eight in the through thickness direction. The shape of seven cracks is curved or winding in the through thickness direction. Four of the cracks are more or less branched. The number of branches for each crack are typically 1 - 3.

4.4.3.2 Austenitic stainless steel

One crack from the nuclear industry was evaluated. The shape in the through thickness direction is winding without any branching. There is no information available on the surface shape.

4.4.4 IGSCC

4.4.4.1 Ferritic low alloy steel

Eight out of 13 evaluated cracks show mainly a straight shape on a macroscopic scale. The remaining five cracks are more or less curved or strongly winding. On a grain size scale all cracks follow a jagged zig-zag crack path caused by the intergranular growth. The number of cracks in the damaged area are typically 1 - 5, with two exceptions where more than ten cracks exist. Macroscopic branching was recorded for five cracks. The number of branches for those cracks were measured as 0.2 - 2.0/mm.

4.4.4.2 Stainless steel

The number of evaluated cracks was 43. Four are from the non-nuclear industry and the remaining cracks from the nuclear industry. 41 cracks are reported in austenitic stainless steel, one in ferritic stainless steel and one in precipitation hardening steel. Six of the cracks are laboratory cracks.

The through thickness shape is winding, straight, bent or zig-zag. Often the shape is a mixture of straight and bent. If the crack is located close to a weld, then it often follows the shape of the weld, see micro graph no 26 in Appendix 2. The crack is bent towards the weld, even though the shape could be characterised as winding in a smaller scale. On a grain size scale the cracks in austenitic stainless steel are more irregular than the cracks in ferritic low alloy steel, due to larger grain size in stainless steel. The dominating surface shape is straight, even though winding, bent or mixed crack shape were found. The number of cracks in the damaged area are mostly less than four. In three cases, all from the non-nuclear industry, more than ten cracks were recorded for mixed IGSCC-TGSCC in austenitic stainless steel. More than five cracks were found in the three cases of pure IGSCC from the nuclear industry. Macro branching is not common for pure IGSCC in austenitic stainless steel. Branching only occur for five cracks, in a range of 0.06-2 branches/mm. The evaluated crack in precipitation hardening stainless steel show a crack branching of 10 branches/mm.

4.4.4.3 Nickel base alloys

Sixteen cracks were evaluated, eleven laboratory cracks and five service cracks from the nuclear industry. One crack is located in Alloy 800 and the remaining 15 in Alloy 600. The evaluation show that there is no difference in shape between laboratory cracks and service cracks from the nuclear industry. The through thickness shape is winding, straight, or zig-zag for IGSCC, and branched for mixed IGSCC/TGSCC. The number of crack branches is 5-8/mm for IGSCC/TGSCC and 0-3/mm for pure IGSCC, except for one IGSCC crack that exhibit 7 branches/mm. The number of cracks in the damaged area is low. A typical range is 1-3. However, there are two cracked areas showing more than ten cracks, one from a laboratory test and one service induced crack from the nuclear industry. The surface shape is reported for two cracks only, they are both straight.

4.4.5 TGSCC

4.4.5.1 Ferritic low alloy steel

Two out of four evaluated cracks, are straight, and the other two curved or winding in the through thickness direction. All cracking appear as single cracks. Only one crack show a tendency to branch, 0.1 branches/mm.

4.4.5.2 Austenitic stainless steel

Out of 26 evaluated cracks 18 are heavily branched in the through thickness direction. The number of cracks in the cracked area is for 15 cases more than five. Four cases of single cracks were observed. The degree of branching was quantified by counting branches longer than five grain diameters. The result is shown in Fig. 5 for 21 cracks, for which the degree of branching was available.

4.4.5.3 Nickel base alloys

All three evaluated cracks are straight. However, two of them show a tendency to branch.

4.4.6 IDSCC

4.4.6.1 Nickel base alloys

Out of 13 evaluated cracks two are service cracks from the nuclear industry, and 11 are laboratory cracks. The through thickness shape was recorded for eight cracks. The shape is winding in five cases, straight in two and one crack is bent. The surface shape is documented in one case only. It is winding. All cracks are single cracks, except one, where the number of cracks is more than five. Only one of the cracks show crack branching, 1.33 branches/mm.

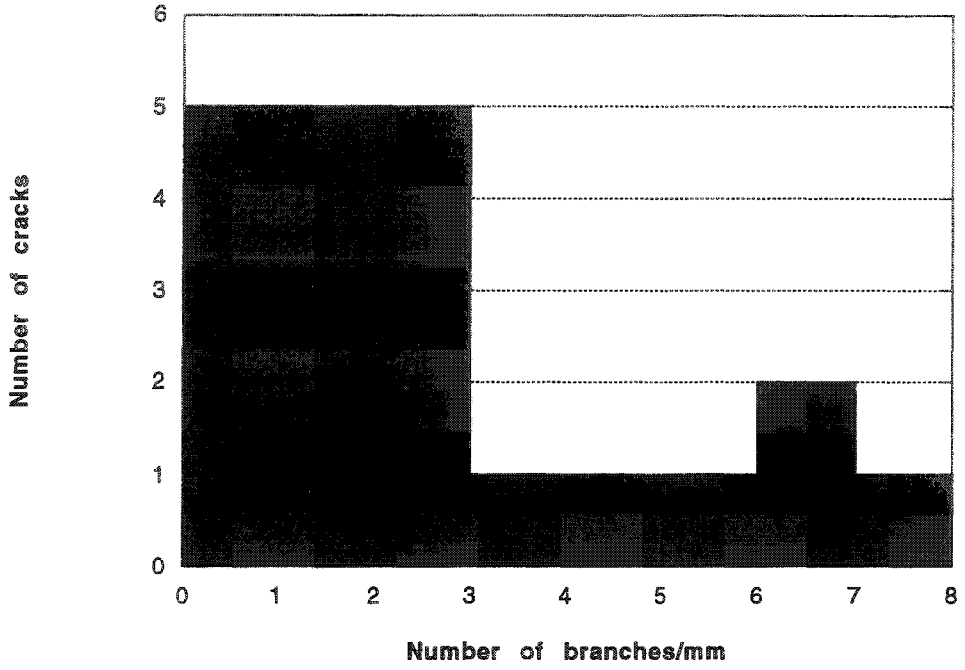

Fig. 5, Degree of branching for 21 TGSCC cracks in austenitic stainless steel.

4.4.7 Weld flaws

The shape of cold cracks and lack of fusion defects are controlled by the weld joint geometry, and thus, macroscopically straight or slightly curved shapes were observed. On a micro scale the cold cracks follow an intergranular crack path and show a jagged zig-zag shape. The lack of fusion flaws are located along the fusion line, which produce straight defects. The hot cracks are controlled by the solidification dendritic pattern, and thus, winding cracks in both macro- and microscopic scale are formed. Hot and cold cracks occur as multiple cracking. The number of cracks in each case is ≥3, and for two of the hot cracks >5. On the contrary, all lack of fusion flaws occur as single defects. None of the weld defects show branching.

4.4.8 Concluding remarks

The results from evaluation of the parameters in Section 4.3 and 4.4 are summarised in Table 3 as typical data.

Parameter		Orientation [°]		Shape		Number of cracks, 7)	Branching
Crack type	Material group	Through thickness direction	Surface direction	Through thickness direction	Surface direction		
Mechanical fatigue	Ferritic low alloy steel	90	1)	straight	straight 5)	1 - 2	no
	Stainless steel	60-90	1)	straight winding	straight 5)	1 - 3	no
Thermal fatigue	Ferritic low alloy steel	90	1)	straight	winding	>10	rarely
	Austenitic stainless steel	85-90	cobble stone pattern	straight bent winding	cobble stone pattern	>5	rarely
Corrosion fatigue	Ferritic low alloy steel	90	1)	straight winding	5)	1 - 3	occasionally
	Austenitic stainless steel	90	1)	winding	5)	2	no
IGSCC	Ferritic low alloy steel	90	1) 2)	straight winding	5)		occasionally 6)
	Stainless steel	80-90	1)	winding zigzag 5)	straight	<4	occasionally 6)
	Nickel base alloy	60-90	1)	winding straight branched	straight	1 - 3	occasionally
TGSCC	Ferritic low alloy steel	75-90	1)	straight	5)	1	occasionally 6)
	Austenitic stainless steel	45-90	0-90	branched	branched	>5	yes
IDSCC	Nickel base alloy	45-90	5)	winding straight	winding	1	rarely
Weld flaws	All material groups	3)	4)	straight	5)	1	6)

Table 3, Typical crack orientation, shape and branching data.

1) Controlled by the major stress direction or geometrical stress raisers.

2) Controlled by residual stresses introduced by welding or cold forming.

3) Lack of fusion flaws and cold cracks are controlled by weld joint geometry.

4) Lack of fusion flaws and cold cracks are parallel to the weld

5) Controlled by weld joint geometry.

6) Common on a micro scale.

7) Number of macro cracks in the damaged area, close to the evaluated crack.

4.5 Crack tip morphology

In this section the results of the crack tip morphology evaluation are reported. The crack tip is characterised by the tip radius. Radii down to 1 μm were measured and smaller radii, < 1 μm, are assigned the value 0.

4.5.1 Mechanical fatigue

4.5.1.1 Ferritic low alloy steels

All seven cracks show unbranched crack tips. Four of them show crack tip radius ≥5 μm and the remaining radii ≤1 μm.

4.5.1.2 Stainless steel

The crack tip radius was evaluated for six cracks. Five of them have a crack tip radius ≤5 μm. One has a crack tip radius of 15 μm.

4.5.2 Thermal fatigue

4.5.2.1 Ferritic low alloy steel

Three out of six evaluated cracks show crack tip radii ≥ 5 μm. The other three cracks have a radius ≤ 2 μm.

4.5.2.2 Austenitic stainless steel

Thermal fatigue cracks in austenitic stainless steel are typically transgranular. The crack tip radius was evaluated only for four out of the 22 recorded cracks. The crack tip radii are in the range of 1-9 μm. Micro-branching close to the crack tip occur for several of the 22 evaluated cracks.

4.5.3 Corrosion fatigue

4.5.3.1 Ferritic low alloy steel

A crack tip radius ≥ 10 μm was measured for eight out of 18 evaluated cracks. The distribution of crack tip radii is shown in Fig. 6. The mean value is 13 μm.

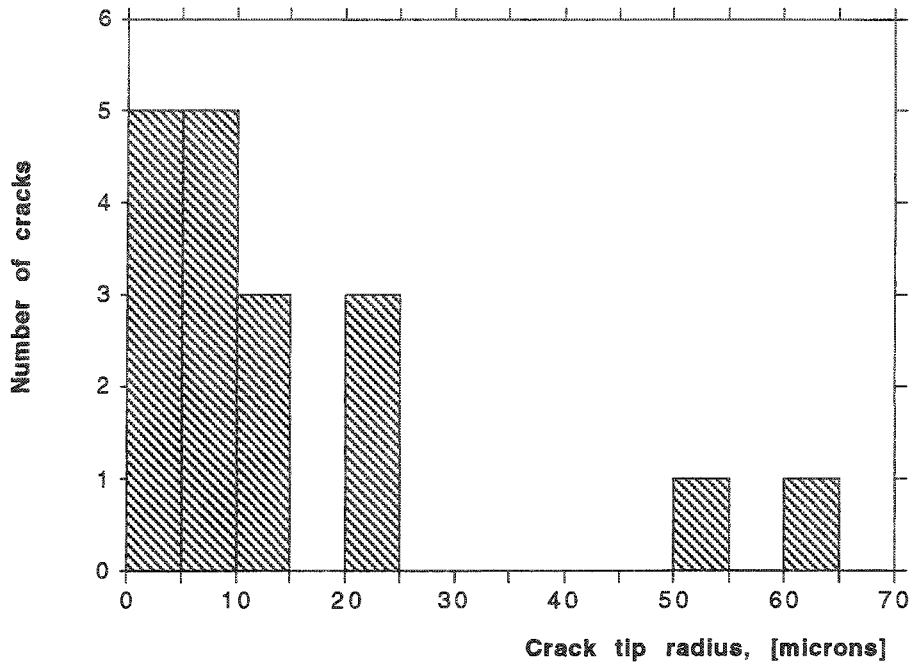

Fig. 6, Crack tip radius for 18 corrosion fatigue cracks in ferritic low alloy steel.

4.5.3.2 Austenitic stainless steel

One crack was evaluated. The crack tip radius is <1μm.

4.5.4 IGSCC

4.5.4.1 Ferritic low alloy steel

Out of eight evaluated cracks six show crack tip radii less than 1 μm.

4.5.4.2 Stainless steel

Twenty-five cracks were evaluated. In all cases the crack tip radii are ≤3μm. However, very often micro branching appears at the crack tip for IGSCC in stainless steel. Typical examples is shown in micro graphs no 29 - 30.

4.5.4.3 Nickel base alloys

For eleven out of 12 evaluated cracks crack tip radii ≤ 3 μm was measured. The remaining crack show a crack tip radius of 10 μm.

4.5.5 TGSCC

4.5.5.1 Ferritic low alloy steel

The crack tip radius was evaluated for three TGSCC cracks. Two of those have a crack tip radius ≥4 μm and the third a radius <1 μm.

4.5.5.2 Austenitic stainless steel

For 14 out of 16 evaluated cracks the crack tip radius is ≤ 2 μm. For ten of them the radius is < 1 μm. The two remaining cracks show enlarged crack tip radii caused by corrosion inside the crack.

4.5.5.3 Nickel base alloys

Two cracks were evaluated, and they show crack tip radius of 2 and < 1 μm, respectively.

4.5.6 IDSCC

4.5.6.1 Nickel base alloys

Three cracks were evaluated. All show crack tip radii less than 2 μm.

4.5.7 Weld flaws

The crack tip radius was only evaluated for two cold cracks, and they both show a tip radius <1 μm.

4.5.8 Concluding remarks

With one exception, all crack mechanisms produce sharp crack tips with a typical radius less than 5 μm. The exception is corrosion fatigue, where corrosion crack blunt the crack tip to typical radii ≥ 8 μm. The most sharp crack tips are produced by IGSCC, where the tip radius typically was less than 1 μm.

Results of the crack tip radius evaluation are compiled in Fig. 7. The median value for IGSCC in all three material groups is 0, i. e. < 1 μm. The dashed lines in Fig. 7 represent the 25% and 75% limits. The absence of dashed lines for some of the data groups are due to the limited number of data points. An interesting result is that some crack mechanisms in some cases show micro-branching at the crack tip. Micro-branching is here defined as branches which are less than five grains in length. The observations of micro-branching at the crack tip were made on photos from failure reports, but no quantification was done in this work.

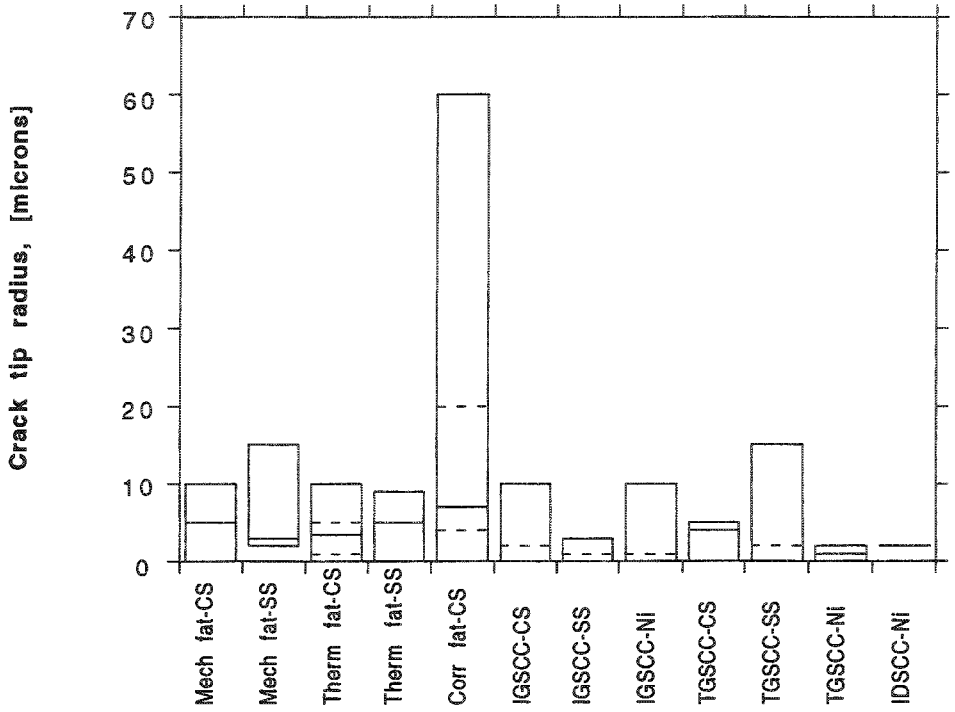

Fig. 7, Comparison of crack tip radius distribution of all data groups except weld flaws. Each box represent 5 - 95% of the data. Lower and upper dashed lines represent 25% and 75% limits, respectively. The solid line shows the median value.

4.6 Crack width

In this section results from the crack width measurements for each crack mechanism/ material group combination are reported. For each group of data the range in crack depth, wall thickness and crack depth/wall thickness ratio is given. The results are displayed in three types of plots.

1) Crack width at surface plotted versus crack depth/wall thickness ratio.
2) Crack width at each measuring point plotted versus distance from crack tip.
3) For selected homogenous groups of data, the crack width at each measuring point is plotted versus distance from crack tip. The three data points of each crack are connected, to get o rough view of the crack width/depth relation.

In addition, statistics of each group of data are shown in tables and in percentile graphs. Eventually, comparisons between the results of the evaluation and literature data are presented.

4.6.1 Mechanical fatigue

4.6.1.1 Ferritic low alloy steels

Seven mechanical fatigue cracks in ferritic low alloy steel were evaluated. The range in crack depth, wall thickness and crack depth/wall thickness ratio is 0.5-15 mm, 5-140 mm and 2 - 100%, respectively. The crack width was measured at three points for each crack. The results are presented in Fig. 8 and 9, where the crack width at surface and midway are plotted versus crack depth/wall thickness ratio and the crack width at each measuring point is plotted versus distance from crack tip, respectively. An anticipated increased crack width with increasing crack depth and crack depth/wall thickness ratio could be observed.

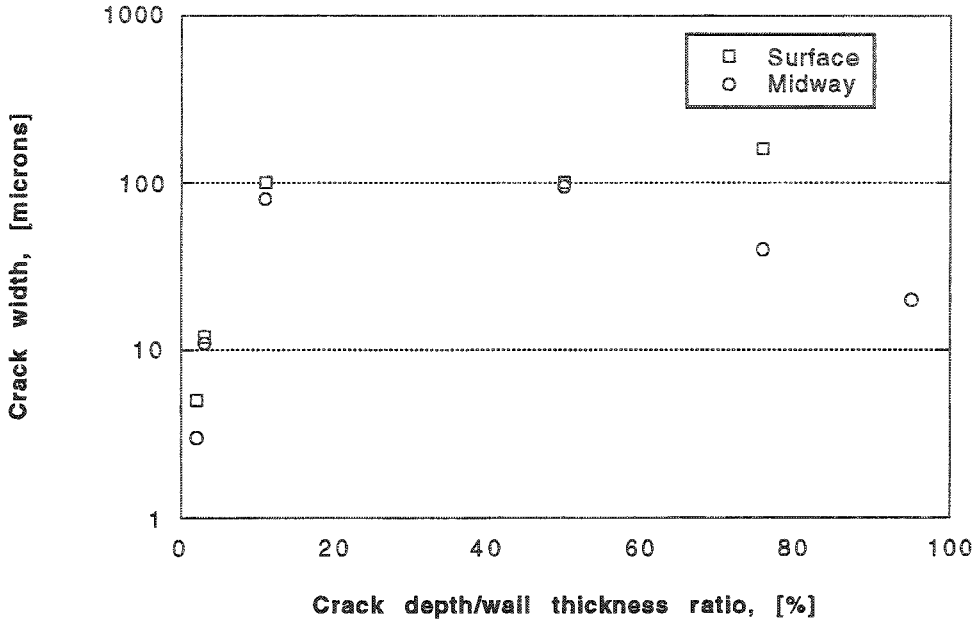

Fig. 8, Crack width at surface and midway for 6 mechanical fatigue cracks versus crack depth/wall thickness ratio.

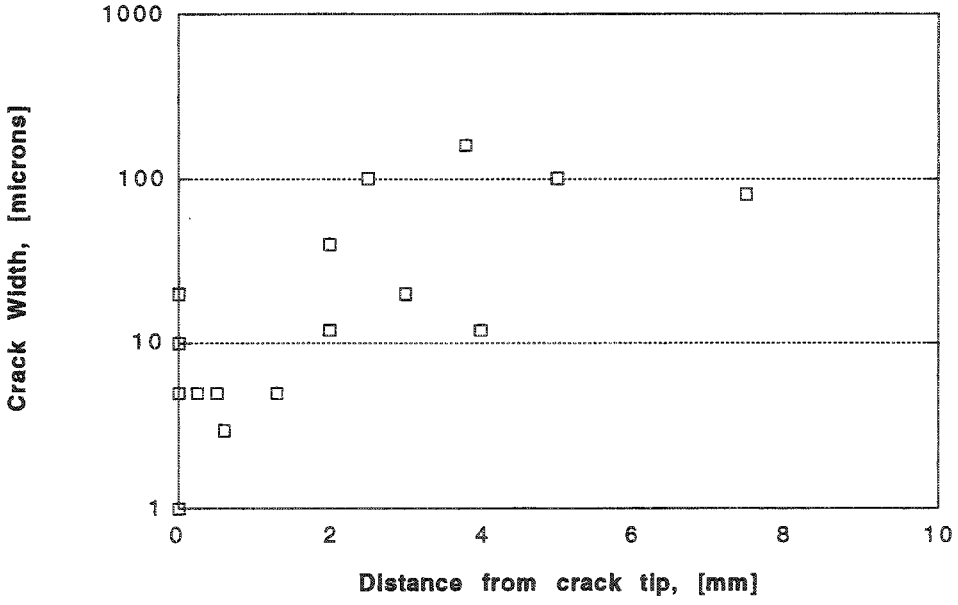

Fig. 9, Crack width at three locations for each crack versus distance from crack tip.

4.6.1.2 Stainless steel

Six cracks were evaluated, one from the nuclear industry (austenitic stainless steel) and five from the non-nuclear industry (two austenitic and three martensitic-austenitic stainless steels). The results are presented in Fig. 10 and 11. The range in crack depth, wall thickness and crack depth/wall thickness ratio is 1-12 mm, 2.8-220 mm and 1-70 %, respectively. This is an inhomogenous group with large scatter in wall thickness and crack/wall thickness ratio. The results are shown in Fig. 10 and 11.

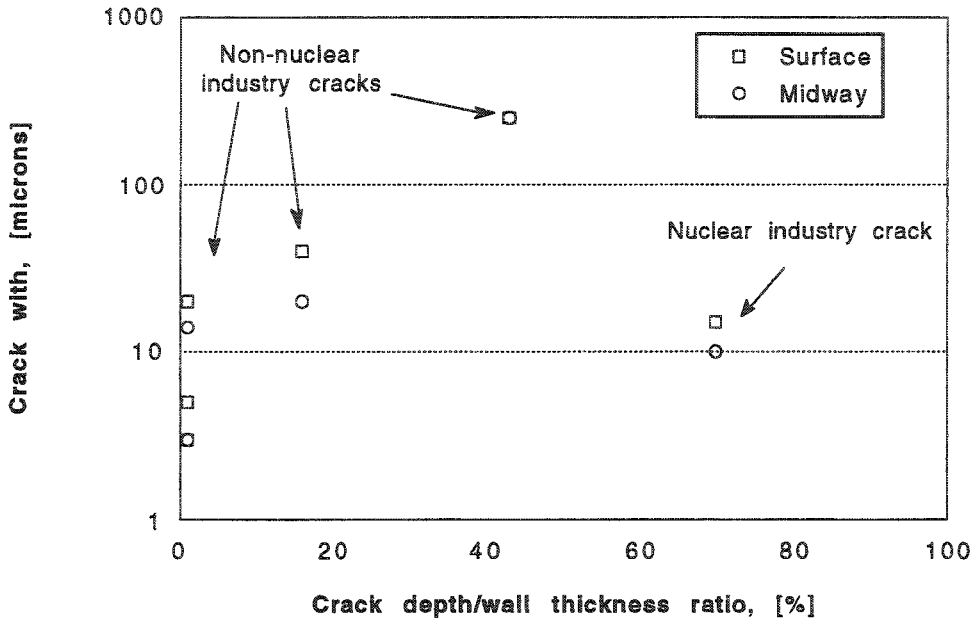

Fig. 10, Crack width at surface and midway for six mechanical fatigue cracks in stainless steel versus crack depth/wall thickness ratio.

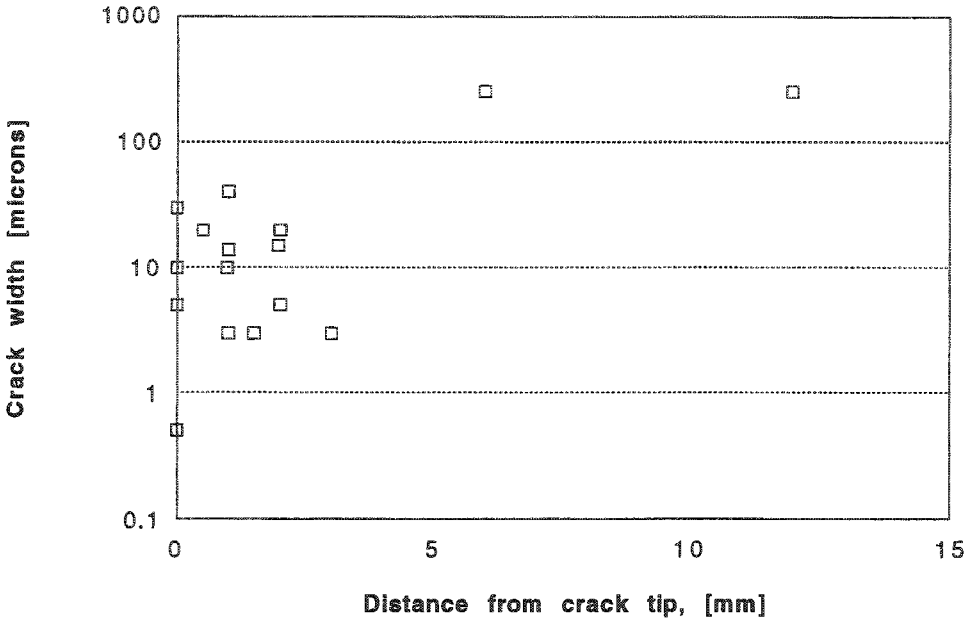

Fig. 11, Crack width at three locations for each crack versus distance from crack tip. Stainless steel.

4.6.2 Thermal fatigue

4.6.2.1 Ferritic low alloy steel

In all, six thermal fatigue cracks in ferritic low alloy steel were evaluated. The range in crack depth, wall thickness and crack depth/wall thickness ratio is 1-2.5 mm, 5-16 mm and 7-50%, respectively. The results are presented in Fig. 12 and 13. Compared to mechanical fatigue, thermal fatigue data are more homogenous, apart from the measured crack widths, which are larger and more scattered. However, the number of cracks is too small for accurate conclusions. The crack width versus distance to the crack tip is shown for four cracks in Fig. 14. All cracks were shallow, in the range 0.5-1 mm. They all show reasonably similar width/depth relation.

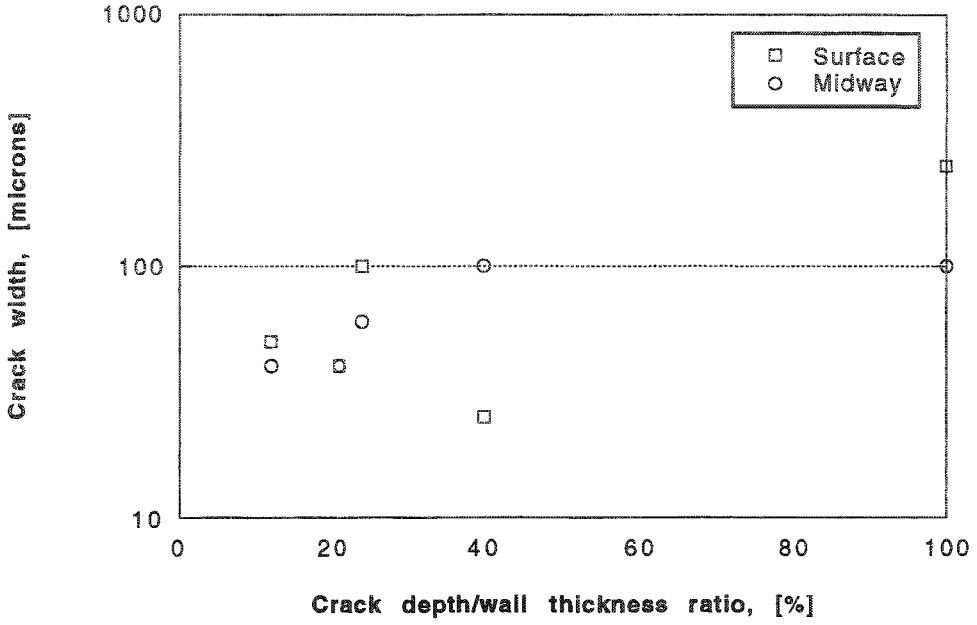

Fig. 12, Crack width at surface and midway for 5 thermal fatigue cracks versus crack depth/wall thickness ratio.

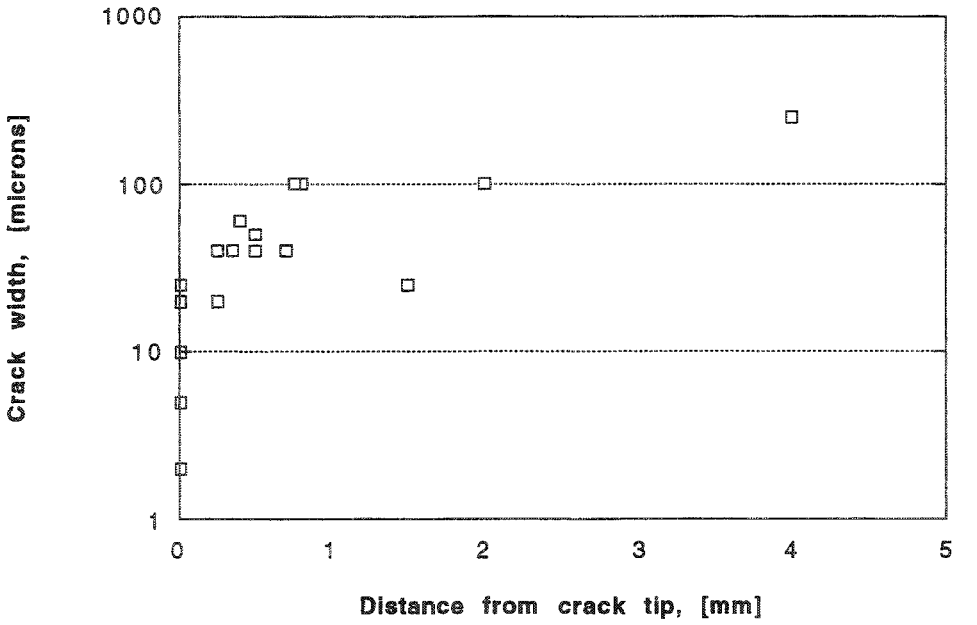

Fig. 13, Crack width at three locations for each crack versus distance from crack tip.

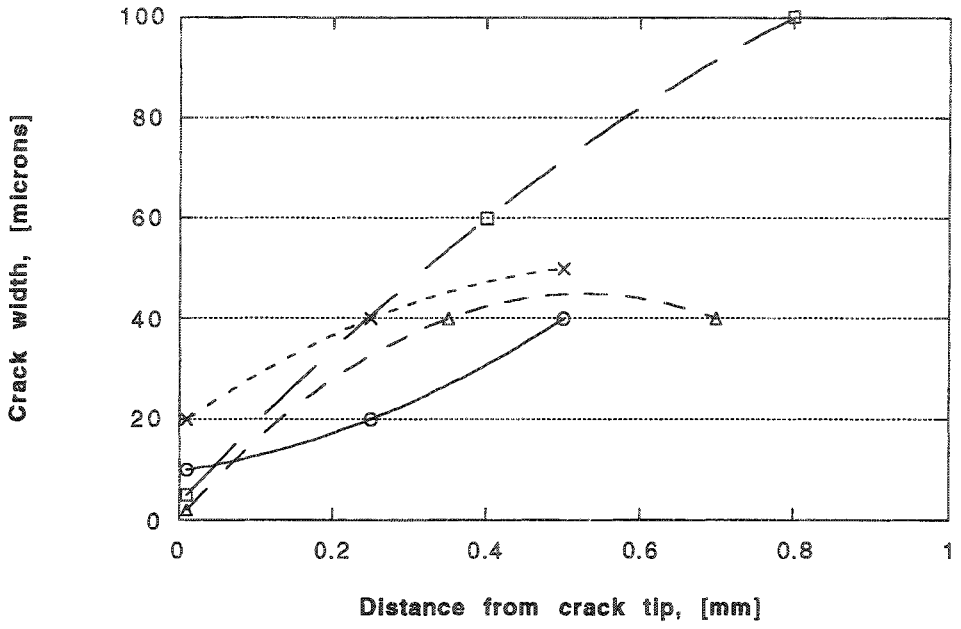

Fig. 14, Crack width at three locations for each crack versus distance from crack tip. Four thermal fatigue cracks with crack depth 0.5-0.8 mm, wall thickness 3-4 mm and crack depth/wall thickness ratio 12-24%.

4.6.2.2 Austenitic stainless steel

The crack width was evaluated for 20 thermal fatigue cracks in austenitic stainless steel. One crack is located in weld material, cladding, and the remaining 19 in base material. The range in crack depth, wall thickness and crack/wall thickness ratio is 1.2 - 19.4 mm, 5 - 40 mm and 3.25 - 100 %, respectively. The results are shown in Fig. 15 - 17. The crack in weld material show a similar crack width behaviour compared to the cracks in base material, see Figure 16.

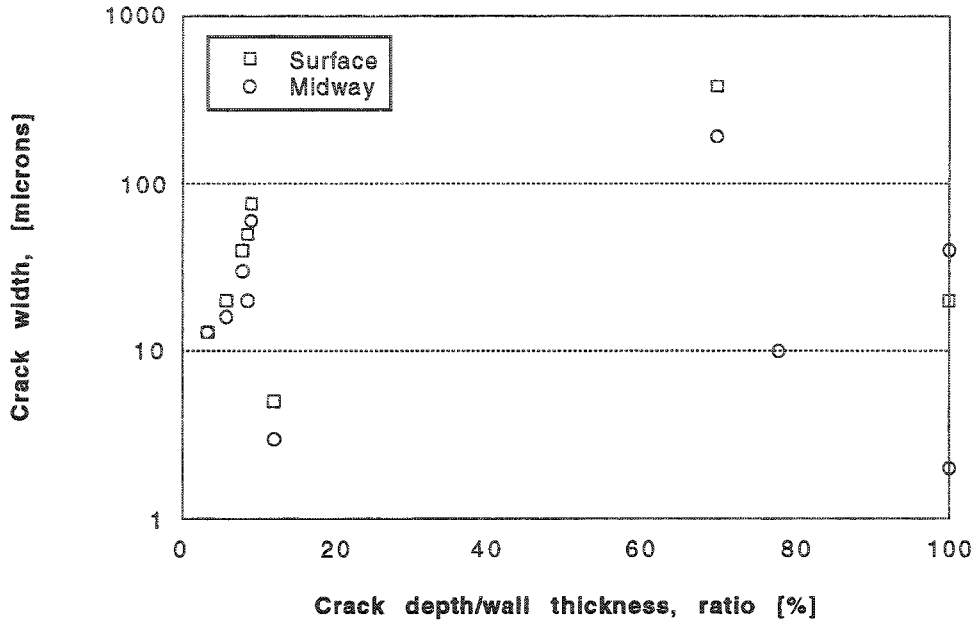

Fig. 15, Crack width at surface and midway for ten thermal fatigue cracks in austenitic stainless steel versus crack depth/wall thickness ratio.

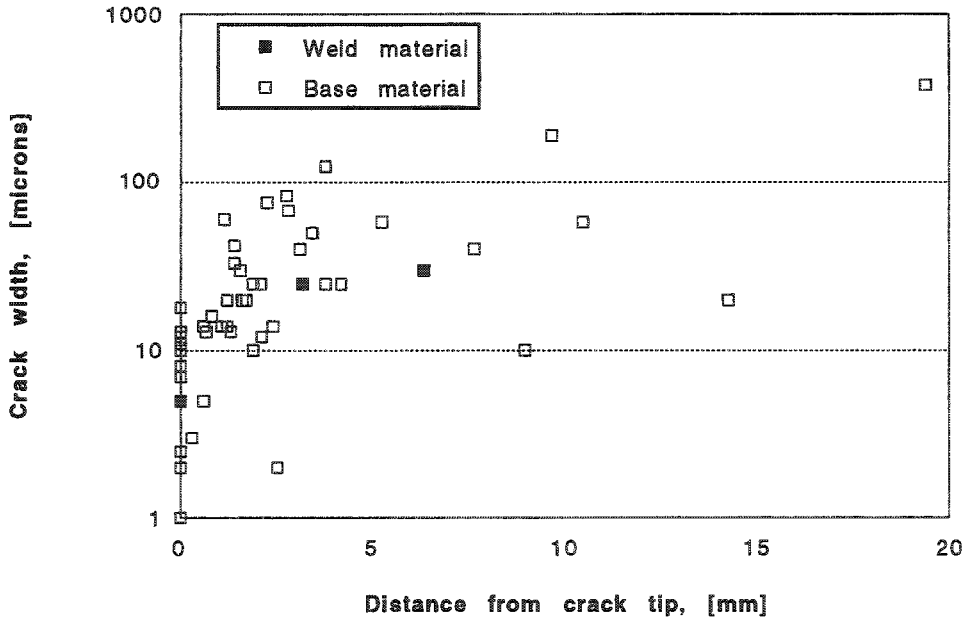

Fig. 16, Crack width at three locations for each crack versus distance from crack tip for 20 thermal fatigue cracks in austenitic stainless steel.

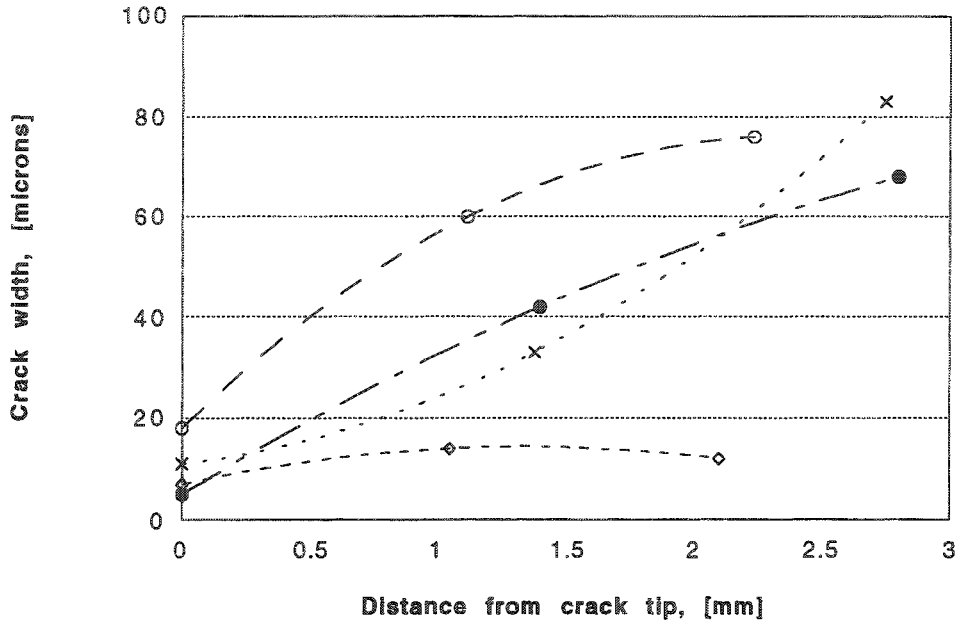

Fig. 17, Crack width at three locations for four thermal fatigue cracks in austenitic stainless steel. Crack depths were in the range 2-3 mm.

4.6.3 Corrosion fatigue

4.6.3.1 Ferritic low alloy steel

In all, 20 corrosion fatigue cracks in ferritic low alloy steel were evaluated. The range in crack depth, wall thickness and crack depth/wall thickness ratio was 0.7 - 15 mm, 4 - 160 mm and 1 - 100%, respectively. The results are presented in Fig. 18 and 19. The number of evaluated cracks is larger compared to the previous two fatigue mechanisms, but the scatter in crack width data is considerably higher. The reason is excessive corrosion inside the cracks, which increase the width. In general the crack widths are larger compared to mechanical and thermal fatigue.

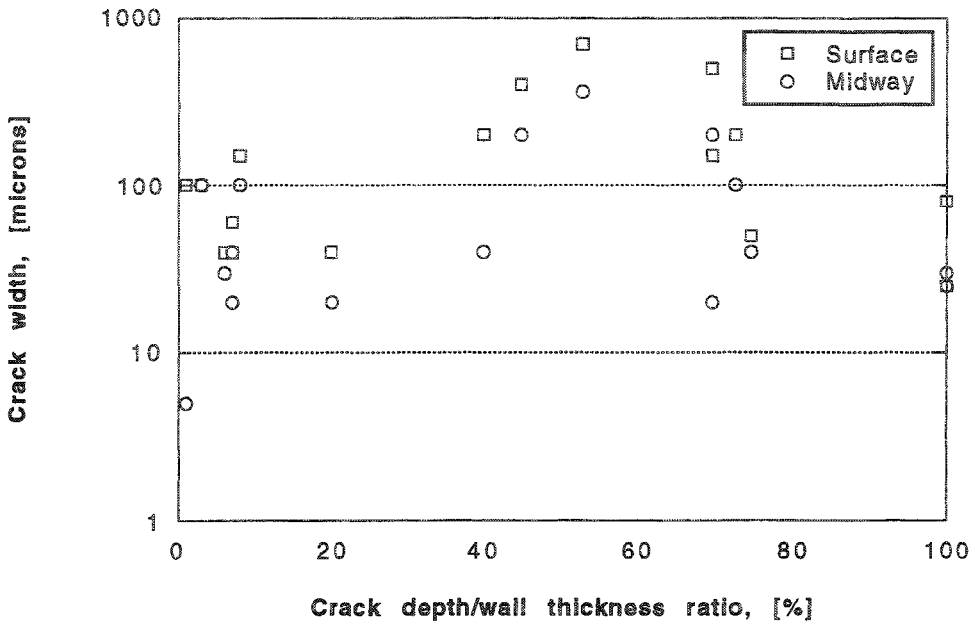

Fig. 18, Crack width at surface and midway for 17 corrosion fatigue cracks versus crack depth/wall thickness ratio.

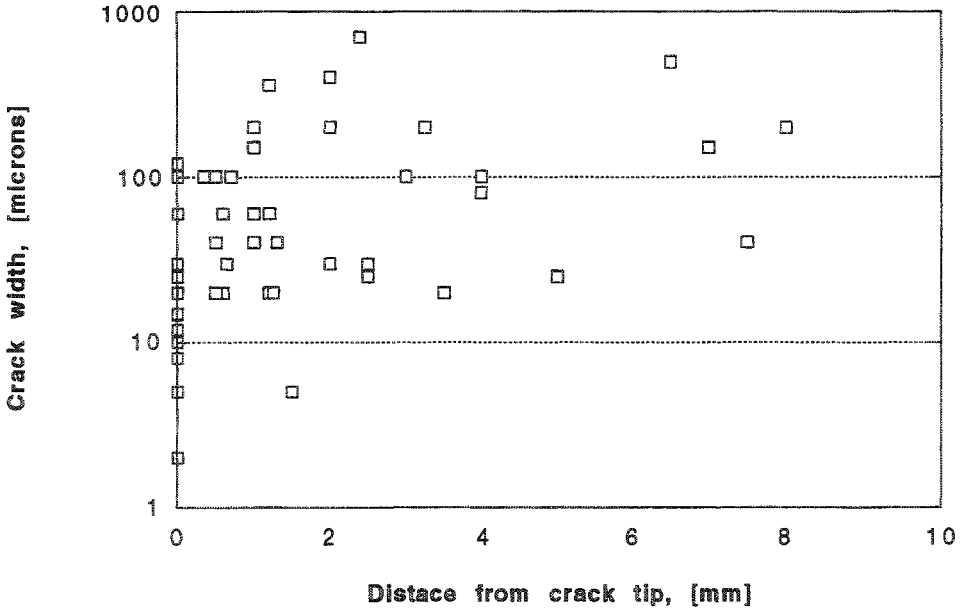

Fig. 19, Crack width at three locations for each crack versus distance from crack tip.

4.6.3.2 Austenitic stainless steel

Only one crack was evaluated, the result is shown in Fig. 20. The crack depth is 2.85 mm and the crack depth/wall thickness ratio is 16.3 %.

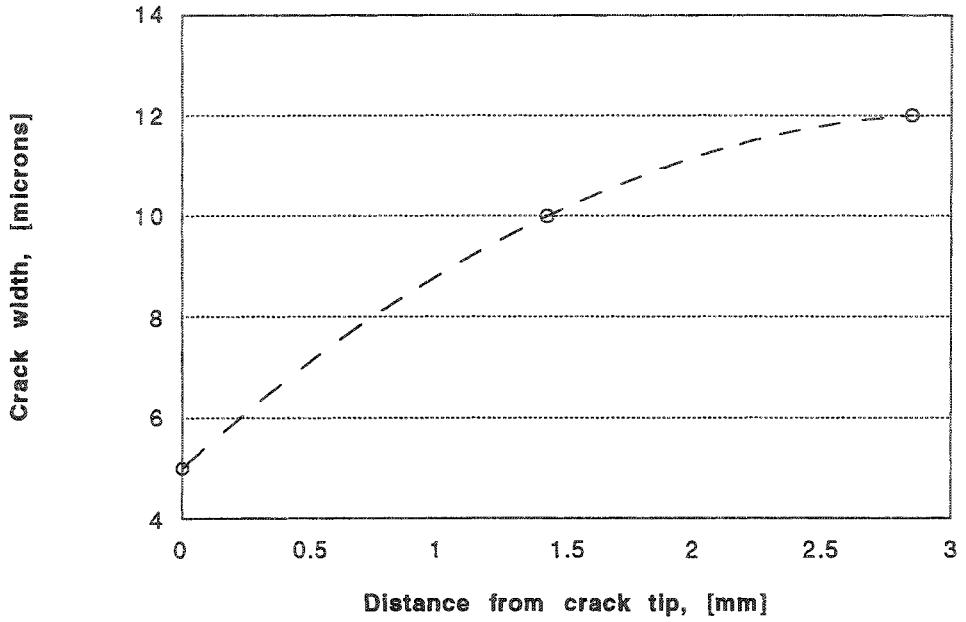

Fig. 20, Crack width at three locations for one corrosion fatigue crack in austenitic stainless steel versus distance from crack tip.

4.6.4 IGSCC

4.6.4.1 Ferritic low alloy steel

13 cracks of IGSCC in ferritic low alloy steel were evaluated. The range in crack depth, wall thickness and crack depth/wall thickness ratio is 1.0 - 23 mm, 5 - 29 mm and 20 - 96%, respectively. The results are presented in Fig. 21-23. In Fig. 21 the crack width at surface and midway are plotted versus the crack depth/wall thickness ratio. In Fig. 22 the crack width is plotted versus distance from crack tip. Three crack width data points from each crack is included in the graph. The crack width increase with increasing depth/wall thickness ratio and with distance from crack tip. The scatter in data is reasonably limited.

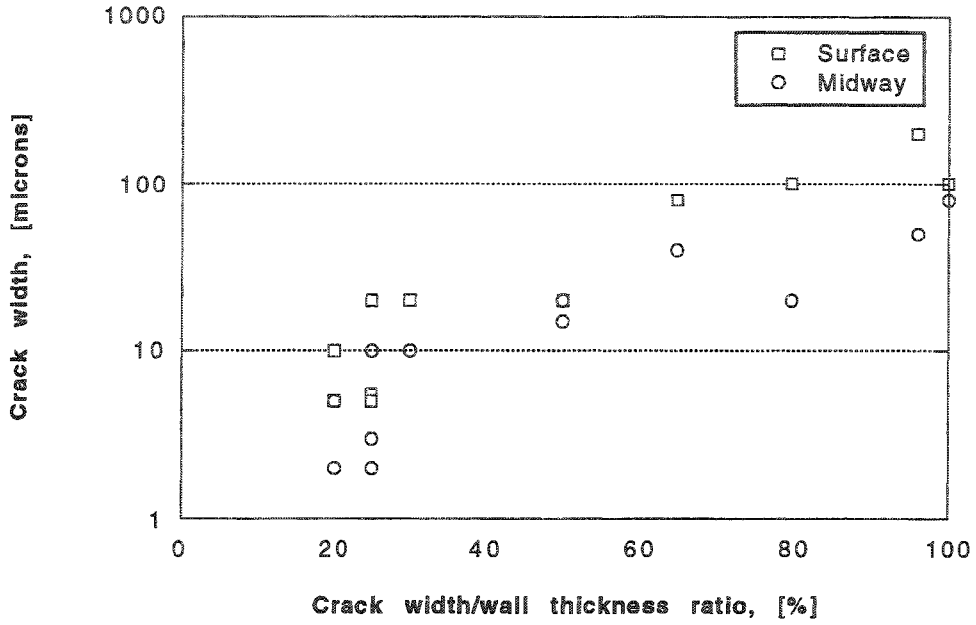

Fig. 21, Crack width at surface and midway for 13 IGSCC versus crack depth/wall thickness ratio.

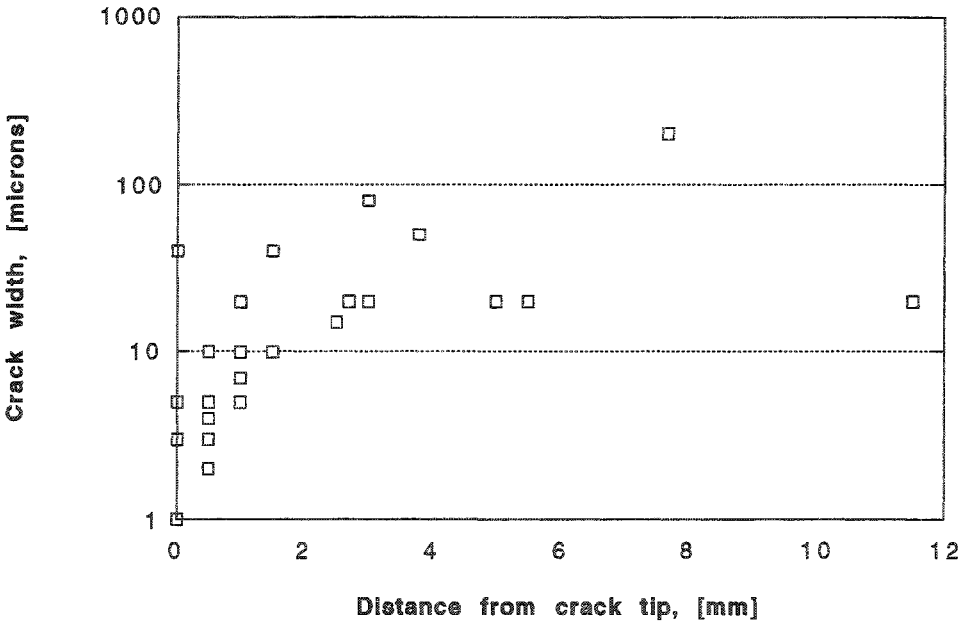

Fig. 22, Crack width at three locations for each crack versus distance from crack tip.

In Fig. 23, ten of the 13 cracks are selected. The selection is made to limit the range in crack depth, wall thickness and crack depth/wall thickness ratio. Three crack width data points are plotted versus distance from crack tip for each crack. A curve fit is made for each set of data to give a rough view of the width versus depth relation. Although, the crack depth range is 1-5 mm, 8 cracks show similar width/depth relations. Two are strongly deviating.

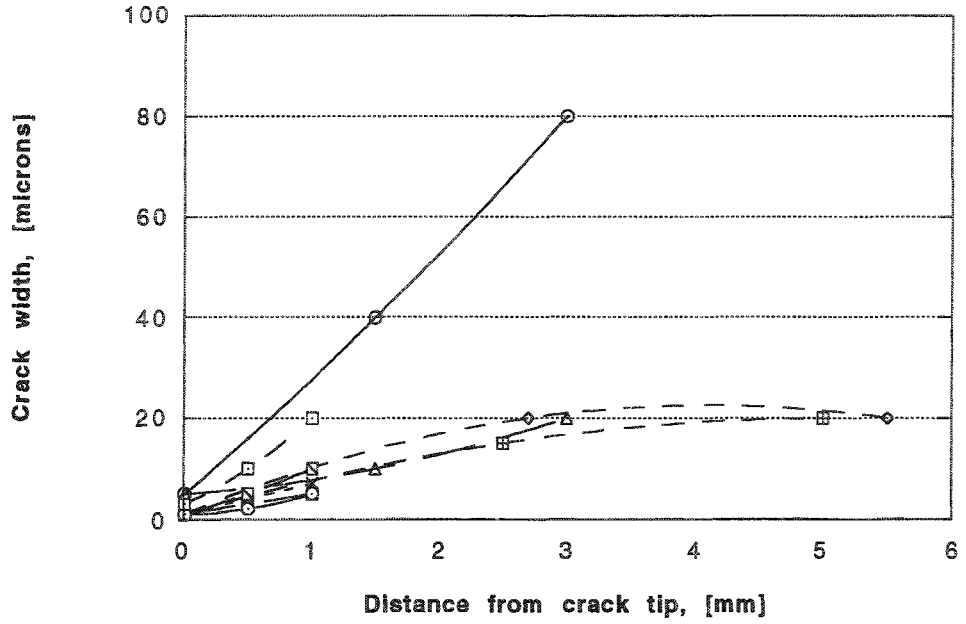

Fig. 23, Crack width at three locations for each crack versus distance from crack tip. Ten cracks of IGSCC with depths 1-5 mm, wall thickness 5-11 mm and crack depth/wall thickness ratio 20-65% were included in the graph.

4.6.4.2 Stainless steel

37 IGSCC cracks in stainless steel were evaluated. Four cracks are from the non-nuclear industry. 35 cracks are from austenitic stainless steel and one crack each from ferritic stainless steel and precipitation hardening austenitic stainless steel. The range in crack depth, wall thickness and crack/wall thickness ratio is 0.3-17 mm, 0.7-40 mm and 2.5-100%, respectively. The results are presented in Fig. 24-26.

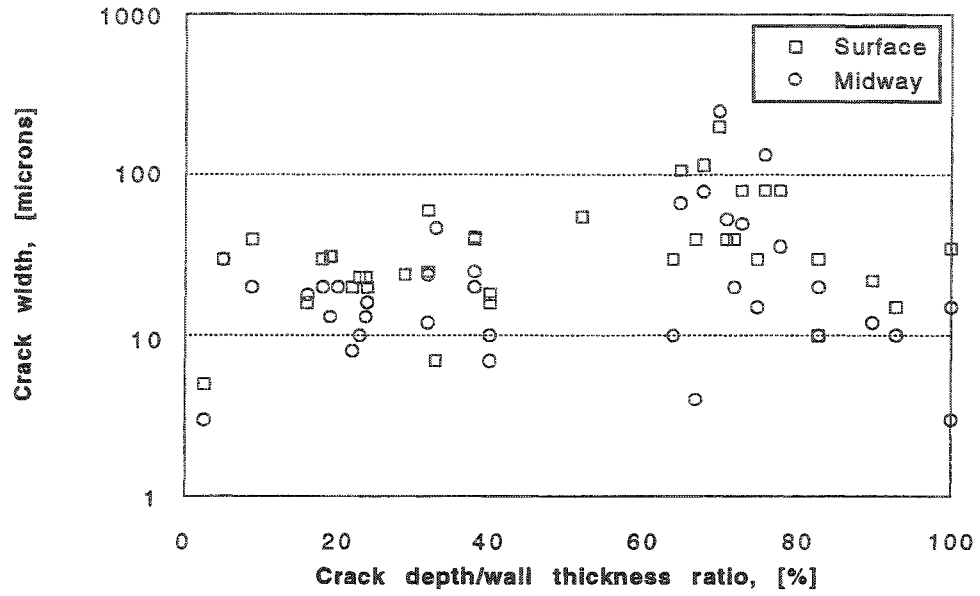

Fig. 24, Crack width at surface and midway for 37 IGSCC versus crack depth/wall thickness ratio.

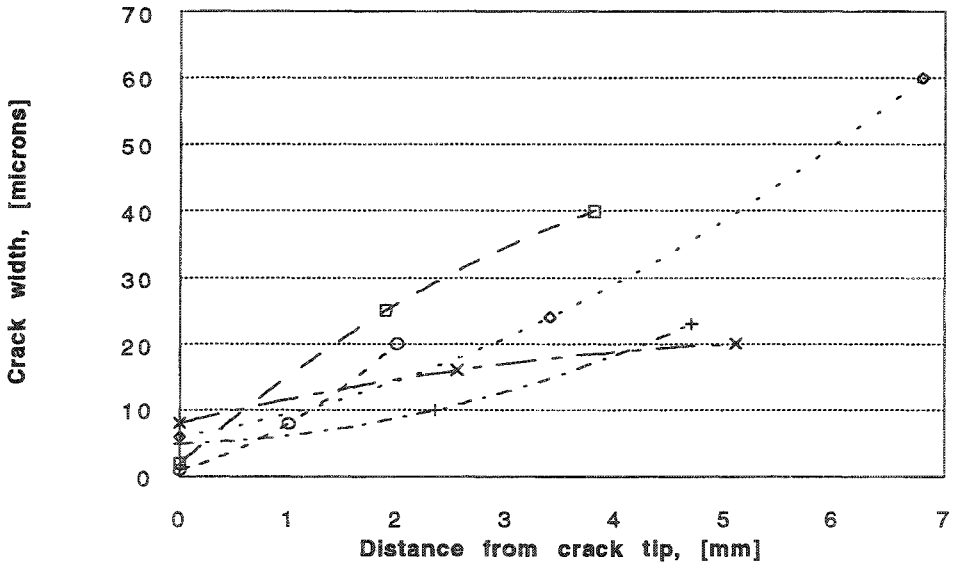

Fig. 25, Crack width at three locations for each crack versus distance from crack tip. Five typical IGSCC cracks in austenitic stainless steel.

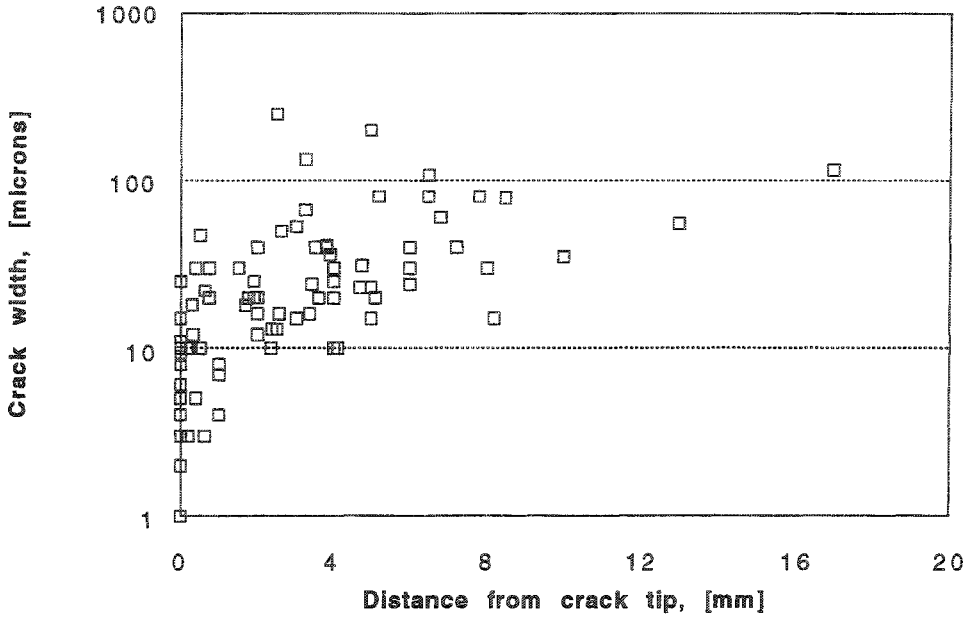

Fig. 26, Crack width at three locations for each crack versus distance from crack tip.

4.6.4.3 Nickel base alloys

Twelve cracks were evaluated. The range in crack depth, wall thickness and crack depth/wall thickness ratio is 0.3 - 8.56, 1 - 8.56 and 50 - 100 %, respectively. The results are shown in Fig. 27 through 29.

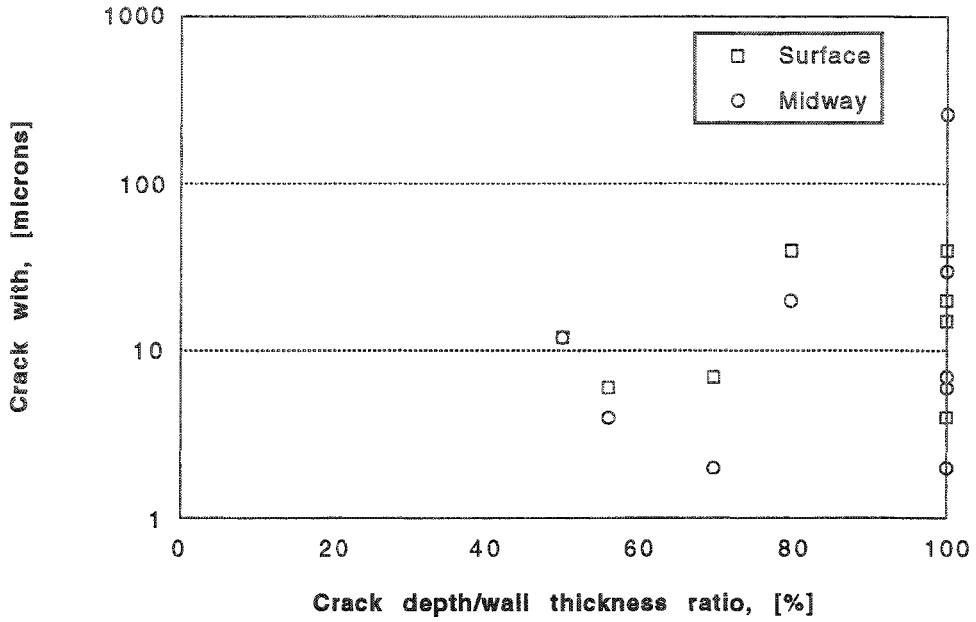

Fig. 27, Crack width at surface and midway for nine IGSCC cracks in Nickel base alloys versus crack depth/wall thickness ratio.

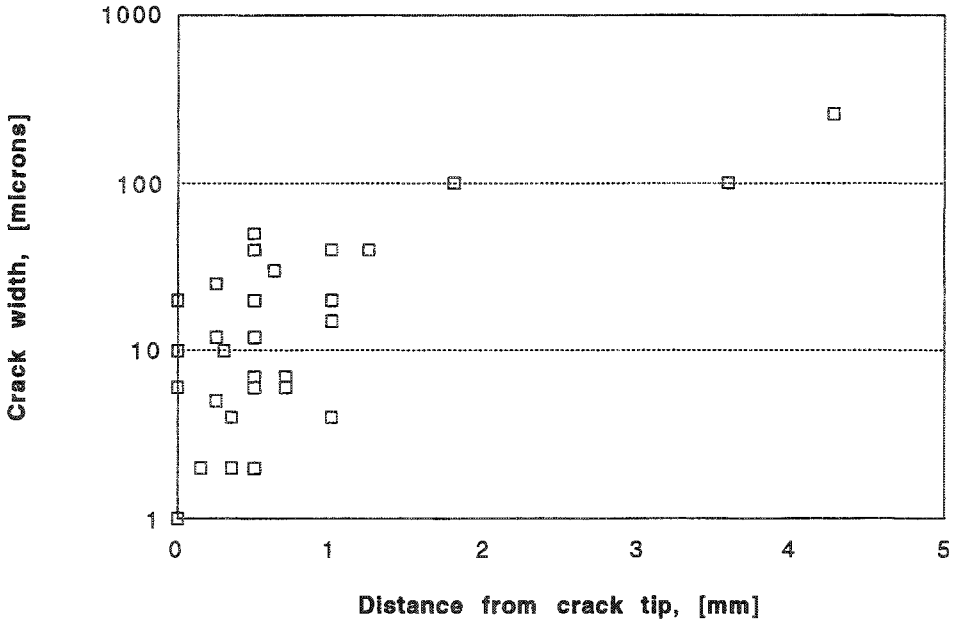

Fig. 28, Crack width at three locations for each crack versus distance from crack tip.

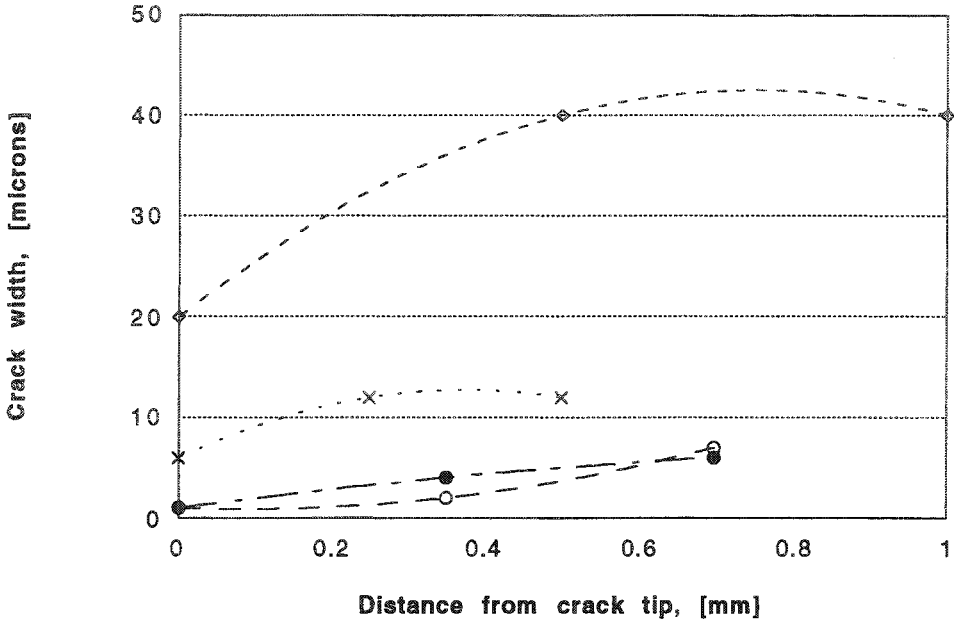

Fig. 29, Crack width at three locations for each crack versus distance from crack tip. Four typical IGSCC cracks in Nickel base alloys.

4.6.5 TGSCC

4.6.5.1 Ferritic low alloy steel

In all, four TGSCC in ferritic low alloy steel were evaluated. The range in crack depth, wall thickness and crack depth/wall thickness ratio is 1-2.5 mm, 5-16 mm and 7-50%, respectively. The results are shown in Fig. 30-32. Compared to IGSCC, TGSCC generally produce wider cracks in ferritic low alloy steels. In spite of the fairly homogenous data set, the four cracks show a large scatter in the width/depth relation, see Fig. 32.

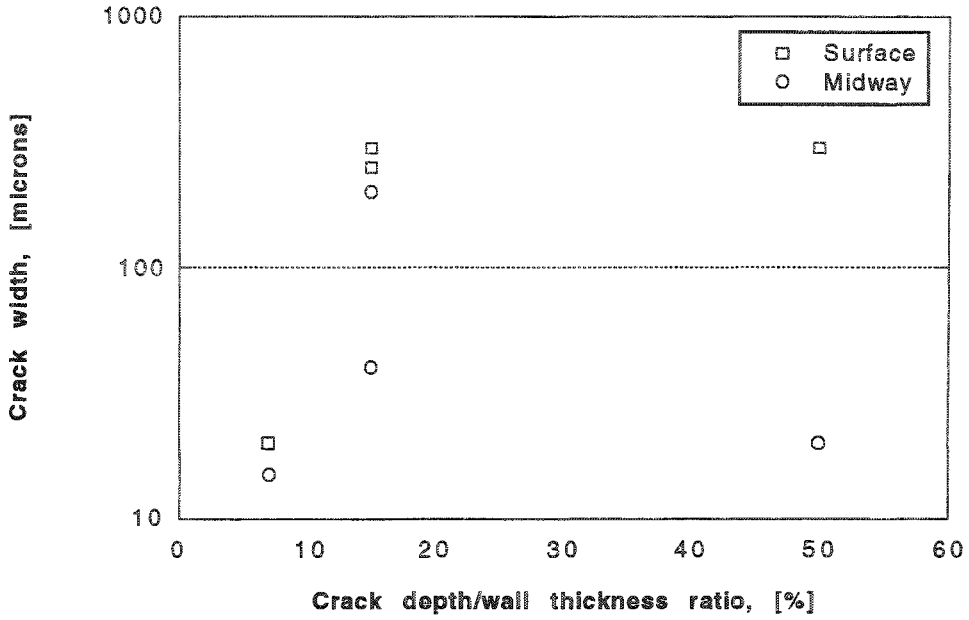

Fig. 30, Crack width at surface and midway for 4 TGSCC cracks versus crack depth/wall thickness ratio.

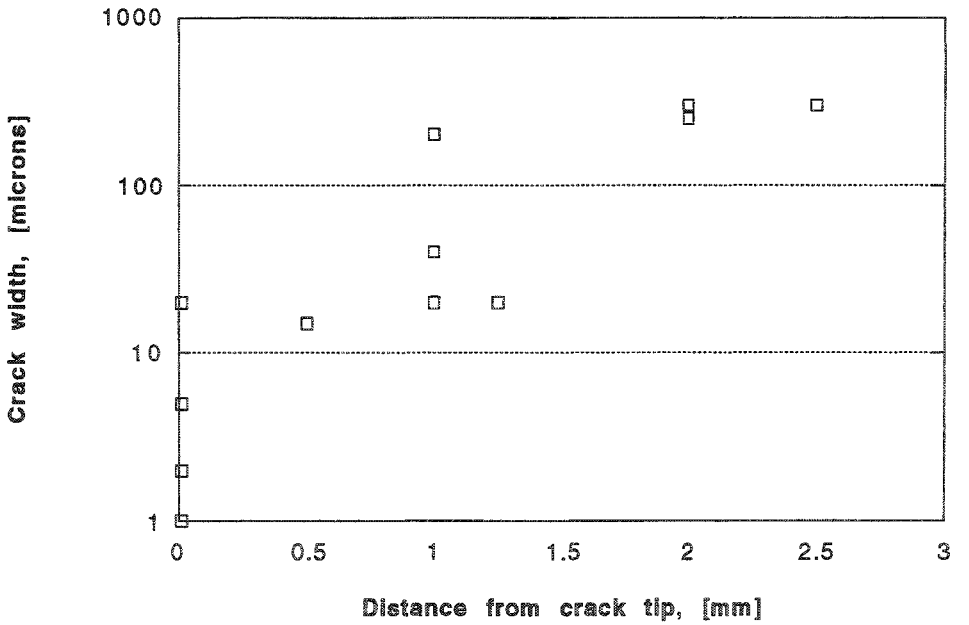

Fig. 31, Crack width at three locations for each crack versus distance from crack tip.

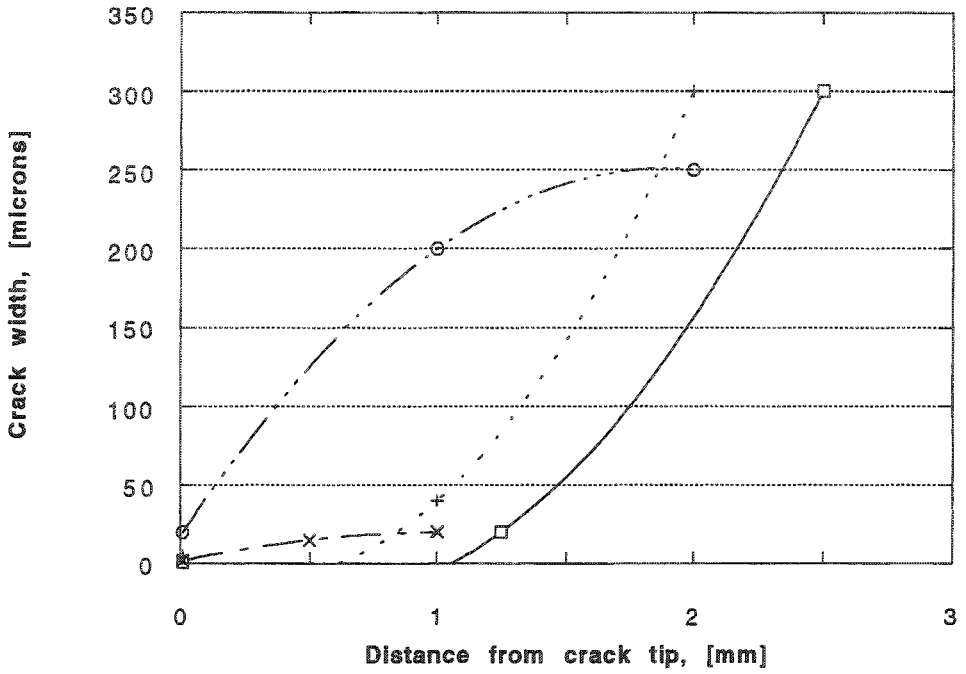

Fig. 32, Crack width at three locations for each crack versus distance from crack tip. Four TGSCC cracks with depths 1-2.5 mm, wall thickness 5-16 mm and crack depth/wall thickness ratio 7-50%.

4.6.5.2 Austenitic stainless steel

The number of evaluated TGSCC cracks in austenitic stainless steel was 26. The range in crack depth, wall thickness and crack depth/wall thickness ratio is 0.5-20 mm, 1-8 mm and 8-100%, respectively. The results are shown in Fig. 33 and 34.

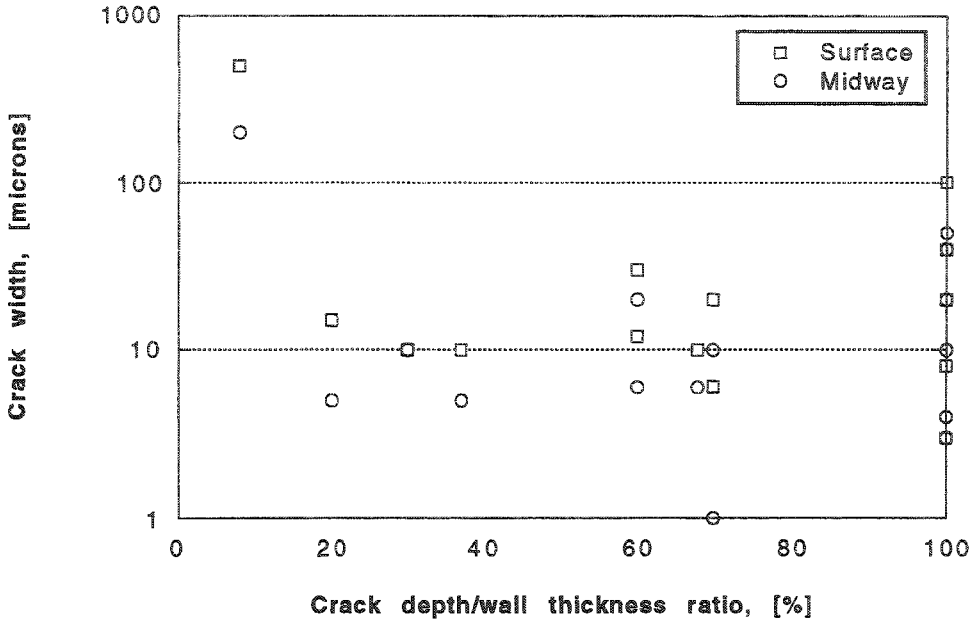

Fig. 33, Crack width at surface and midway for 14 TGSCC cracks versus crack depth/wall thickness ratio.

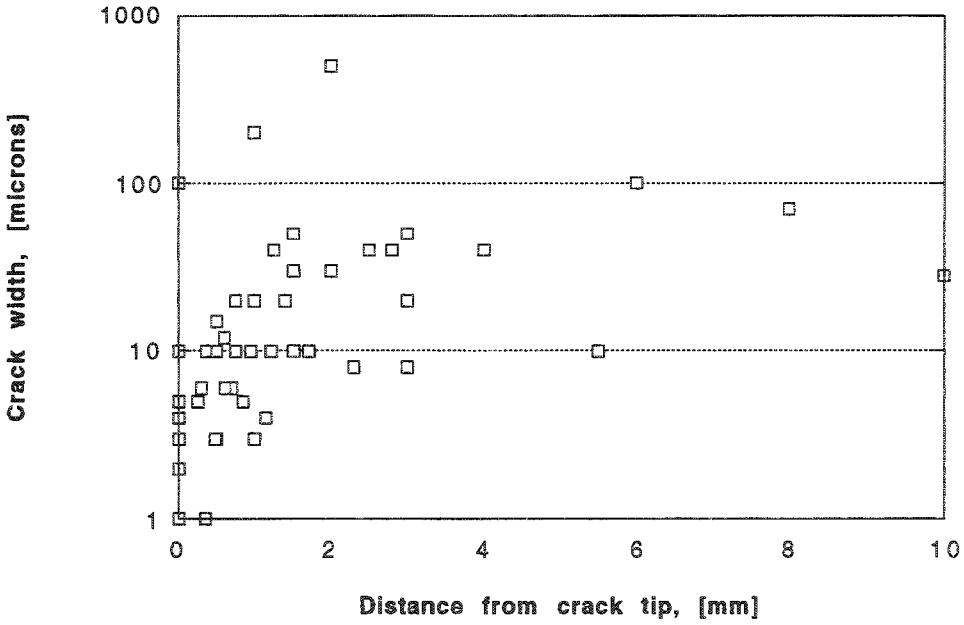

Fig. 34, Crack width at three locations for each crack versus distance from crack tip.

4.6.5.3 Nickel base alloys

Only three cracks were evaluated. As there were a large scatter in the crack widths no further evaluation seemed meaningful.

4.6.6 IDSCC

4.6.6.1 Nickel base alloys

Six cracks were evaluated, one is a service induced crack from the nuclear industry and five are laboratory induced cracks. There is no difference in the crack width data between the two groups. Consequently all are evaluated as one group of data. The range in crack depth, wall thickness and crack depth/wall thickness is 0.5 - 3 mm, 3 - 7.62 mm and 16 - 33 %, respectively. The results are shown in Fig. 35 through 37.

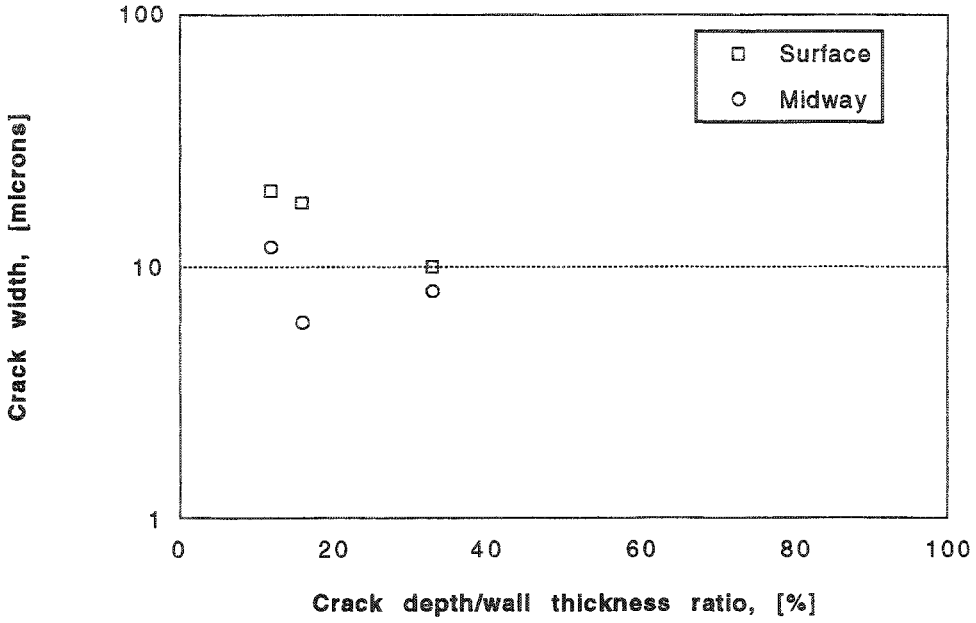

Fig. 35, Crack width at surface and midway for three IDSCC cracks versus crack depth/wall thickness ratio.

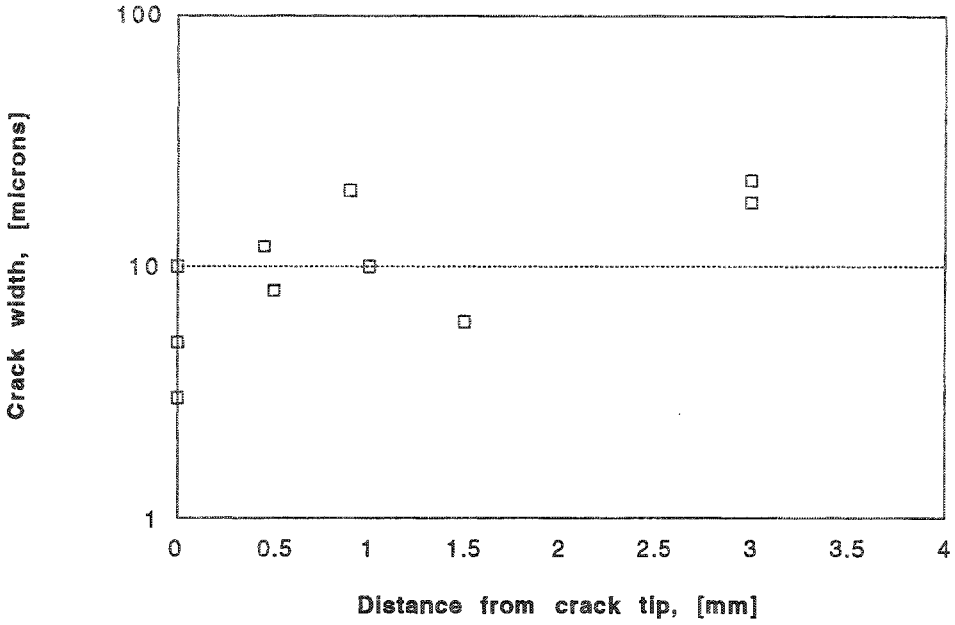

Fig. 36, Crack width at three locations for each crack versus distance from crack tip.

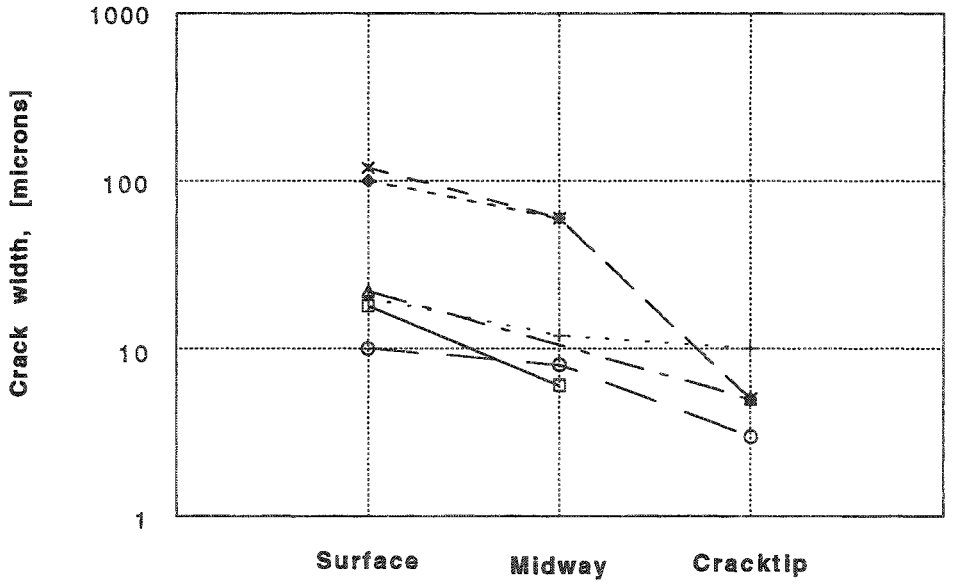

Fig. 37, Crack width at surface, midway and at crack tip for six IDSCC cracks in Alloy 182 and Alloy 82.

4.6.7 Weld flaws

Eleven out of 13 evaluated weld flaws are typically narrow showing crack widths at the surface between 10 and 40 μm. One exception is a hot crack, which is 250 μm wide at the surface. However, the evaluated weld flaws of each type were too few for any meaningful compilations or reliable conclusions.

4.6.8 Comparison of crack width data

4.6.8.1 Statistics on crack width of fatigue cracking

A comparison of fatigue crack width data in ferritic low alloy steels were made and the results are shown in Table 4 and in Fig. 38, which show median values, solid line, 25% and 75% limits, lower and upper dashed lines, and total scatter, the solid line box. Although, similar mean and median crack widths are shown for all data, the scatter in corrosion fatigue data is considerable compared to the other two mechanisms. A similar comparison is made for mechanical and thermal fatigue cracks in stainless steels, see Table 5 and Fig. 39. The two data groups show similar crack widths.

Fig. 40 demonstrates a comparison of the crack width versus crack depth/wall thickness for the three fatigue mechanisms in ferritic low alloy steels. In Fig. 41 the crack width along the crack versus distance to the crack tip is shown. In both plots the mechanical and thermal fatigue data are close and reasonably well gathered, while corrosion fatigue data is severely scattered. A similar comparison is made for stainless steels in Fig. 42 and 43.

	Crack width at surface [μm]			Crack width inside the crack [μm]					
	mechanical fatigue	thermal fatigue	corrosion fatigue	mechanical fatigue		thermal fatigue		corrosion fatigue	
				mid-way	crack tip	mid-way	crack tip	mid-way	crack tip
Number of observations	6	6	20	7	7	6	6	20	20
minimum	5	25	20	3	1	20	2	5	2
maximum	160	250	700	100	20	100	25	360	120
mean value	63.7	84.2	149	37.1	8.1	60	12	72.5	26.3
median	56	45	70	20	10	50	10	35	15
RMS	87.4	114	231	51.5	10.2	67.3	14.5	112	41.1
standard deviation	65.5	85.2	181	38.6	6.6	33.5	8.8	88.2	32.4

Table 4, Crack width statistics of fatigue cracks in ferritic low alloy steels.

	Crack width at surface [μm]			Crack width inside the crack [μm]					
	mechanical fatigue	thermal fatigue	corrosion fatigue	mechanical fatigue		thermal fatigue		corrosion fatigue	
				mid-way	crack tip	mid-way	crack tip	mid-way	crack tip
Number of observations	6	18	1	6	6	20	20	1	1
minimum	3	5	-	3	0.5	2	1	-	
maximum	250	380	-	250	30	190	18	-	
mean value	55.5	59.1	12	50	9.33	32.2	7.9	10	5
median	17.5	27.5	-	12	7.5	22.5	9	-	-
RMS	103.9	102.4	-	103	13.7	51	9	-	-
standard deviation	96.2	86.0	-	98.2	11	40.5	4.4	-	-

Table 5, Crack width statistics of fatigue cracks in stainless steels.

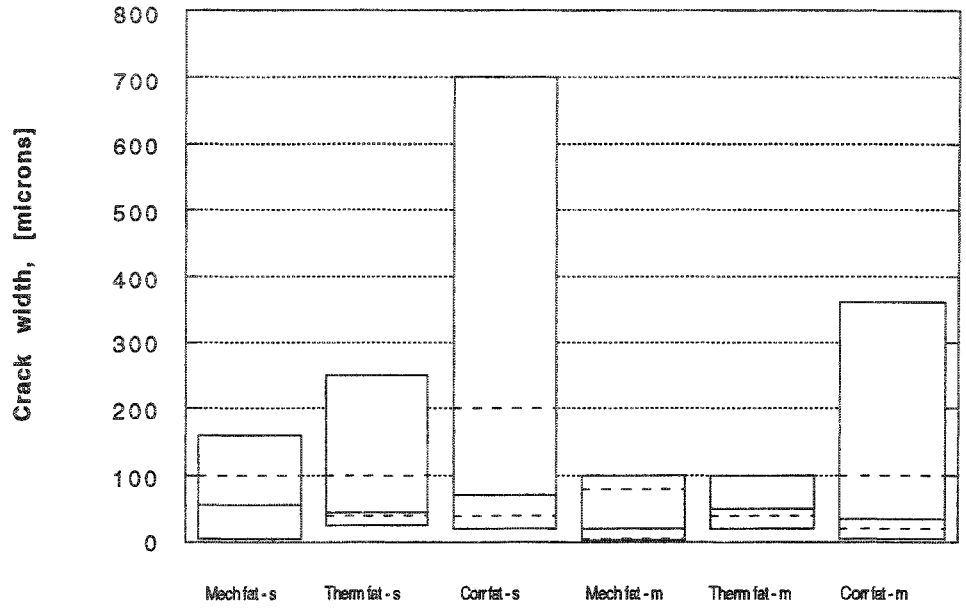

Fig. 38, Range of crack widths at surface (s) and midway (m) locations of fatigue cracks in ferritic low alloy steels.

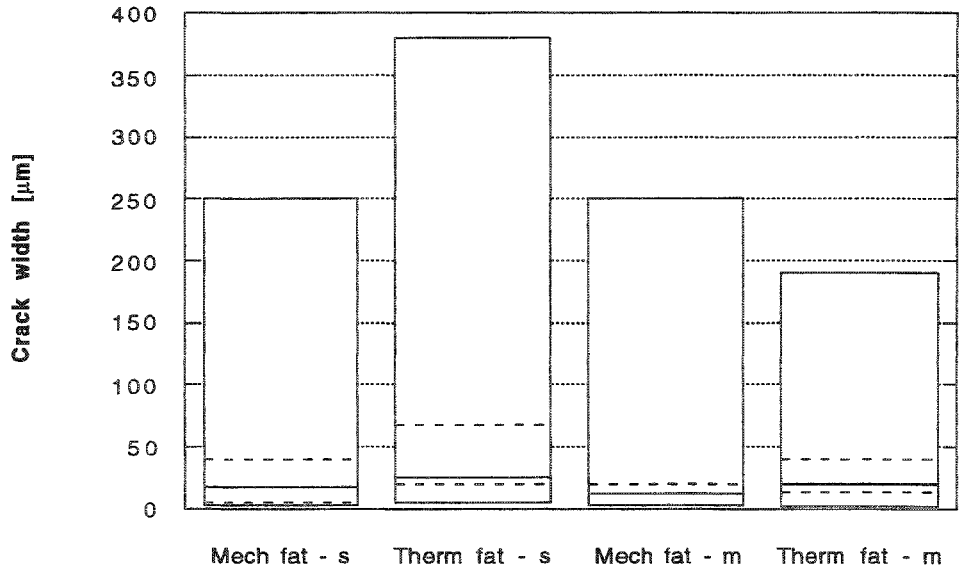

Fig. 39, Range of crack widths at surface (s) and midway (m) locations of fatigue cracks in stainless steel.

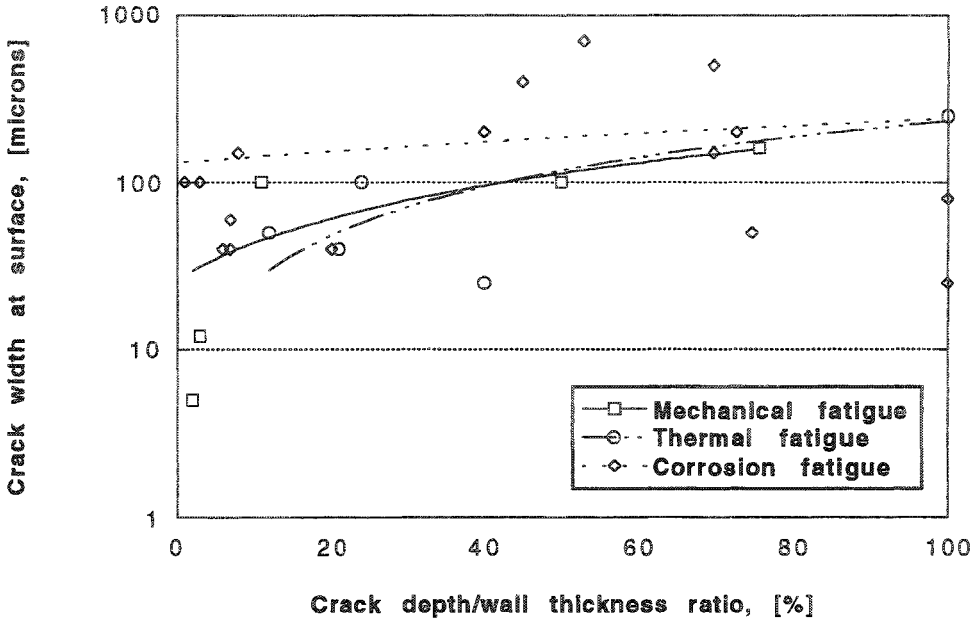

Fig. 40, Crack width at surface for fatigue cracks in ferritic low alloy steel versus crack depth/wall thickness ratio.

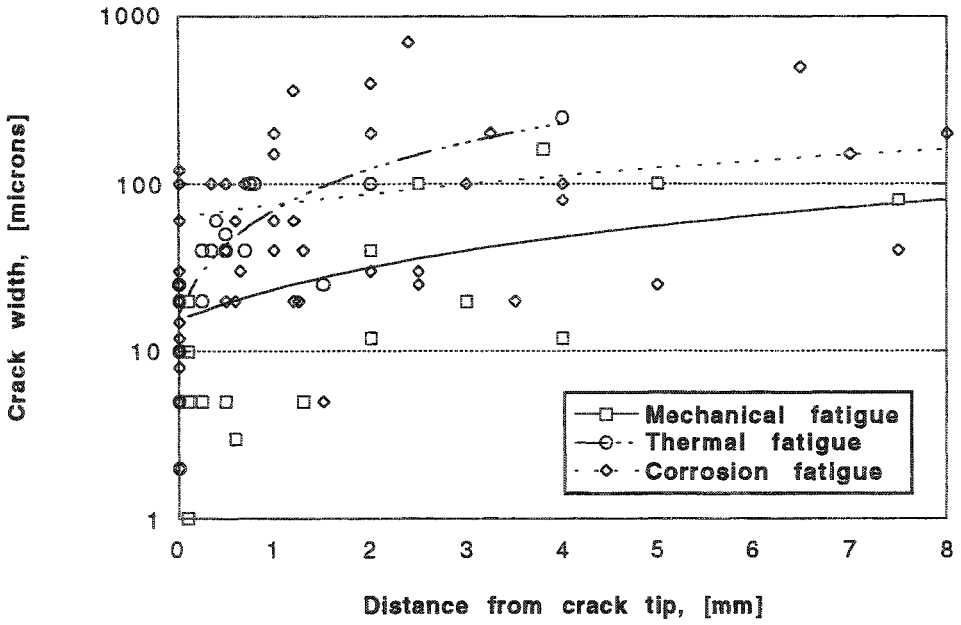

Fig. 41, Crack width at three locations for each crack versus distance from crack tip, ferritic low alloy steel.

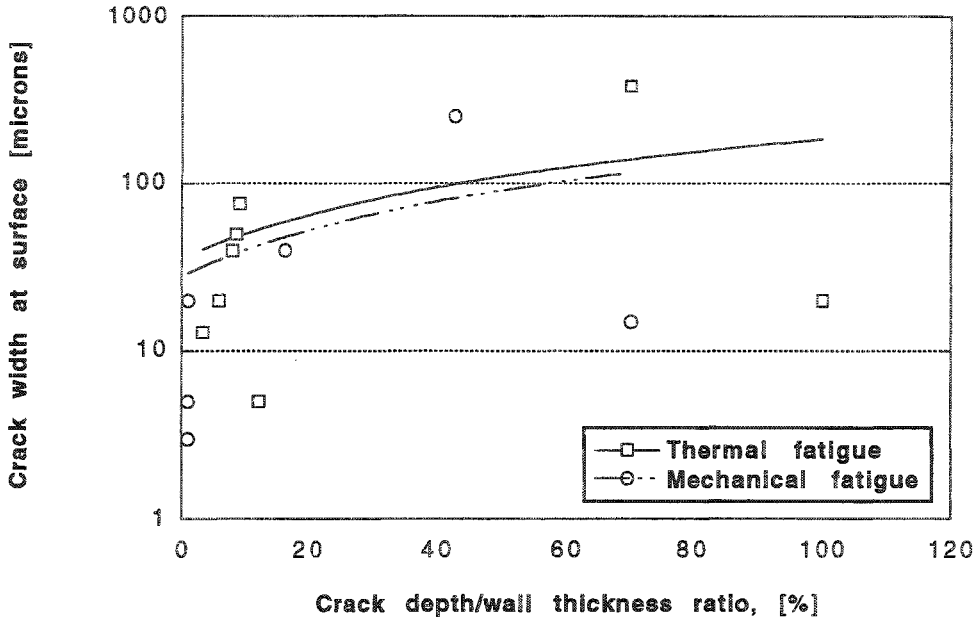

Fig. 42, Crack width at surface for fatigue cracks in stainless steel versus crack depth/wall thickness ratio.

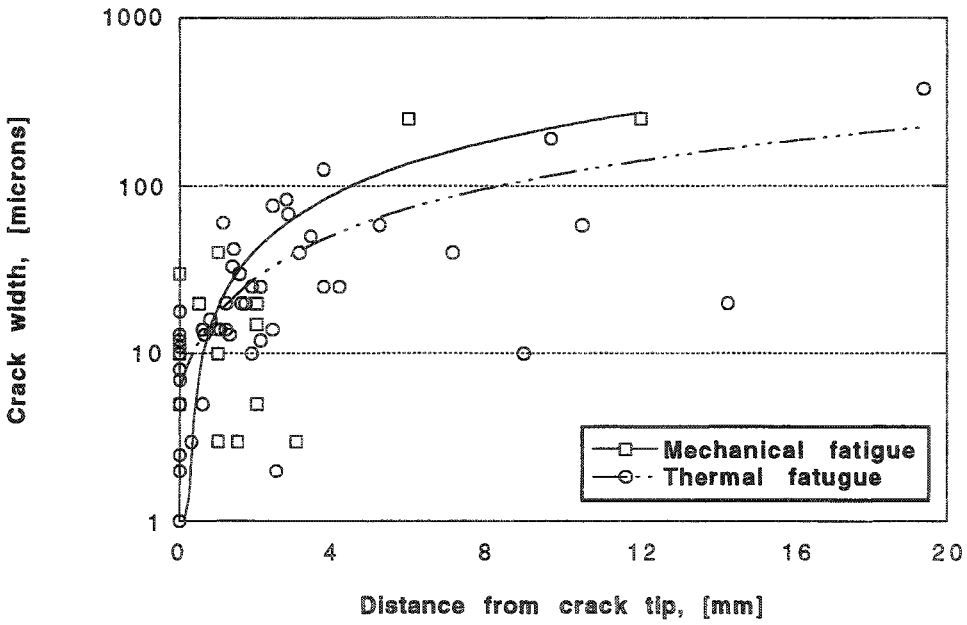

Fig. 43, Crack width at three locations for each crack versus distance from crack tip, stainless steel.

4.6.8.2 Statistics on crack width of SCC

Statistics on crack width of IGSCC and TGSCC cracks are shown in Tables 6 - 8. The range in data and median values for both data groups are displayed in Fig. 44. A comparison of IGSCC crack widths in the three material groups show no significant differences. However, there is a tendency that the widest cracks appears in stainless steel and the most narrow in nickel base alloys. The number of TGSCC cracks in ferritic low alloy steel and nickel base alloys are too few for an evaluation or comparison. TGSCC in stainless steels show similar crack widths compared to IGSCC.

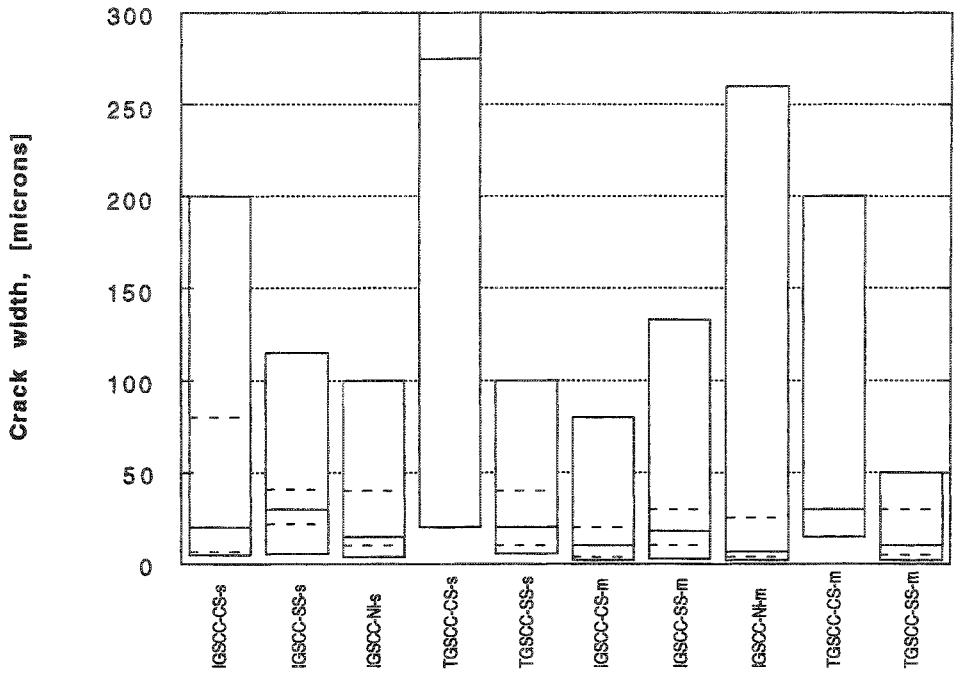

Fig. 44, Range of crack widths at surface (s) and midway (m) of stress corrosion cracks

	Crack width at surface [μm]		Crack width inside the crack [μm]			
	IGSCC low alloy	IGSCC austenitic	IGSCC low alloy		IGSCC austenitic	
			mid-way	crack tip	mid-way	crack tip
Number of observations	13	33	13	12	33	32
minimum	5	5	2	1	3	1
maximum	200	200	80	40	250	25
mean value	45.5	43.2	20.1	5.3	32.3	5.4
median	20	30	10	1	18	3
RMS	72.4	57.8	30.1	11.8	56.7	7.8
standard deviation	58.6	39.0	23.4	11.0	47.2	5.8

Table 6, Crack width statistics of IGSCC for low alloy steel and austenitic stainless steel.

	Crack width at surface [μm]		Crack width inside the crack [μm]			
	IDSCC nickel base	IGSCC nickel base	IDSCC nickel base		IGSCC nickel base	
			mid-way	crack tip	mid-way	crack tip
Number of observations	6	15	6	5	17	14
minimum	10	4	6	3	2	1
maximum	120	100	60	10	260	20
mean value	48.33	24.1	27.7	5.6	30.5	4.1
median	21	15	16	5	7	1
RMS	65.5	34.2	36.2	6.1	69.1	6.8
standard deviation	48.4	25.2	25.5	2.6	63.9	5.7

Table 7, Crack width statistics of IDSCC and IGSCC for nickel base alloy.

	Crack width at surface [μm]			Crack width inside the crack [μm]					
	TGSCC low alloy	TGSCC austenitic	TGSCC nickel base	TGSCC low alloy		TGSCC austenitic		TGSCC nickel base	
				mid-way	crack tip	mid-way	crack tip	mid-way	crack tip
Number of observations	4	21	-	4	4	25	20	-	-
minimum	20	3	-	15	1	1	1	-	-
maximum	300	500	-	200	20	200	100	-	-
mean value	217	49.1	-	68.8	7	24.3	8.6	-	-
median	275	20	-	30	3.5	10	3.5	-	-
RMS	246	115	-	103	10.4	46.0	22.8	-	-
standard deviation	134	106	-	88.2	8.8	39.9	21.7	-	-

Table 8, Crack width statistics of TGSCC

4.6.9 Literature data on crack width

In a work by MacDonald [3] results from crack width measurements of 169 IGSCC cracks in BWR piping are presented. The crack width was measured at the inner surface of the pipe by means of a low power binocular microscope. The crack depth was measured by ultrasonic testing or by destructive testing, i.e. metallografic examination. Statistics from the crack width measurements and plots on crack width versus crack depth/wall thickness ratio are shown in Table 9 and Fig. 45 and 46, respectively.

Results from crack width measurements are shown by Lapides in two reports [2, 4]. The crack width and depth data were derived from metallographic examinations of IGSCC in pipes removed from service. The crack width was measured both at the surface and at various locations along the crack. Lapides claims there is no correlation between crack width, crack depth and pipe dimensions. For a given crack depth, the width is assumed to be controlled by bending moments, applied loads and service age. Thus, he suggest the data to be presented as a lower bound value and as an interval.

Lapides also states that fatigue cracking, from light water reactor service, resembles parallel-sided slots, except for the sharp tip section. On the contrary, he found that the crack width of IGSCC is an exponential function of crack depth. Crack width data from

reference 2 are re-plotted versus crack depth/wall thickness ratio in Fig. 47. Statistics on crack width data are shown in Table 9 and in Fig. 45.

Crack width data on IGSCC in PWR components of austenitic stainless steel are reported by Stenefjäll in a yet not published document [5]. Statistics of these data are shown in Table 9 and Fig. 45.

By comparing data in the literature, and by comparing them with the results from this work, a reasonably good agreement is established for crack widths of IGSCC in stainless steels, Table 9 and Fig. 45 and 48. The median crack width is between 30 and 45 μm. The results of Lapides give the highest median value and the largest scatter. The results in this work and those of Stenefjäll show the lowest median values and smallest scatter. One conclusion of this comparison is that crack width measurements on metallographic samples, [2], [4], [5] and in this work give an equally good accuracy as measurements made directly on the metal surface [3].

Compilations of crack width data of fatigue cracks were made by Skånberg [6], who in turn refers to results published by Lapides, Doctor and Stenefjäll. A large number of data points on mechanical fatigue cracking in cladded ferritic low alloy steel are reported together with some data points from thermal fatigue in cast austenitic stainless steels and corrosion fatigue in Type 304 stainless steel. All cracks were produced in the laboratory and the specimens used were of equal or almost equal thickness. The crack width measurements were all made at the crack/surface intersection. The crack width data are replotted versus crack depth/wall thickness ratio in Fig. 49, and range/median values are compiled in Fig. 50. Compared with the results of this work the data in [6] show more narrow crack widths for mechanical and thermal fatigue but similar crack widths for corrosion fatigue cracks. This may partly be explained by the fact that all the crack width data of Doctor/Stenefjäll were obtained in laboratory experiments, where both loading and environmental conditions were well controlled. The major part of the cracks evaluated in this work are service induced, hence, less controlled loading conditions and corrosion attack may contribute to increased crack widths.

	Crack width at surface of IGSCC in stainless steels[μm]			
	MacDonald [3]	Lapides [2]	Stenefjäll [5]	This work
Number of observations	169	25	5	26
minimum	5.1	10	19	5
maximum	310	380	54	107
mean value	54.2	73.2	36.6	37.2
median	40.6	45	37	30
RMS	67.8	108	38.3	44.4
standard deviation	40.8	81.6	12.5	24.8

Table 9, Statistics on crack width at surface of IGSCC in austenitic stainless steels. Comparison between results of this work and literature data, [2], [3] and [5].

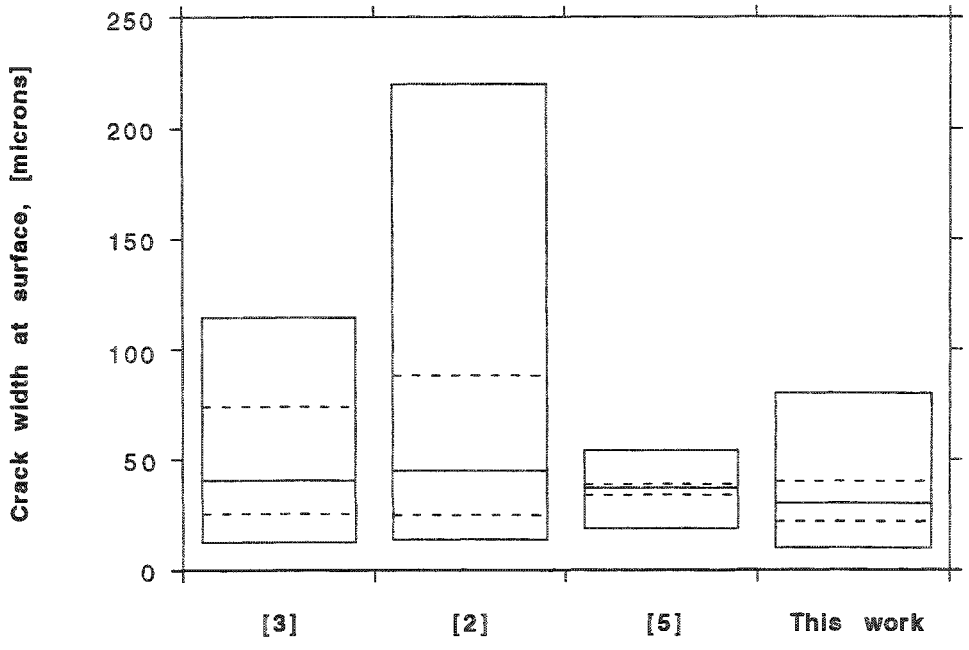

Fig. 45, Range of crack widths at surface of IGSCC cracks in austenitic stainless steels. Comparison between results of this work and literature data, [2], [3] and [5].

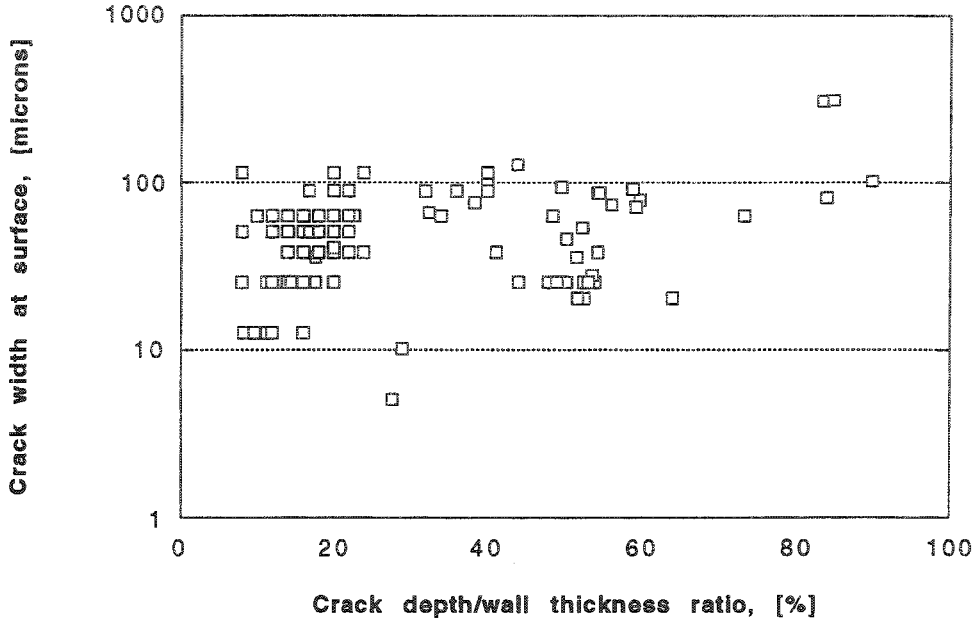

Fig. 46, Crack width at surface for 169 IGSCC cracks versus crack depth/wall thickness ratio [3].

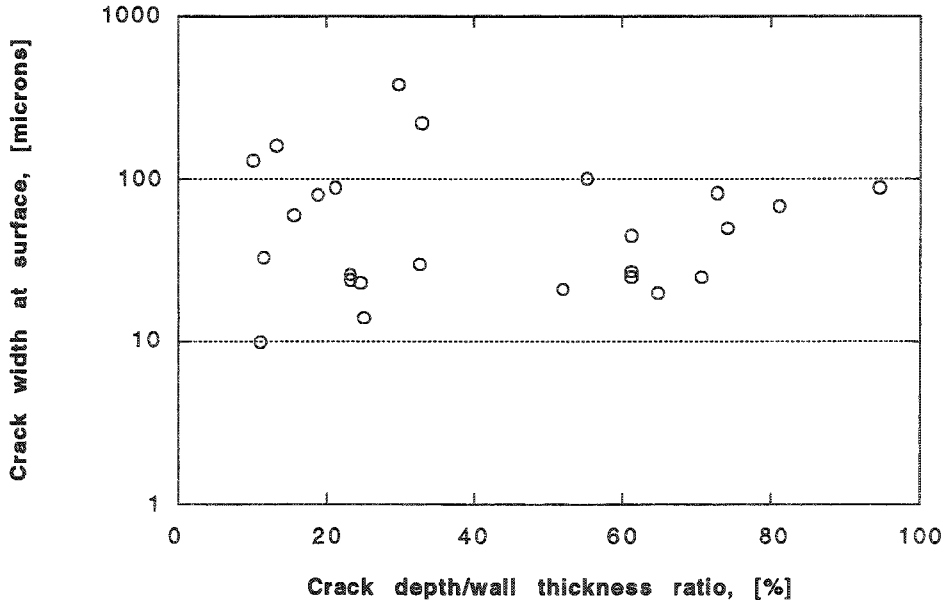

Fig. 47, Crack width at surface for 25 IGSCC cracks versus crack depth/wall thickness ratio [2].

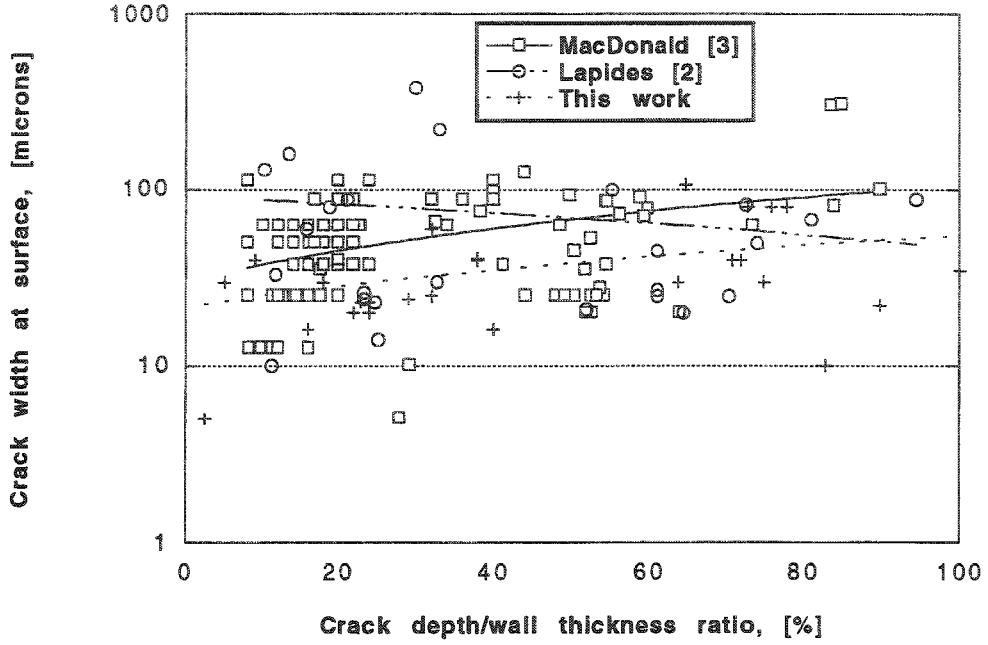

Fig. 48, Crack width at surface for IGSCC versus crack depth/wall thickness ratio. Comparison between [2], [3], and results of this work.

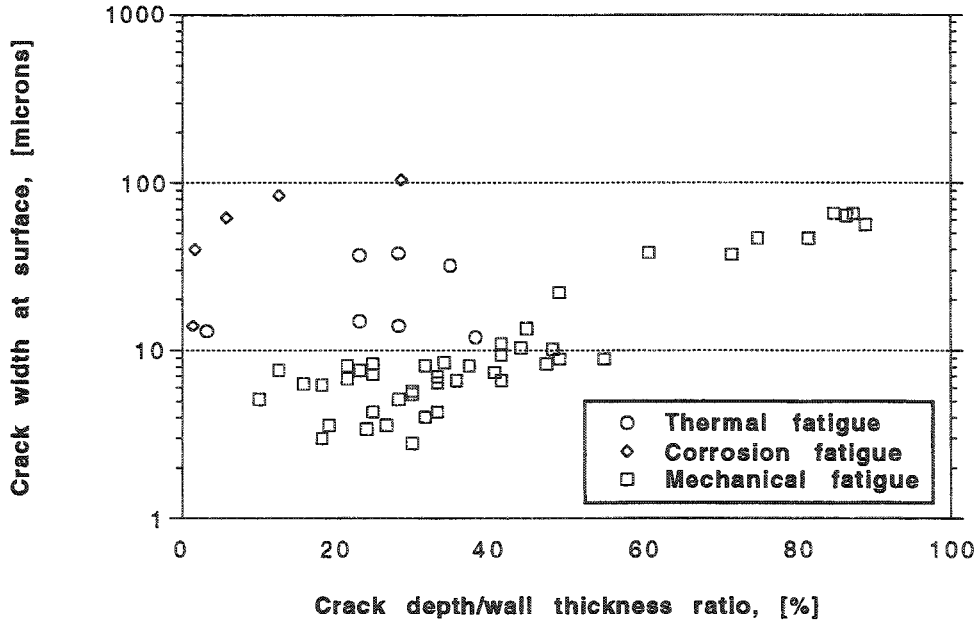

Fig. 49, Crack width at surface versus crack depth/wall thickness ratio of fatigue cracks in austenitic stainless steels [6].

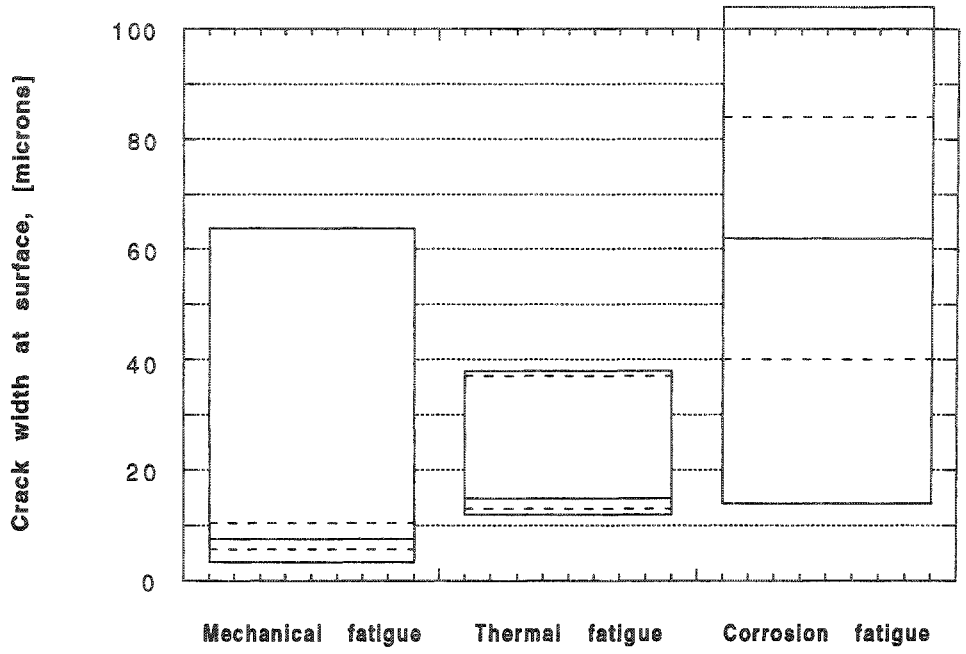

Fig. 50, Range of crack widths at surface of fatigue cracks in austenitic stainless steels [6].

4.6.10 Effects of crack closure

As mentioned previously the crack width is strongly dependent on the stresses acting perpendicular to the crack extension directions. When cutting out a piece of material around a crack the crack width often is affected due to redistribution of residual stresses or by adding external loads during the cutting or the sample preparation.

Another factor directly influencing the crack width, and hence, NDT detectability and crack sizing, is crack closure. This phenomenon has been extensively studied for many years. One of those studies was carried out by Brickstad in 1991 [10]. In that work crack closure was divided in two categories, namely, service induced and crack growth induced crack closure. During service induced crack closure the closure is controlled by either external loads, such as, mechanical, thermal or hydrostatic loads, or internal loads, such as, weld residual stresses or residual stresses from cold forming. Crack closure during crack growth occurs due to local plastic residual strain in the vicinity of the crack surfaces behind a growing crack. The residual strain is a remnant of the plastic zone in front of the

crack. Fatigue cracks are inclined to exhibit more crack closure than stress corrosion cracks due to the typical cyclic load conditions during fatigue.

The effect of service induced crack closure was studied for five specific cases.

- Surface cracks parallel to a circumferential weld of a thick wall pipe.
- Surface cracks parallel to a circumferential weld of a thin wall pipe.
- Under clad cracks of a low alloy ferritic steel clad with austenitic stainless steel.
- Surface cracks in feed water nozzles subject to thermal loads.
- Surface cracks in cold bent pipes.

The results of these studies indicated that crack closure may occur for deep internal surface cracks in thick wall piping during shut down periods of a nuclear power plant. Crack closure of corresponding cracks in thin walled piping was found less probable. Crack closure of under clad cracks was also predicted. Severe thermal transients in feed water nozzles were found to induce plastic strain in the surface layer of the material and hence cause crack closure. A brief analysis of cold bent pipes indicated crack closure both in service and during shut down conditions at certain positions along the pipe circumference.

The effect of crack growth induced closure was claimed to be less well known, and thus, more difficult to predict. Although, crack closure of thermal fatigue cracks at mixing tees, where water of different temperature mix, was found possible.

Considering crack width estimations, the effect of crack closure must be accounted for, especially in heavy wall sections adjacent to welds, in cold formed regions and where the surface is subject to severe thermal loads.

4.6.11 Concluding remarks on crack width

Crack width data from this work and literature data are shown in Fig. 51. According to the result of this work typical crack widths at the surface for mechanical and thermal fatigue cracks are 25-50 μm. However, crack width data below 25 μm are reported in reference 6. Possible reasons for that are presented in section 4.6.9. A reasonably good agreement with literature data is established for IGSCC, showing crack widths of 20 - 30 μm in this work and approximately 40 μm in the literature.

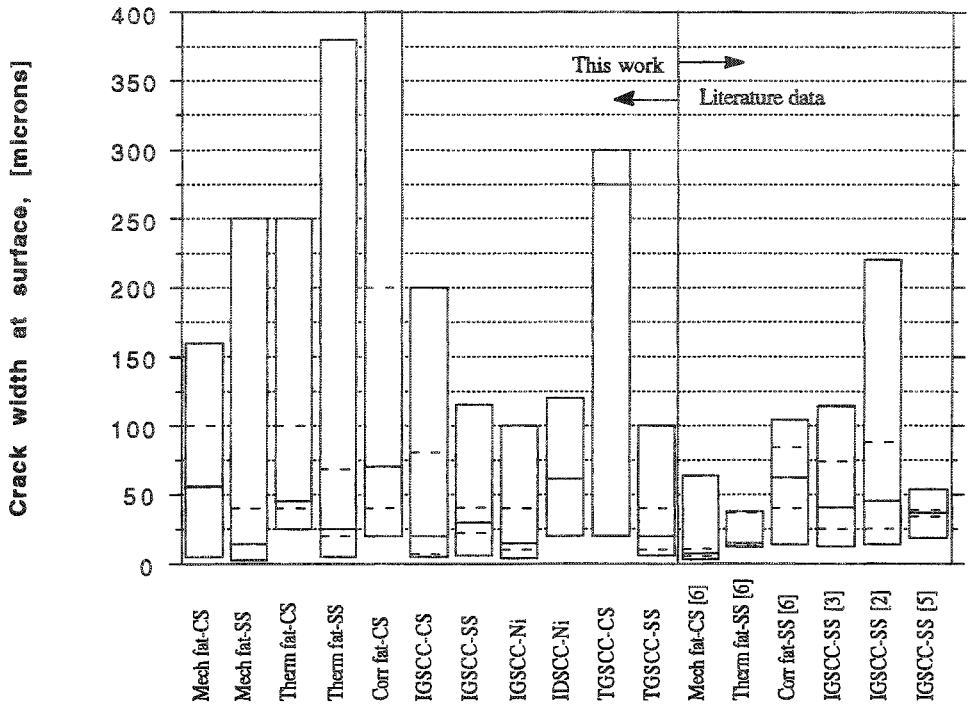

Fig. 51, Comparison of this work and literature data on crack widths at the surface of fatigue and stress corrosion cracks.

4.7 Crack surface roughness

In this section results from measurements of crack surface roughness are reported. The parameters evaluated are profile top height, R_z, and profile wave length, measured as a correlation length, λ_0. Both parameters are defined in section 3. The results are shown in percentile plots, showing median values and degree of scatter and in tables showing statistics on both parameters. In addition, comparisons are made with data from the literature.

4.7.1 Fatigue

4.7.1.1 Ferritic low alloy steels

Results from the evaluation of seven mechanical fatigue, six thermal fatigue and 20 corrosion fatigue cracks are shown in Table 10 and Fig. 52 and 53. Mechanical and thermal fatigue cracks show lower and less scattered R_z-values compared to corrosion fatigue cracks. The highest λ_0-values were measured for mechanical fatigue cracks, while thermal and corrosion fatigue cracks show lower and less scattered correlation lengths.

4.7.1.2 Austenitic stainless steel

Results from the evaluation of seven mechanical fatigue and 20 thermal fatigue cracks are shown in Table 11 and Fig. 52 and 53. Mechanical fatigue cracking in stainless steel produce surfaces with a comparable roughness to ferritic low alloy steel. One data point, 212 μm, is much higher than the others, hence, the scatter in this data group is large. Thermal fatigue cracks show considerably higher and more scattered Rz-values compared to ferritic steel. The correlation length is larger for mechanical than for thermal fatigue cracking, as in ferritic low alloy steel. The values are also approximately the same.

	Crack surface roughness, Rz, [μm]			Correlation length, λ_0, [μm]		
	mechanical fatigue	thermal fatigue	corrosion fatigue	mechanical fatigue	thermal fatigue	corrosion fatigue
Number of observations	6	4	18	5	6	19
minimum	12	6	5	25	16	14
maximum	40	20	100	870	230	270
mean value	23.7	12.2	38.6	405	82.5	78.5
median	22.5	11.5	28	390	50	43
RMS	25.5	13.5	46.5	493	113	108
standard deviation	10.3	6.45	26.6	315	84.6	76.4

Table 10, Statistics on surface roughness and correlation length data for fatigue cracks in ferritic low alloy steel

	Crack surface roughness, Rz, [μm]		Correlation length, λ_0, [μm]	
	mechanical fatigue	thermal fatigue	mechanical fatigue	thermal fatigue
Number of observations	6	20	7	20
minimum	10	6	30	27
maximum	212	140	1000	138
mean value	49.3	65.2	272.1	85.6
median	13.5	65.2	111	94.5
RMS	88.3	74.4	424.7	92.8
standard deviation	80.2	36	352.1	36.8

Table 11, Statistics on surface roughness and correlation length data for fatigue cracks in stainless steel

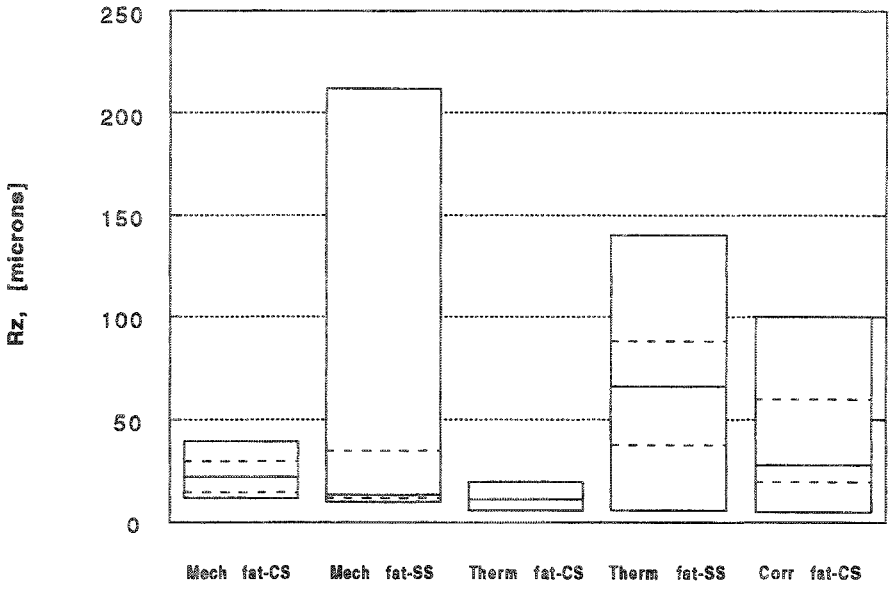

Fig. 52, Comparison of surface roughness, R_z, of fatigue cracks in ferritic low alloy steels and stainless steels.

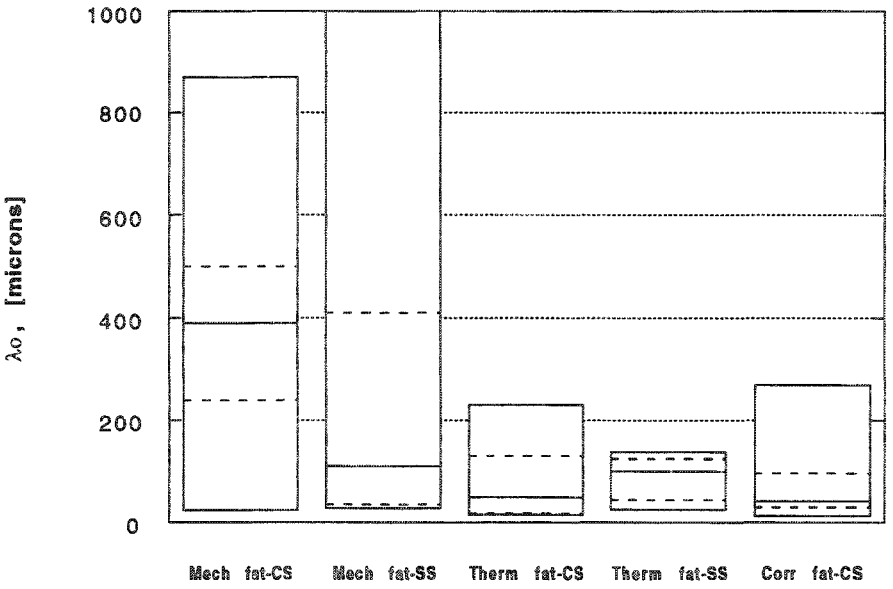

Fig. 53, Comparison of correlation length, λ_0, of fatigue cracks in ferritic low alloy steels and stainless steels.

4.7.2 IGSCC and IDSCC

Results from the evaluation of 13 cases of IGSCC in ferritic low alloy steels, 37 cases of IGSCC in stainless steels, 13 cases of IGSCC and 13 cases of IDSCC in nickel base alloys are shown in Table 12 and in Fig. 54 and 55. The crack surface roughness is approximately the same for IGSCC in ferritic low alloy steels and nickel base alloys, but considerably larger for IGSCC in stainless steels and for IDSCC in nickel base alloys. The largest correlation length is observed for IDSCC in nickel base alloys, while the other three groups show values below 50 μm.

	Crack surface roughness, Rz, [μm]				Correlation length, λ_0, [μm]			
	IGSCC low alloy	IGSCC stain-less	IGSCC nickel base	IDSCC nickel bas	IGSCC low alloy	IGSCC stain-less	IGSCC nickel base	IDSCC nickel bas
Number of observations	13	37	16	13	10	35	14	12
minimum	10	8	8	5	12	3	3.1	17
maximum	128	169	142	288	210	156	100	228
mean value	44.8	71.9	40.7	121.6	53.8	54.7	26.1	102.3
median	32	68	27	78.6	15.5	42	12.5	97
RMS	55.0	83	51.9	158.8	91.1	66.3	38.2	121.4
standard deviation	33.4	42.2	33.3	106.4	77.4	38	28.9	68.3

Table 12, Statistics on surface roughness and correlation length data for IGSCC and IDSCC, in various types of material.

4.7.3 TGSCC

Results from the evaluation of four cracks in ferritic low alloy steels, 24 cracks in stainless steels and three cases of TGSCC in nickel base alloys are shown in Table 13 and Fig. 54 and 55. The number of cracks are too few for comparison in all groups of material, but stainless steel. In addition, the surface roughness and in particular the correlation length are less useful parameters for heavy branched cracks, as TGSCC cracks generally are.

	Crack surface roughness, Rz, [μm]			Correlation length, λ_0, [μm]		
	TGSCC low alloy	TGSCC stainless	TGSCC nickel base	TGSCC low alloy	TGSCC stainless	TGSCC nickel base
Number of observations	4	24	3	4	12	2
minimum	20	10	17	28	15	7
maximum	136	90	34	1300	83	15
mean value	58	37.4	24.7	365	33.8	11
median	38	34.5	23	66	30.5	11
RMS	73.8	44.0	25.6	61	38.7	-
standard deviation	52.7	23.6	8.6	623	19.7	-

Table 13, Statistics on surface roughness and correlation length data for TGSCC

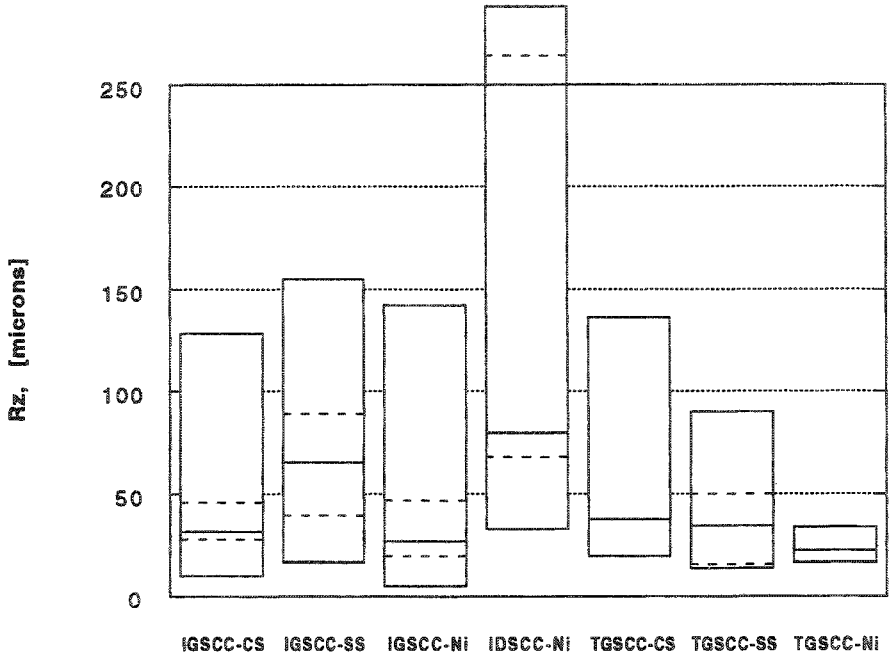

Fig. 54, Comparison of surface roughness, R_z, of SCC in ferritic low alloy steels, stainless steels and nickel base alloys.

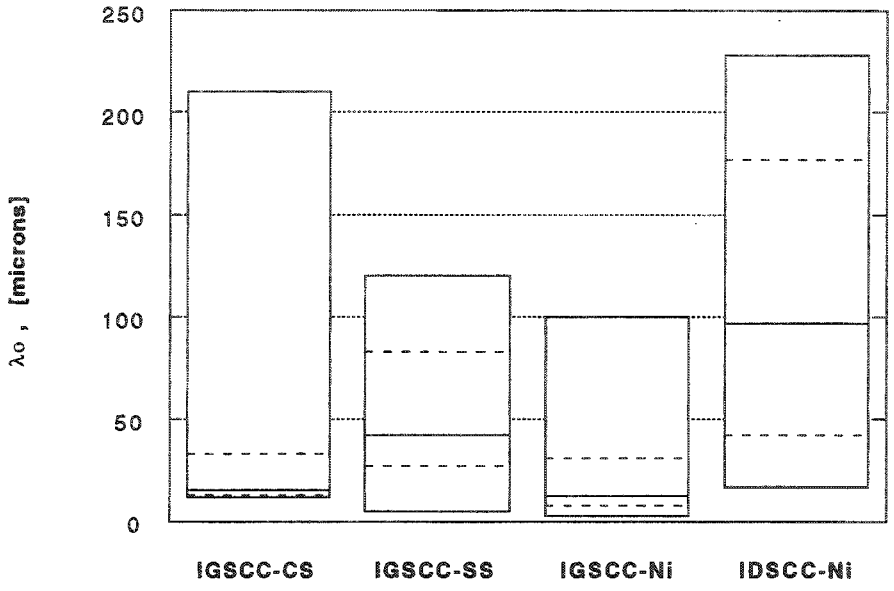

Fig. 55, Comparison of correlation length, λ_0, of SCC in ferritic low alloy steels, stainless steels and nickel base alloys.

4.7.5 Comparison of surface roughness data

A comparison of crack surface roughness data for fatigue, IGSCC, IDSCC and TGSCC in low alloy steels, stainless steels and nickel base alloys is shown in Fig. 56. Correlation lengths from the same data groups are compared in Fig. 57.

Most data groups show a surface roughness, R_z, in the same range. Typically, less than 30 μm. The exceptions are IGSCC and thermal fatigue in stainless steels and IDSCC in nickel base alloys, which show R_z-values typically in the range of 70 - 80 μm. Crack surfaces of IGSCC in ferritic low alloy steels are less rough than in austenitic stainless steels, which may be explained by the more fine grained structure in ferritic low alloy steels.

An evaluation of the correlation length, λ_0, show considerable deviation for mechanical fatigue cracking in ferritic low alloy and stainless steels compared to all other groups. Typical correlation lengths for these exceptions are in the range 300 - 400 μm, while the other data groups show values below 100 μm.

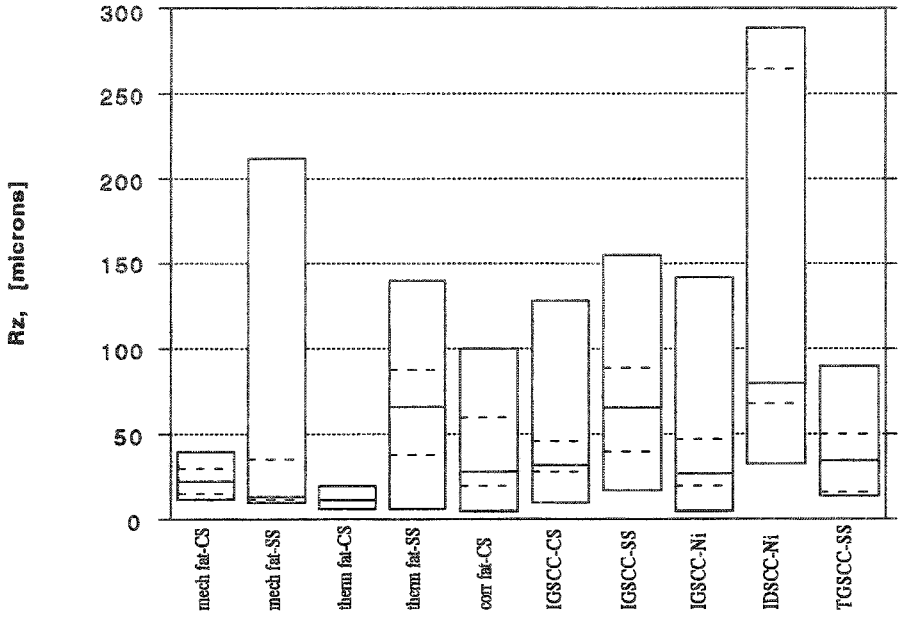

Fig. 56, Comparison of surface roughness, R_z, for fatigue and SCC.

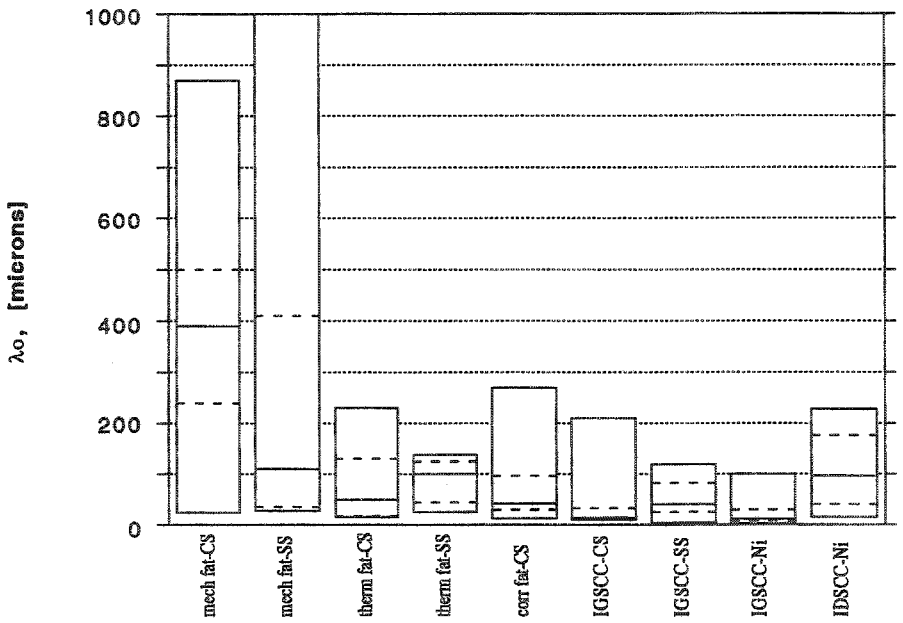

Fig. 57, Comparison of correlation length, λ_0, for fatigue and SCC.

4.7.6 Weld flaws

Three cases each of lack of fusion, hot cracking and cold cracking were evaluated. Lack of fusion flaws show a typical smooth surface topography, and thus, low Rz-values. Hot and cold cracks also produce low Rz-values, with the exception of one hot crack. The correlation lengths were only evaluated for the cold cracks. The results are shown in Table 14.

Weld flaw type	**Rz**	λ_0
Lack of fusion	13, 22, 37	no data
Hot cracks	27, 43, 155	25, 42, 250
Cold cracks	30, 30, 80	no data

Table 14, Surface roughness and correlation length data for weld flaws.

4.7.7 Literature data on surface roughness

The literature review yielded data on crack surface roughness covering two areas of interest. These were the influence of surface roughness on ultra sonic testing detection and the influence on leak rate in through wall cracks. There exist several methods to measure surface roughness, and there are many definitions which depend on how the measurement is made. Two measuring methods are possible, direct measurement on a surface with a surface roughness measuring device or measurements on a micro graph over a cross section of the crack. The most common measures are R_{RMS}, R_a and R_z.

Manning [7], Wooldridge and Steel [1] and Egerbo et al [8] all report surface roughness data obtained from direct surface measurements made on fatigue test specimens of austenitic stainless and ferritic low alloy steels. The results are reported either as R_{RMS} or R_a-values. The data, converted to R_a-values, are compiled in Fig. 58. Fatigue cracking in both ferritic low alloy steels and stainless steels produce similar surface roughness median values, which are in the range 5-7 μm. The exception which is slightly higher shows values close to 12 μm [1].

A document, yet not published, by Stenefjäll [5] report surface roughness data derived from R_a measurements made on cross-sections of IGSCC in austenitic stainless steel components. The data are shown in Fig. 59. Wilkowski et al [9] evaluated surface roughness data as R_{RMS} on cross-sections. They distinguish local surface roughness from global, where local roughness are measured on a grain size scale and global roughness

are measured in regions between macroscopic crack turns larger than 45°. The literature data from [5] and [9] are compared for low alloy and stainless steels in Fig. 59. The data in [9] are converted to R_a for the comparison. The local surface roughness values reported in [9] show good agreement with the literature data above and with the data produced in this work. However, the global surface roughness data in [9] are much higher than the other data used for the comparison. The surface roughness data presented in [5] also deviate strongly from the data of this work, probably due to the evaluation methods used. The data in [5] are in the same range as the global surface roughness data of [9].

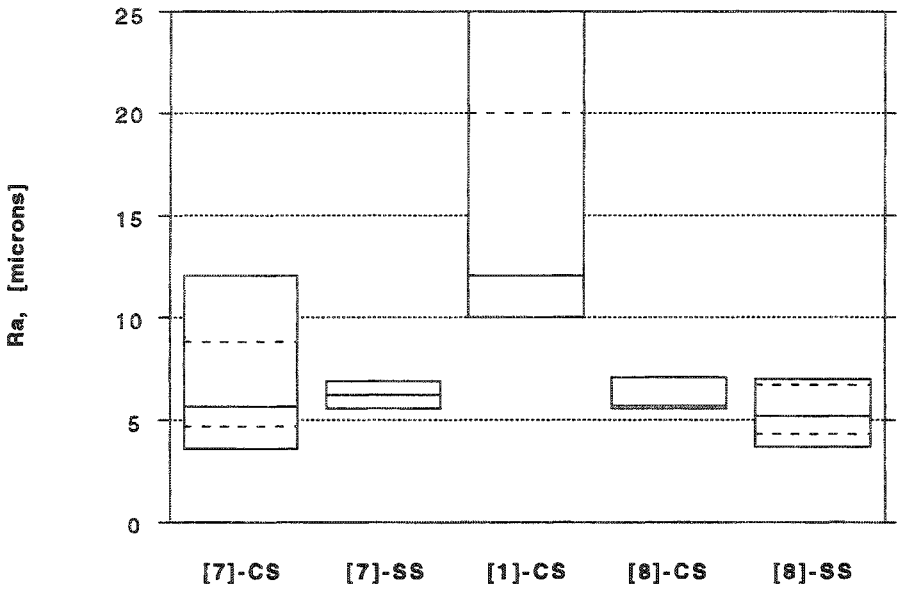

Fig. 58, Range in surface roughness, R_a, of fatigue cracks, from [7], [1] and [8].

4.7.8 Concluding remarks on surface roughness

Crack surface roughness data obtained in this work and in the literature are shown in Fig. 60. All data are converted to R_a for the comparison. A reasonably good agreement with literature data is established for fatigue cracks, all showing R_a-values between 3 and 12 μm. The only exception is data for thermal fatigue in stainless steels of this work, which show a larger surface roughness, with a median value of 16.5 μm. For IGSCC in stainless steels, the local data reported in [9] are much lower than the data derived in this work, a median value of 7 μm compared to 17 μm.

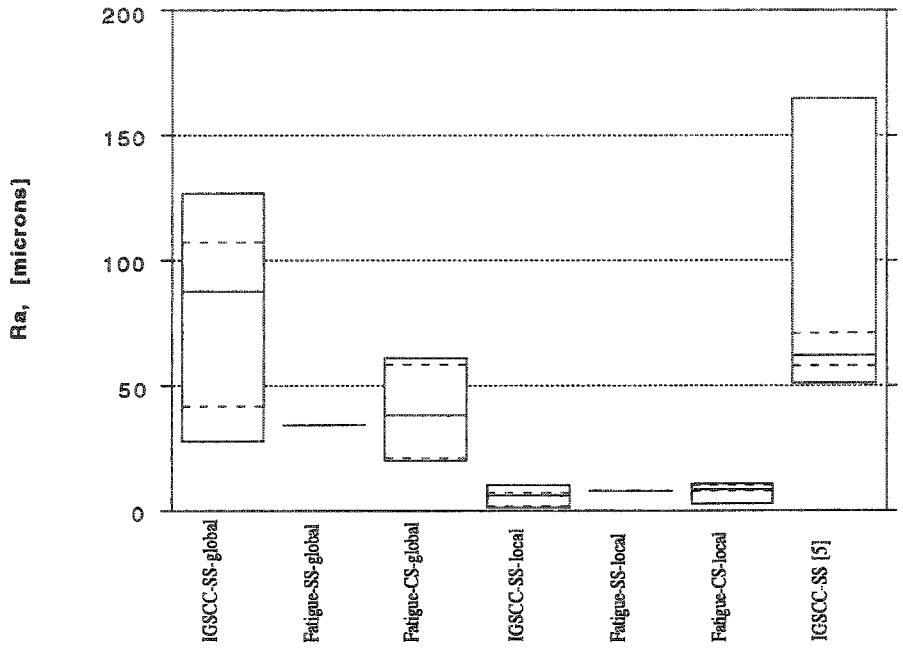

Fig. 59, Range of crack surface roughness, R_a, of fatigue and stress corrosion cracks reported by [9] and [5].

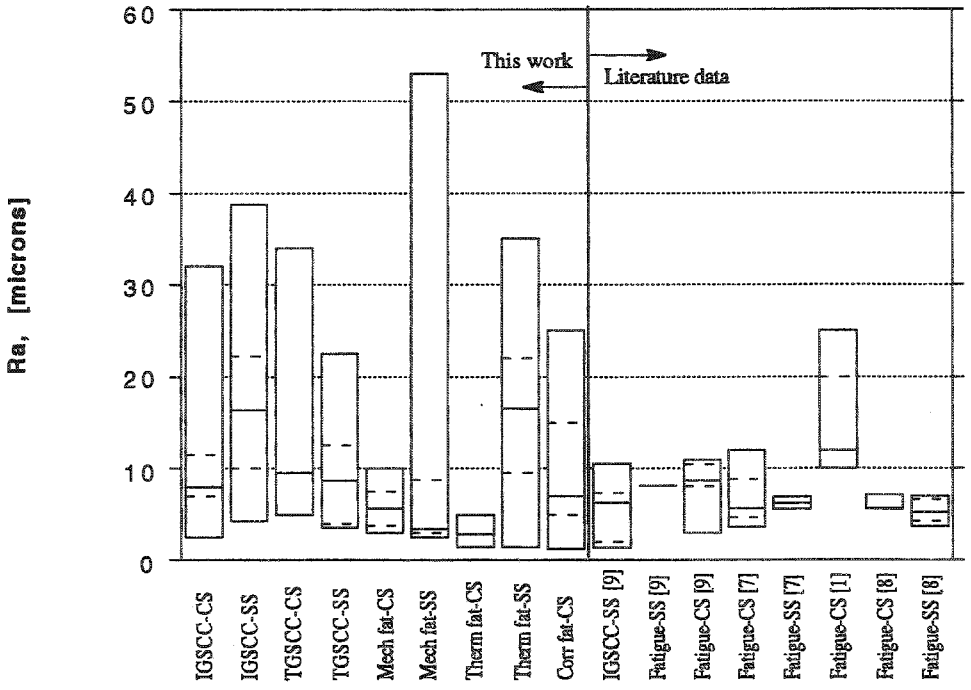

Fig. 60, Comparison of surface roughness data, R_a, for fatigue and stress corrosion cracks derived from this work and the literature.

5 Suggested further work

During the evaluation of morphology parameters from failure analysis reports it was quite obvious that the majority of the failure investigations did not aim to measure the type of parameters needed for this work. Although, some of the parameters are used to diagnose the failure mechanisms, several of them are of less importance when performing a failure analysis. Some reports did not even provide documentation, micro graphs etc., accurate enough for further evaluation.

To establish a more comprehensive and reliable parameter database it is necessary to perform extended investigations on a number of future failure cases, aiming to accurately determine the morphology parameters. A number of 20 - 30 cases for each data group is probably enough to provide statistical significance. The ordinary failure investigation procedure then need to be extended with supplementary evaluations to determine all major morphology parameters defined in section 3. Compared to the amount of work necessary to conduct an ordinary failure analysis the suggested supplementary evaluations probably would be a minor effort.

A procedure to perform such an extended failure investigation is proposed below.

- Record material grade and condition, heat treatment, cold forming etc.
- Record design and service conditions.
- Record component dimensions.
- Record crack length, crack site, crack surface orientation and macroscopic crack features.
- Measure crack width at the surface inter-section at several points along the crack.
- Sectioning should be done midway between the surface crack tips and when necessary at several other points along the crack.
- On the cross-section(s) the following parameters should be evaluated:

    - Through thickness orientation (angle between crack and surface)
    - Macroscopic shape
    - Macroscopic branching and crack tip branching
    - Crack tip radius
    - Crack width at several points along the crack depth
    - Surface roughness
    - The amount of non-metallic oxides inside the crack

6 References

1 Wooldridge A. B., Steel G., The influence of crack growth condition and compressive stress on the ultrasonic detection and sizing of fatigue cracks, CEGB, NW/SSD/RR/45/80, April 1980.

2 Lapides M. E., Evaluation of Miniac radiography for in-service inspection of cast austenitic piping and components in PWR nuclear units, EPRI Report NP-xxxx, September 1984.

3 MacDonald D. E., IGSCC Detection in BWR Piping Using the Miniac, EPRI Report NP-3828, February 1985.

4 Lapides M. E., A note on radiographic detection of IGSCC, Supplement to EPRI Report NP 3164-SR, February 1984.

5 Stenefjäll T., Private communications, September 1994.

6 Skånberg L., Validation of NDT-systems (in Swedish), SKI Report No 94:25.

7 Manning P. T., The surface topography of some fatigue crack surfaces, CEGB, May 1979.

8 Egerbo A., Evertsson S., Norrgård M., Sundqvist, Thorén B, Influence of defect type on ultrasonic detection - pre-study (in Swedish), SKI report 13.2-989/87, April 1989.

9 Rahman S., Ghadiali N., Paul D., Wilkowski G., Probabilistic pipe fracture evaluations for leak-rate detection applications, NUREG/CR-6004, June 1992.

10 Brickstad B., Investigation of crack closure effects in Swedish nuclear power plants (in Swedish), SKI-Report TR 91:1, January 1991.

Database template

General data

Service/Lab	Service	Nuclear/non nuclear	Nuclear
Identification	O1 system 211	Reference	RM 87-371
Crack mechanism	TGSCC	Crack location	Flange
Material grade	SS 2333	Material group	Austenitic stainless steel
Material condition		Delivery form	Forging
Loading conditions		Service temperature	286
Dy [mm]		Wall thickness	

Crack morphology data

Crack dimension [mm]	Length	1,3	Depth	0,95	Depth/w.t. [%]
Distance to.. [mm]					
Through thickness angle	90		Surface angle	0	
Trough thicknes shape	Straight, branched		Surface shape	Straight	
Number of cracks	>5		C-S pattern distance		
Macroscopic branching	0,01				
Grain size [µm]			Micro-structure	Equiaxed grains	
Rz [µm]	23,8	L [mm]	0,85	λ_0 [mm]	30
Crack width [µm] Surface	10	Midway	3	Tip	2
Influence of sampling	1		Crack tip radius [µm]	0	
Amount of oxides Surface	1	Midway	1	Tip	1

Sketch over crack location and shape

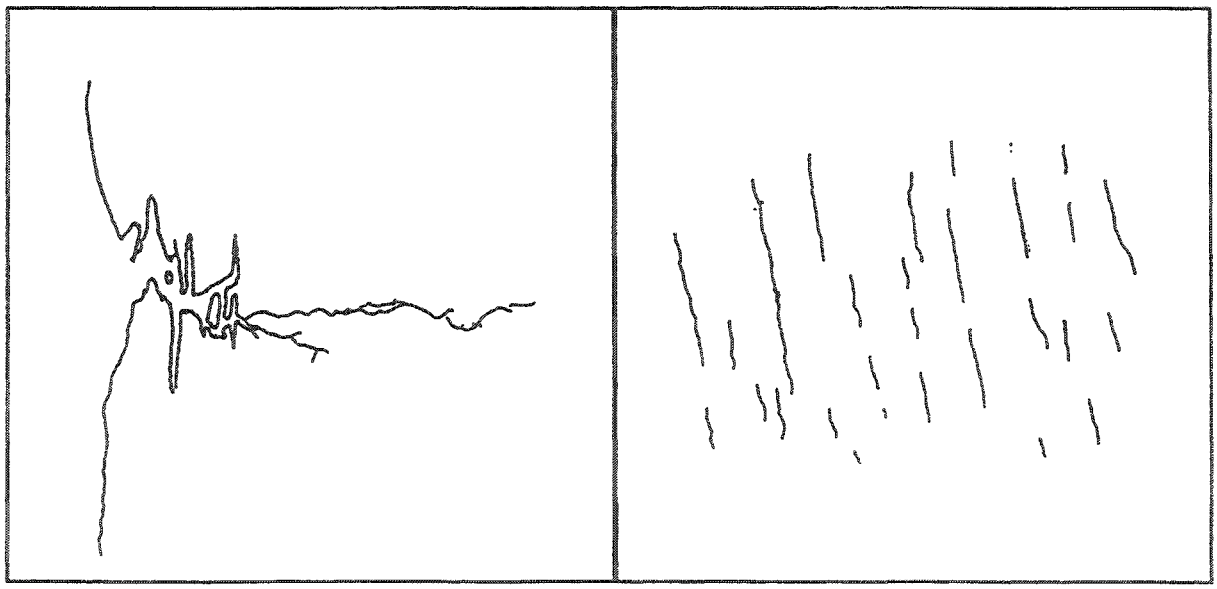

Examples of characteristic crack features displayed by macro and micro graphs

Mechanical fatigue in ferritic low alloy steel

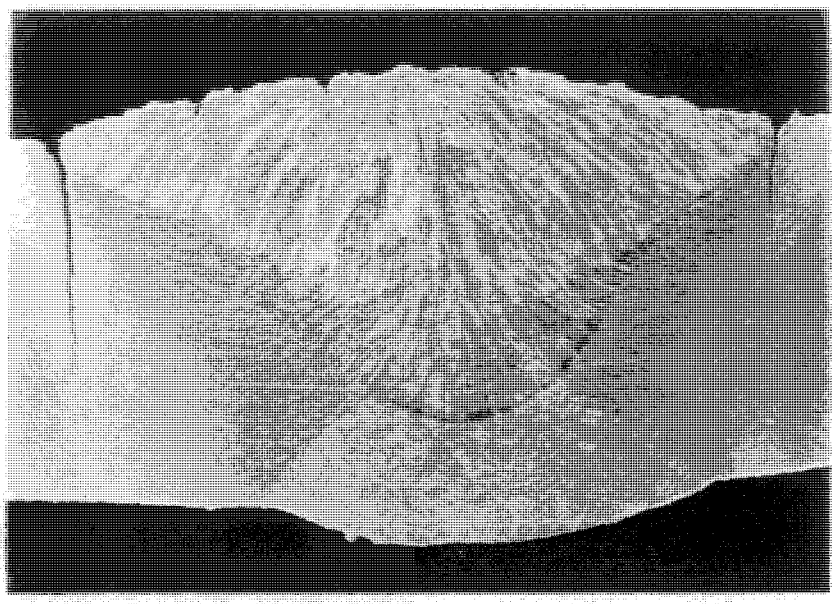

Micro graph 1 Mechanical fatigue in steam boiler shell made of mild carbon steel, non-nuclear industry. Cross section. Note, typical location at weld fusion line and the straight unbranched features. Magnification 4.5 X.

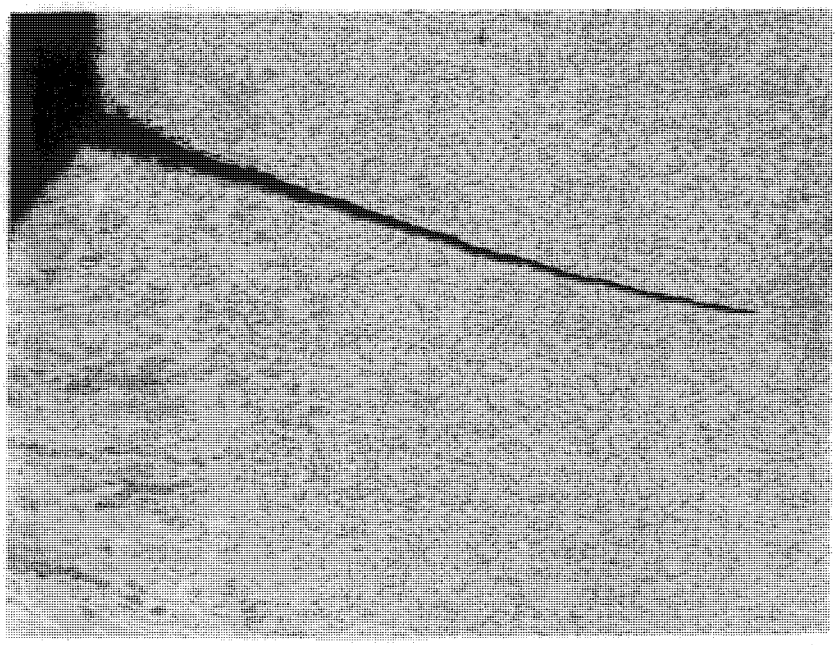

Micro graph 2 Mechanical fatigue of steam boiler shell made of mild carbon steel, non-nuclear industry. Cross section. Note, typical straight and unbranched crack growth. Magnification 25 X

Mechanical fatigue in ferritic low alloy steel

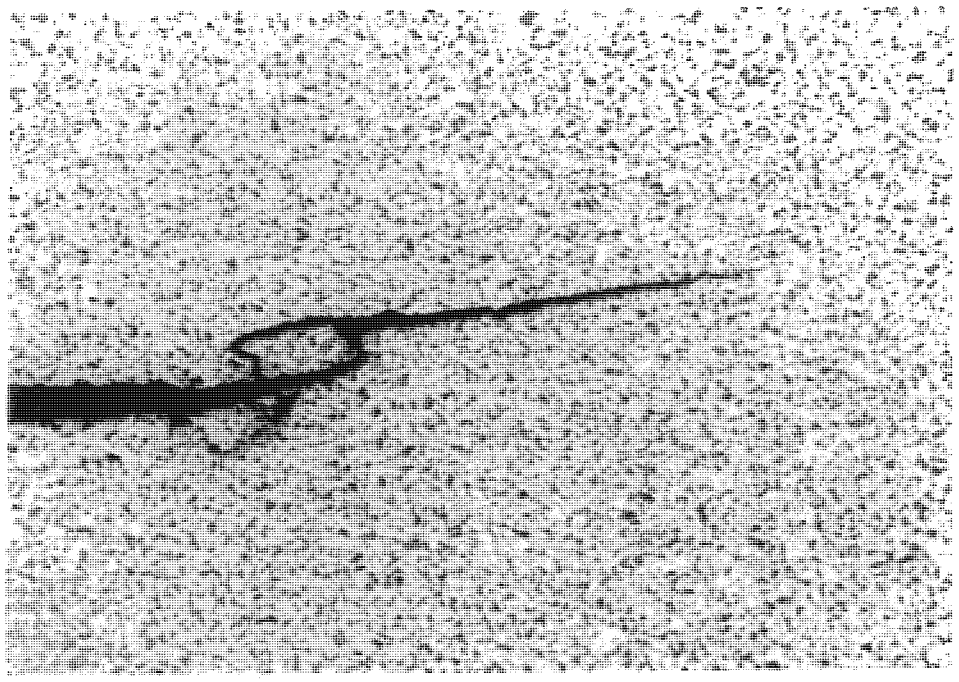

Micro graph 3 Mechanical fatigue in steam boiler tube made of ferritic low alloy high temperature steel, non-nuclear industry. Note pointed unbranched crack tip.
Magnification 50 X.

Mechanical fatigue in stainless steel

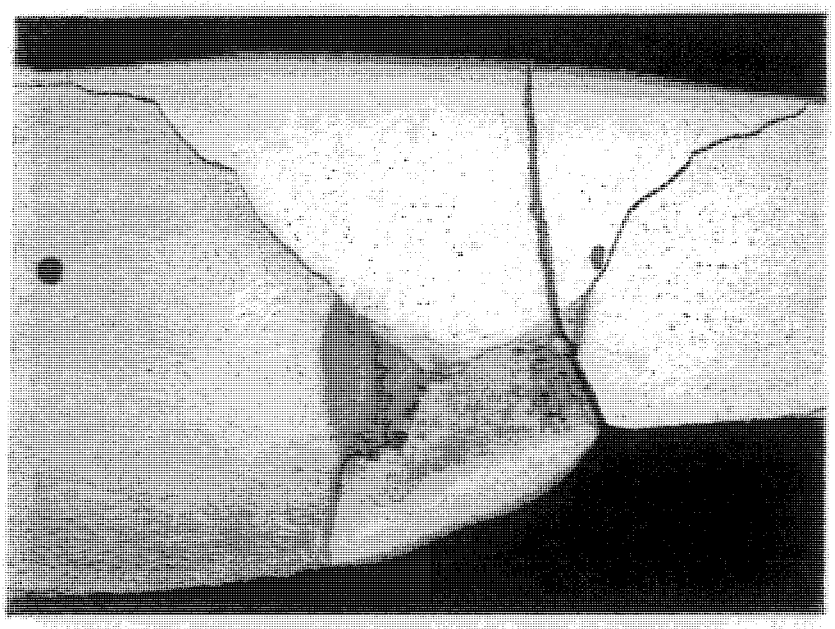

Micro graph 4 Mechanical fatigue in an austenitic stainless steel pipe, nuclear industry. Cross section. The crack has been initiated at a sharp notch between the root run and the pipe.
Magnification 5.5 X.

Mechanical fatigue in stainless steel

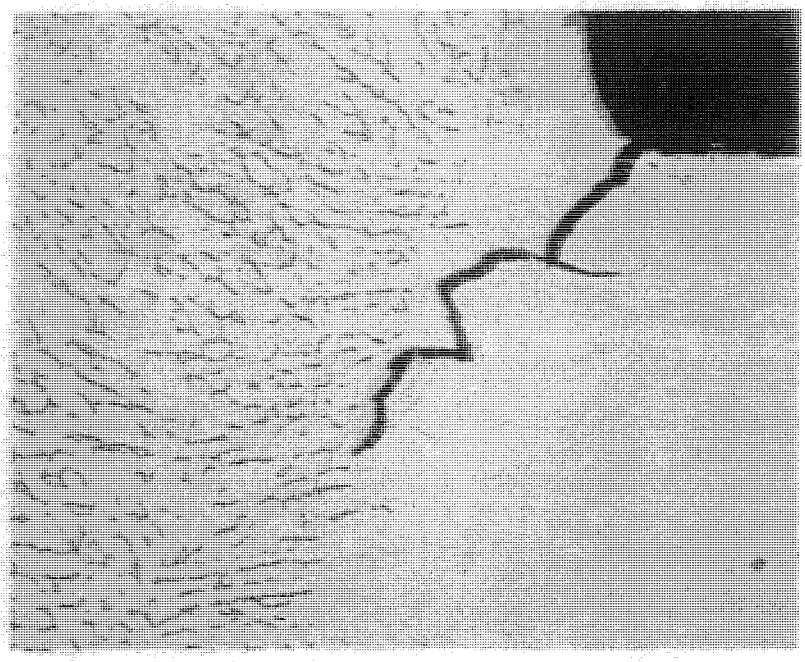

Micro graph 5 Mechanical fatigue in an austenitic stainless steel pipe, nuclear industry. Note, transgranular and winding crack growth. Magnification 200 X.

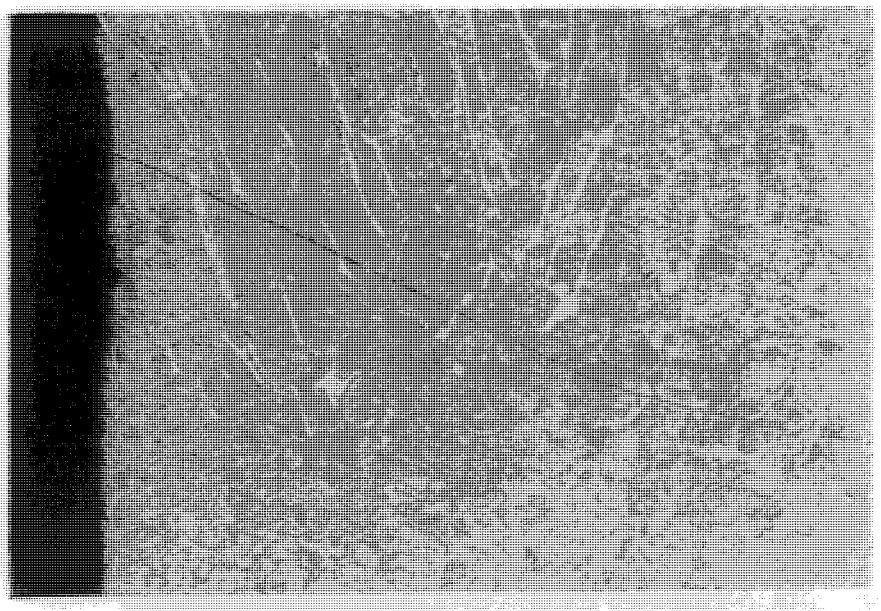

Micro graph 6 Mechanical fatigue in a pulp processing machine shaft made of martensitic/austenitic stainless steel, non-nuclear industry. Cross section. Note, narrow, straight and unbranched micro-structure independent crack growth. Magnification 12 X.

Thermal fatigue in ferritic low alloy steel

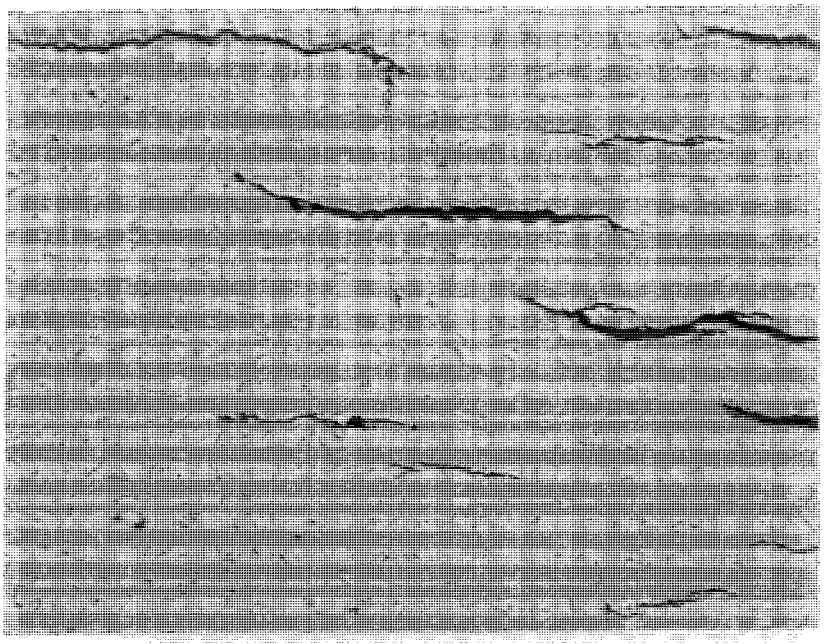

Micro graph 7 Thermal fatigue in steam boiler shell made of mild carbon steel, non-nuclear industry. Surface section. Note, high density of almost parallel cracks.
Magnification 50 X.

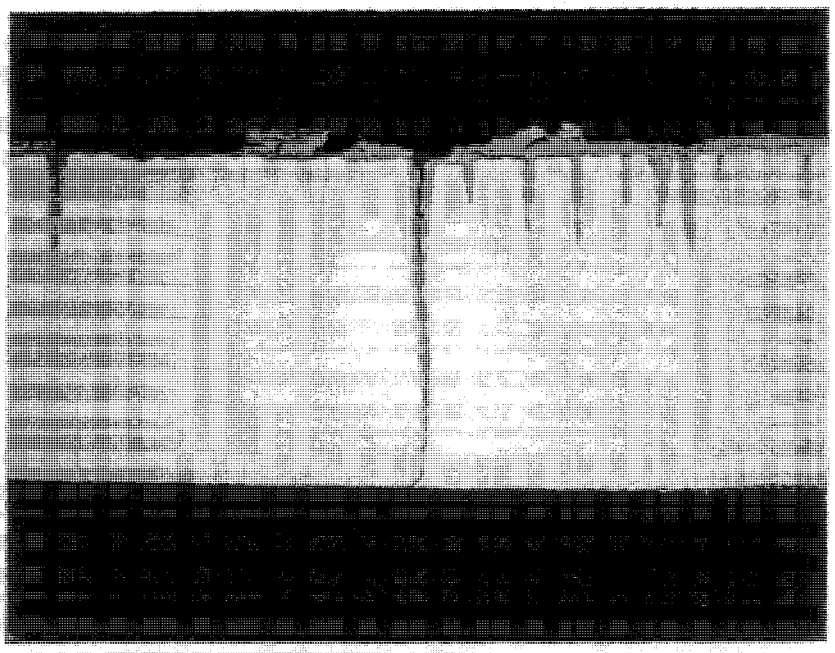

Micro graph 8 Thermal fatigue in steam boiler soot blower tube made of low alloy high temperature steel, non-nuclear industry. Cross section. Note, narrow spaced straight unbranched cracks filled with oxide.
Magnification 12 X.

Thermal fatigue in ferritic low alloy steel

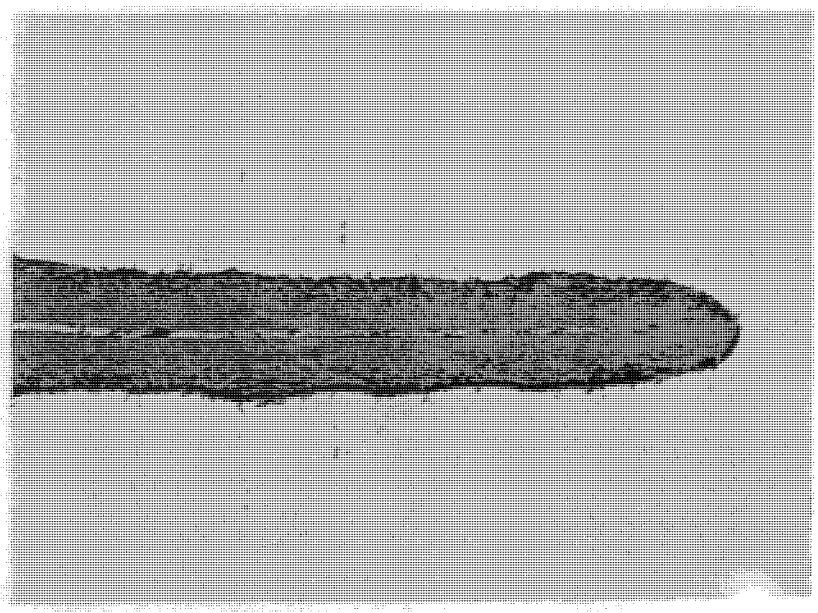

Micro graph 9 Thermal fatigue in steam boiler tube made of mild carbon steel. Note, blunted oxide filled crack tip. Magnification 200 X.

Thermal fatigue in stainless steel

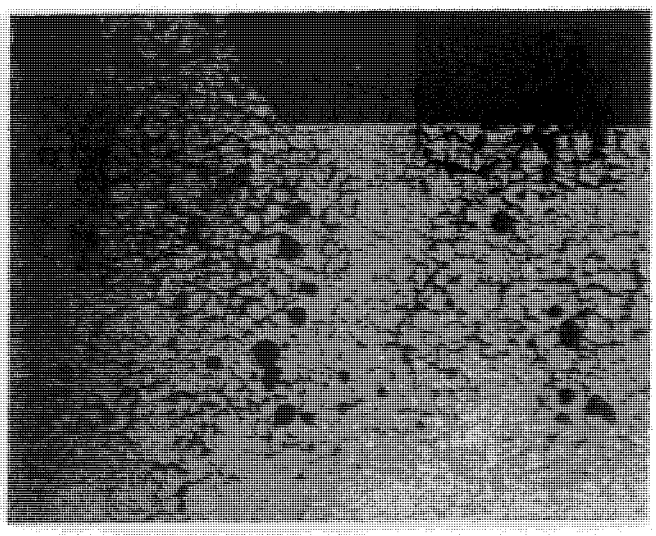

Micro graph 10 Cobble stone pattern, due to thermal fatigue at the inside of an austenitic stainless steel pipe, nuclear industry. The photo is taken after a dye penetrant test. Magnification ≈1 X.

Thermal fatigue in stainless steel

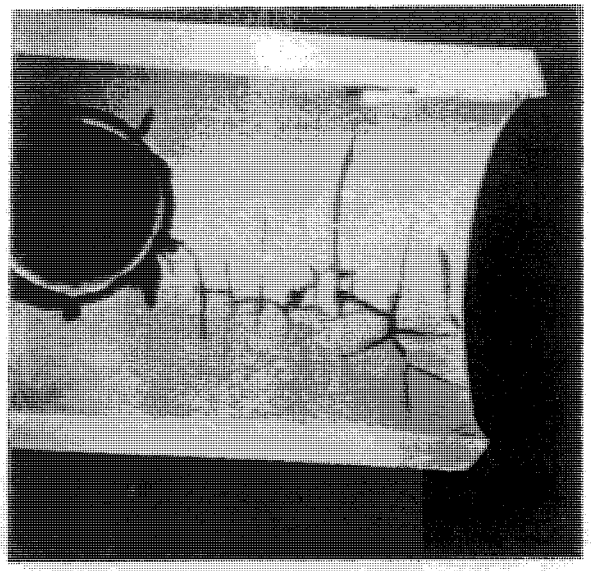

Micro graph 11 Cobble stone pattern due to thermal fatigue inside a tee, austenitic stainless steel, nuclear industry. Note, the non-symmetrical location of the cobble stone pattern.
Magnification ≈0.5 X.

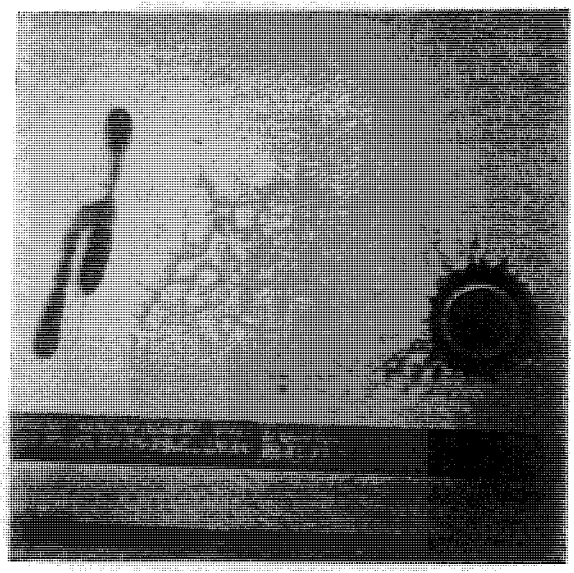

Micro graph 12 Section of a pipe showing cobble stone pattern due to thermal fatigue, nuclear industry. The photo is taken after a dye penetrant test.
Magnification ≈ 0.4 X.

Thermal fatigue in stainless steel

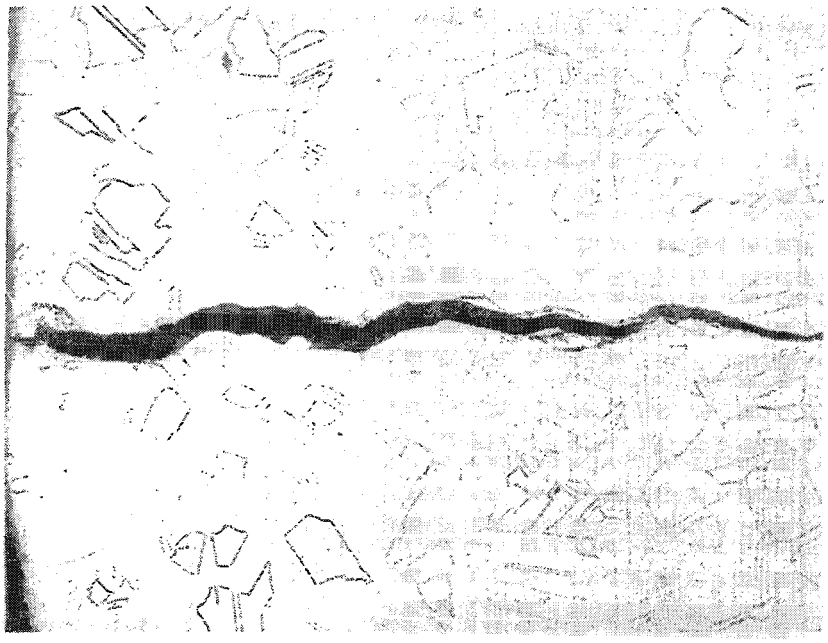

Micro graph 13 Thermal fatigue crack in an austenitic stainless steel pipe, nuclear industry. Cross section. Note, transgranular crack growth without branching.
Magnification 50 X.

Micro graph 14 Thermal fatigue crack in an angle tee made of austenitic stainless steel, nuclear industry. Cross section. Note, micro branching at the crack tip.
Magnification 50 X.

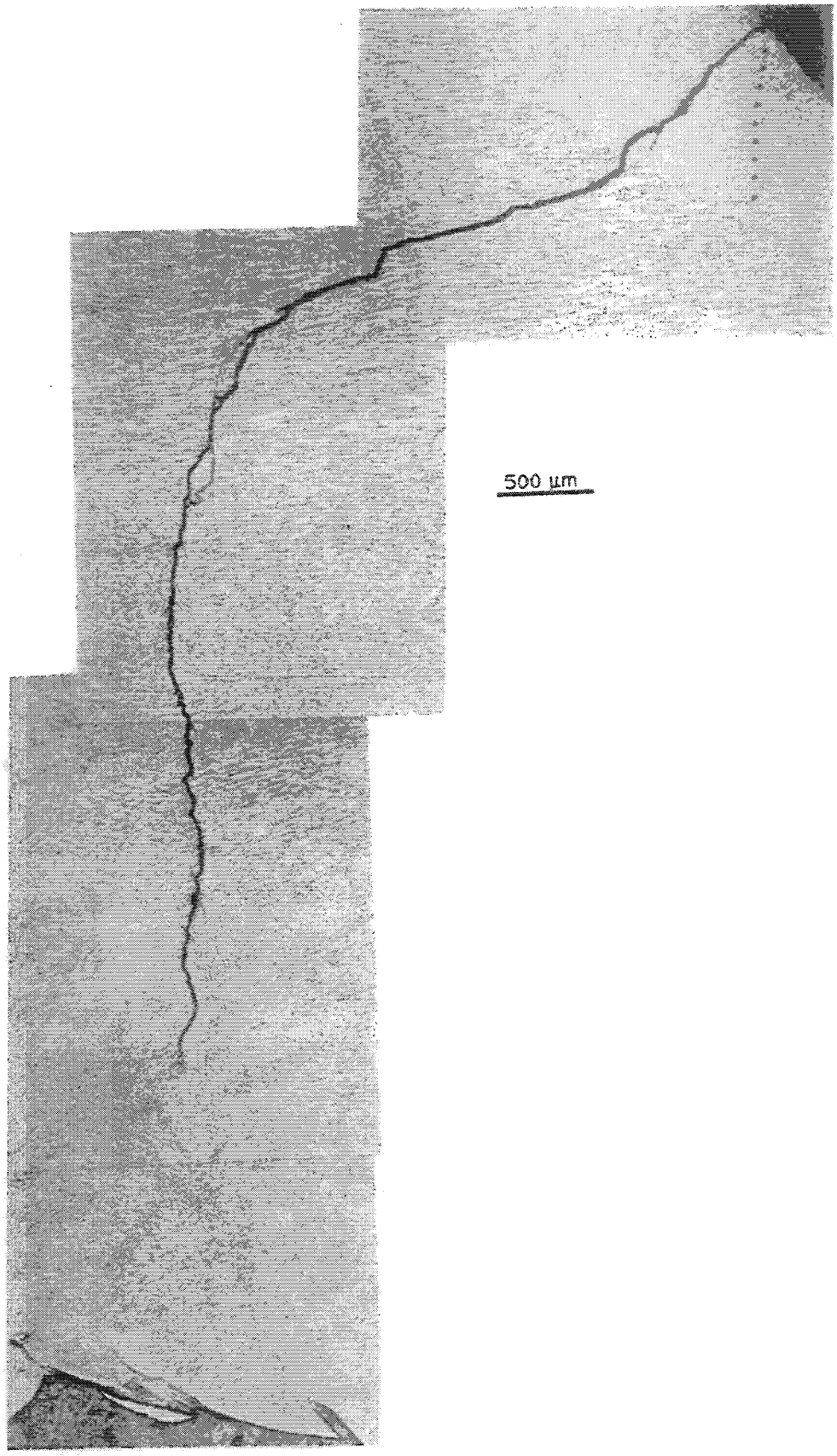

Micro graph 15 Thermal fatigue crack in austenitic stainless steel cladding, nuclear industry. Note, the bent shape of the crack and the tendency for micro branching at the crack tip. Magnification 30 X.

Corrosion fatigue in ferritic low alloy steel

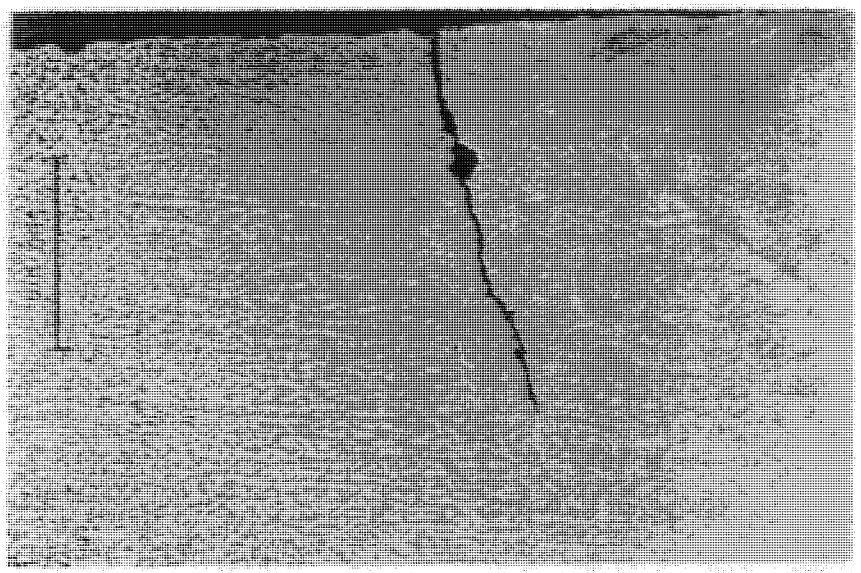

Micro graph 16 Corrosion fatigue in feed water vessel made of mild carbon steel, non-nuclear industry. Cross section. Note, typical location near weld fusion line and orientation affected by weld geometry. Magnification 50 X.

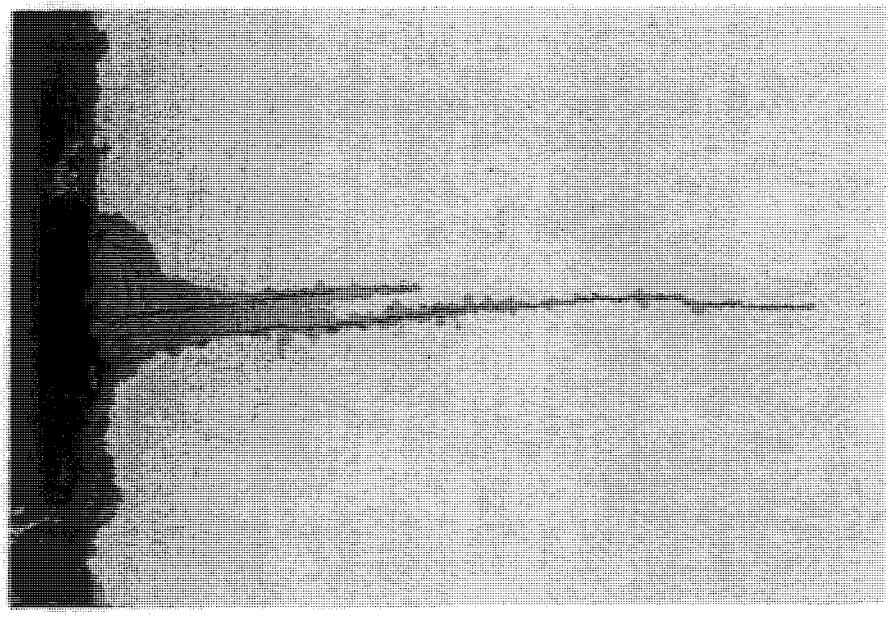

Micro graph 17 Corrosion fatigue in steam boiler shell made of mild carbon steel, non-nuclear industry. Cross section. Note, corrosion widening of crack and branching tendency. Magnification 50 X.

Mixed thermal and corrosion fatigue in ferritic low alloy steel

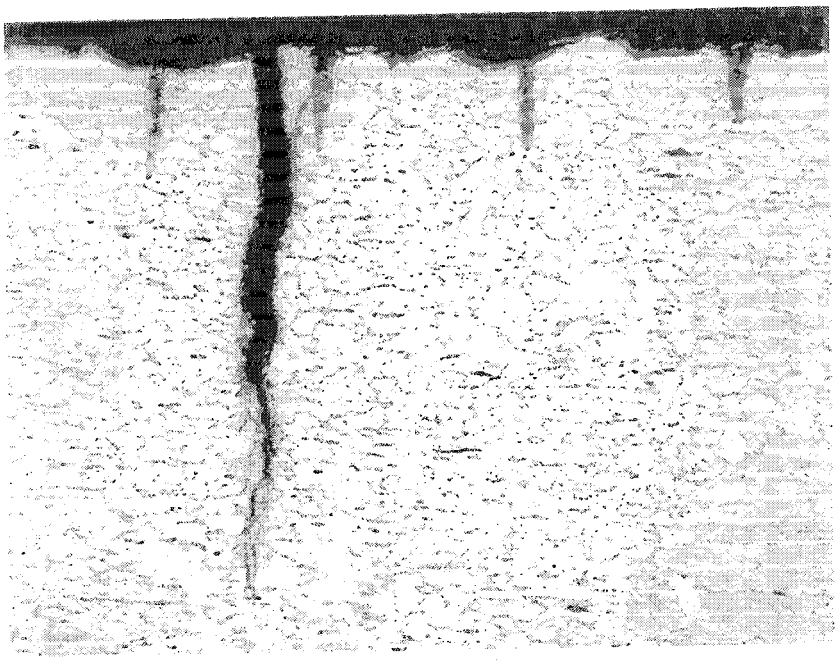

Micro graph 18 Mixed thermal and corrosion fatigue in steam boiler tube made of mild carbon steel, non-nuclear industry. Cross section. Note, partly branching of one crack. Magnification 100 X.

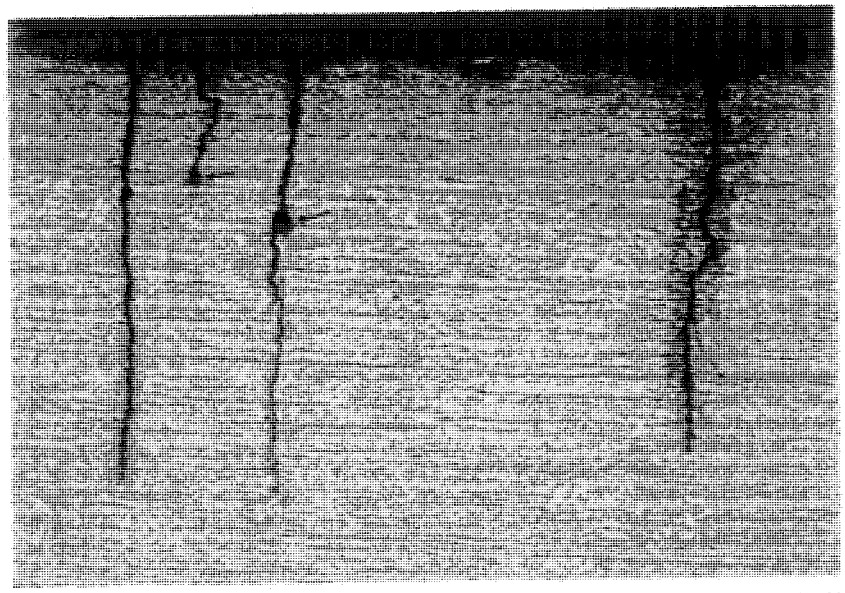

Micro graph 19 Mixed thermal and corrosion fatigue in steam boiler shell made of mild carbon steel, non-nuclear industry. Cross section. Note, local corrosion along some cracks due to increased oxygen content during shut down periods.
Magnification 50 X.

IGSCC in ferritic low alloy steel

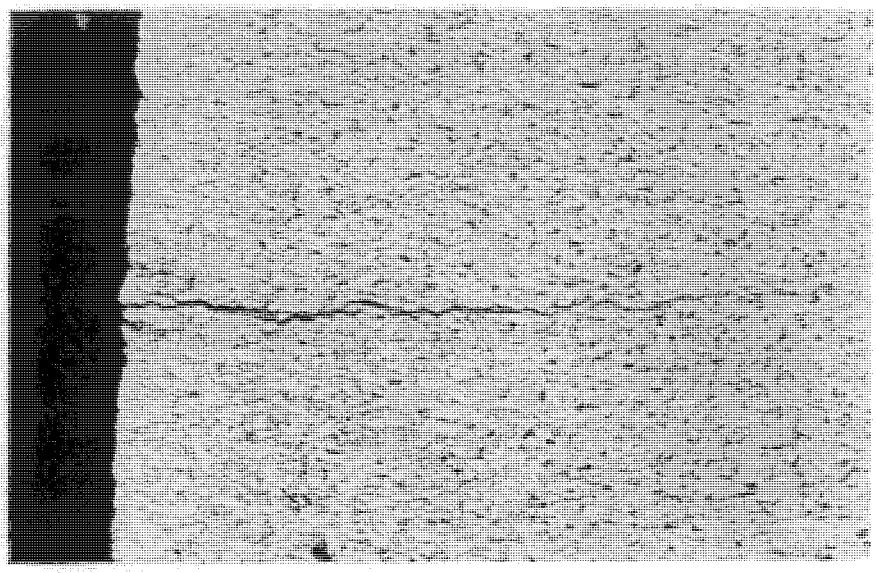

Micro graph 20 IGSCC in cold bent steam boiler tube made of mild carbon steel, non-nuclear industry. Cross section. Note, narrow crack width and micro crack branching in parent metal.
Magnification 100 X.

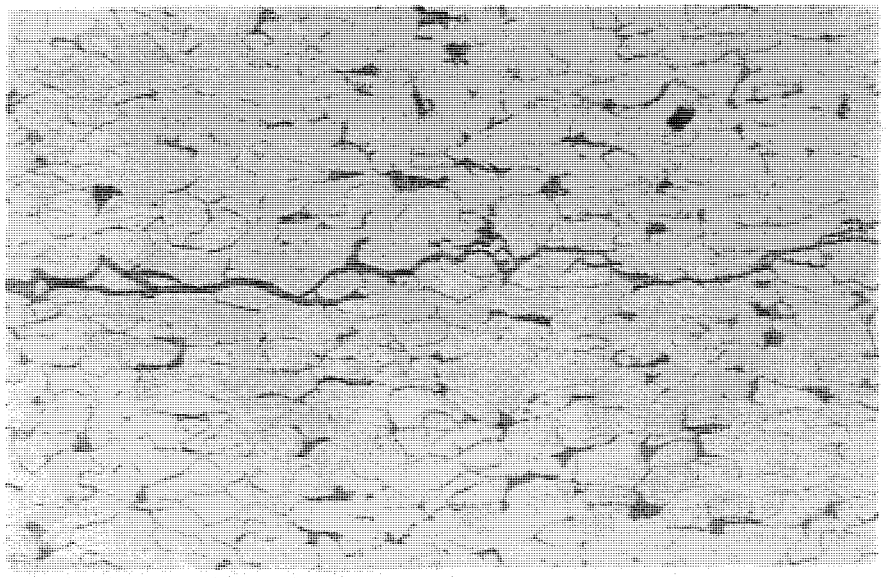

Micro graph 21 IGSCC in cold bent steam boiler tube made of mild carbon steel, non-nuclear industry. Cross section. Note, narrow crack width and micro crack branching located in parent metal.
Magnification 400 X.

Mixed IGSCC and TGSCC in ferritic low alloy steel

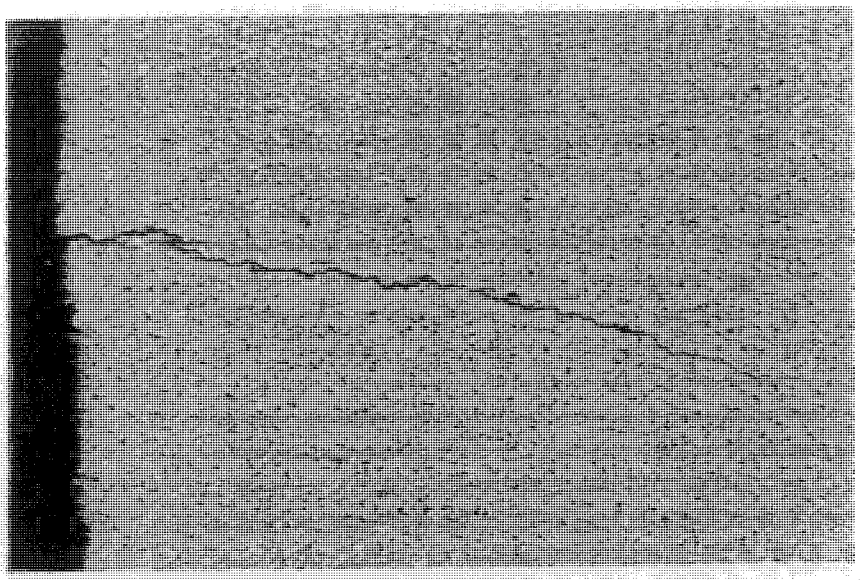

Micro graph 22 Mixed IGSCC and TGSCC in steam boiler tube made of mild carbon steel, non-nuclear industry. Cross section. Note, narrow crack width and micro crack branching in parent metal. Magnification 100 X.

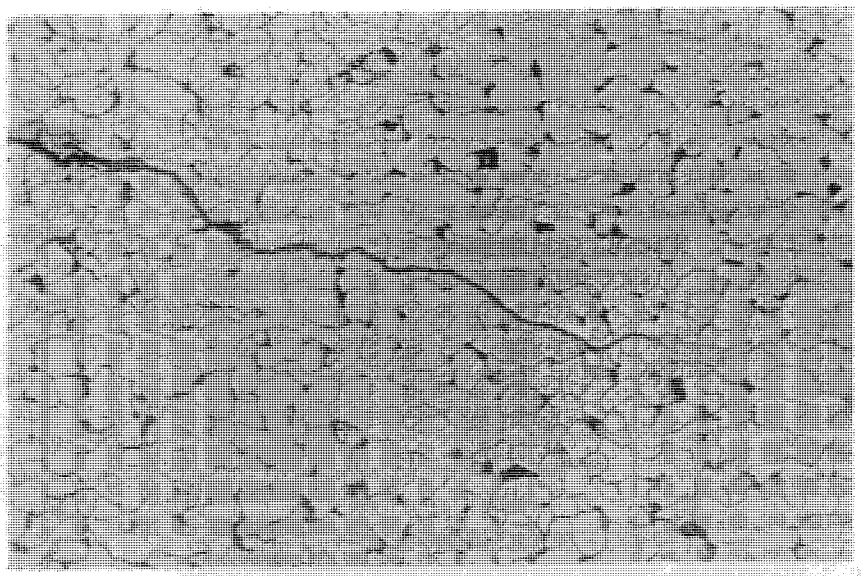

Micro graph 23 Mixed IGSCC and TGSCC in steam boiler tube made of mild carbon steel, non-nuclear industry. Cross section. Note, narrow crack width and micro crack branching in parent metal. Magnification 400 X.

IGSCC in stainless steel

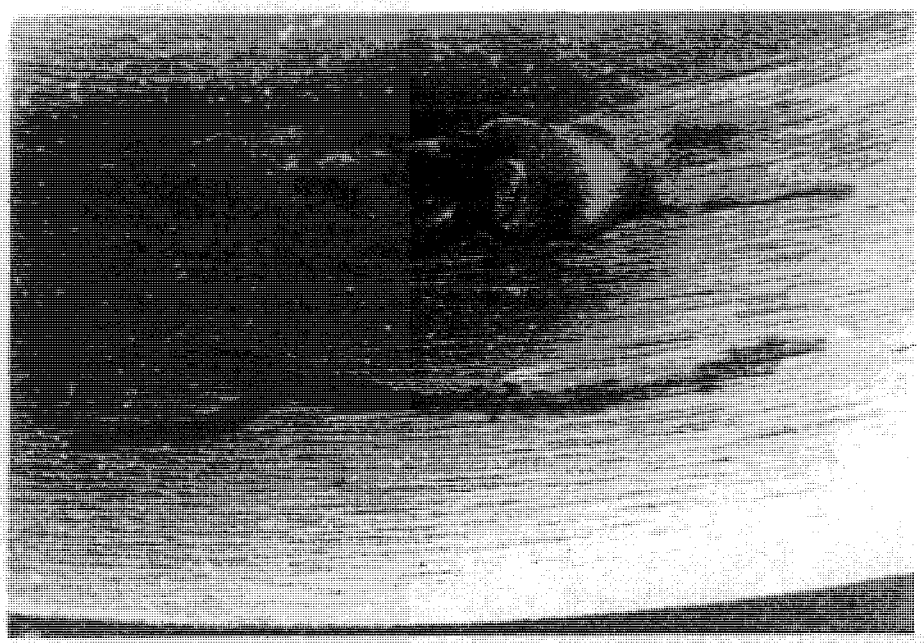

Micro graph 24 IGSCC crack close to a weld repair in an austenitic stainless steel pipe, nuclear industry. Surface view. Photo after a dye penetrant test. The crack are located app. 8 mm from the weld. Magnification 2.3 X.

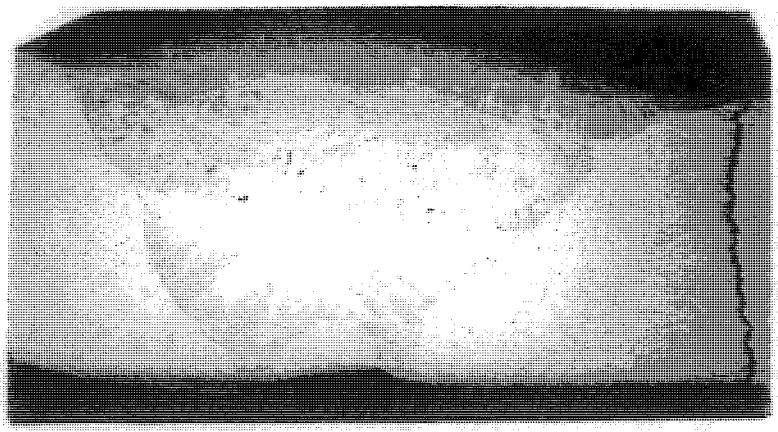

Micro graph 25 IGSCC crack in an austenitic stainless steel pipe, nuclear industry. Cross section. Magnification 4.5 X.

IGSCC in stainless steel

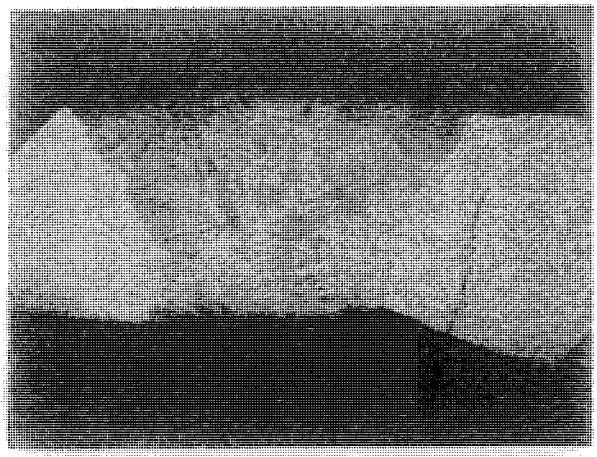

Micro graph 26 IGSCC crack in an austenitic stainless steel pipe, nuclear industry. Cross section.
Magnification 2.5 X.

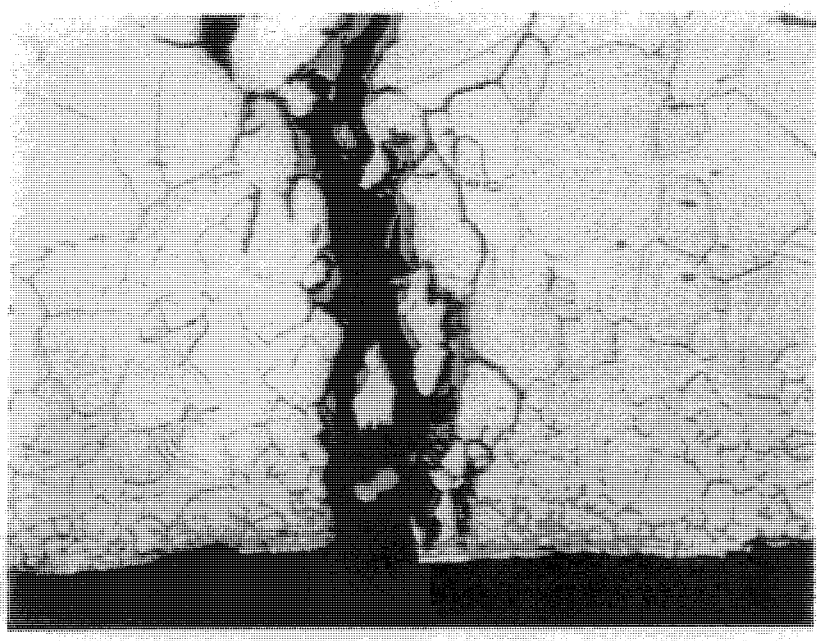

Micro graph 27 IGSCC crack at the inside surface of an austenitic stainless steel pipe, nuclear industry. Note, the heavy oxidised crack and the large amount of micro branching.
Magnification 420 X.

IGSCC in stainless steel

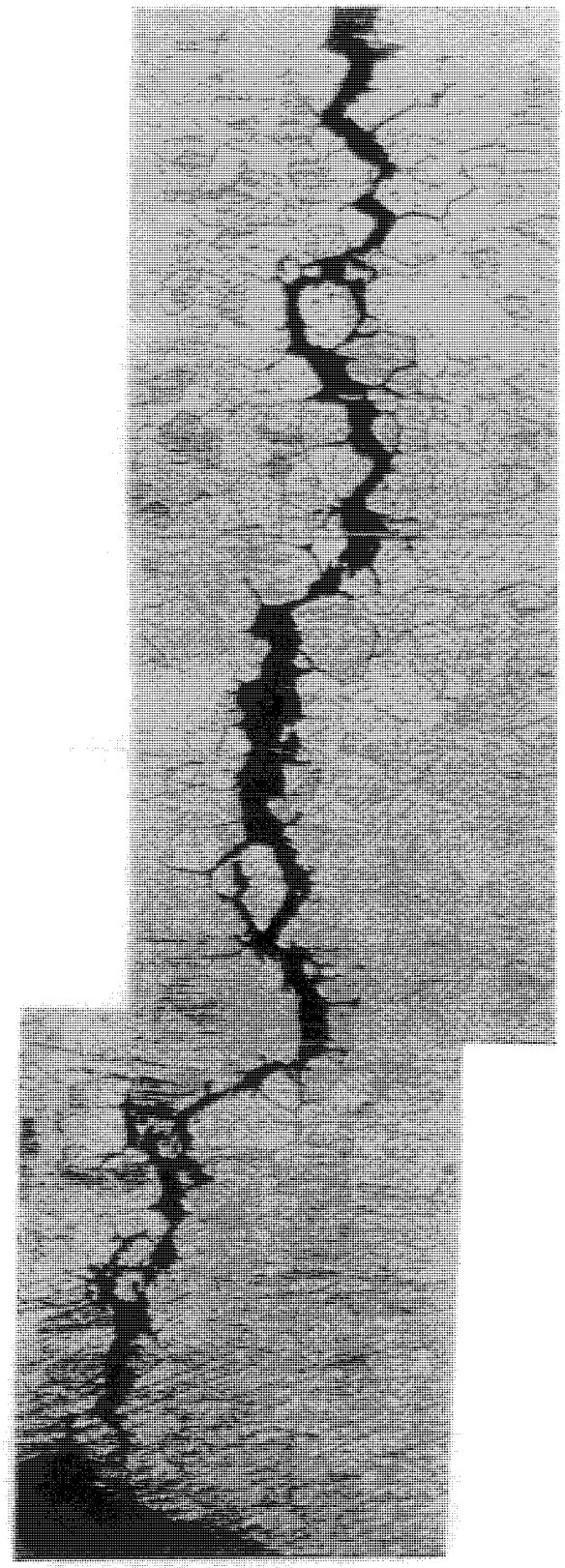

Micro graph 28 Part of an IGSCC crack in an austenitic stainless steel pipe, nuclear industry. Cross section. Note the winding and intergranular crack propagation.
Magnification 37.5 X.

IGSCC in stainless steel

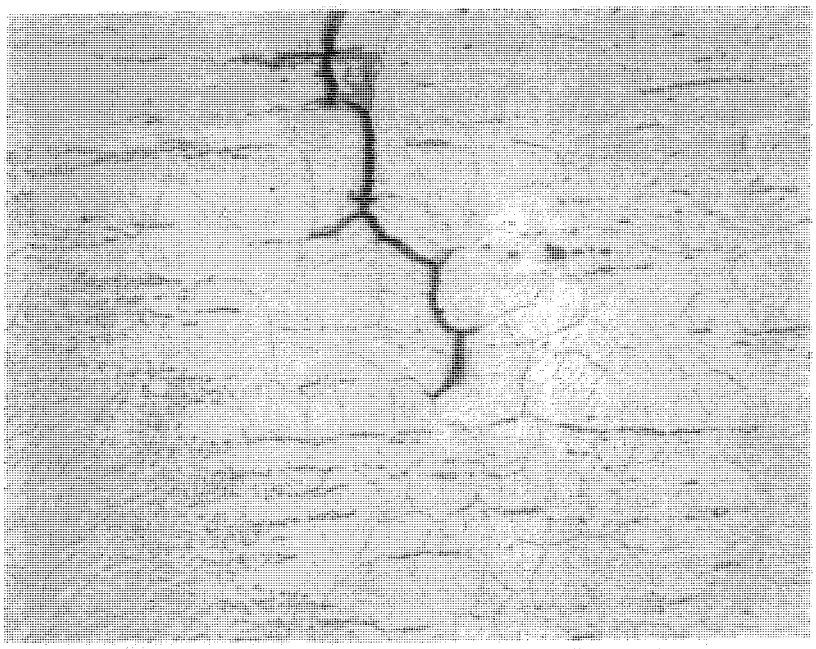

Micro graph 29 IGSCC crack tip region of the crack shown in micro graph 12, nuclear industry. The crack propagates parallel to the fusion line. Magnification 170 X.

Micro graph 30 IGSCC crack tip region close to a weld in an austenitic stainless steel pipe, nuclear industry. Crack arrest at the fusion line. Note, the micro branching and the intergranular crack growth. Magnification 200 X.

IGSCC in stainless steel

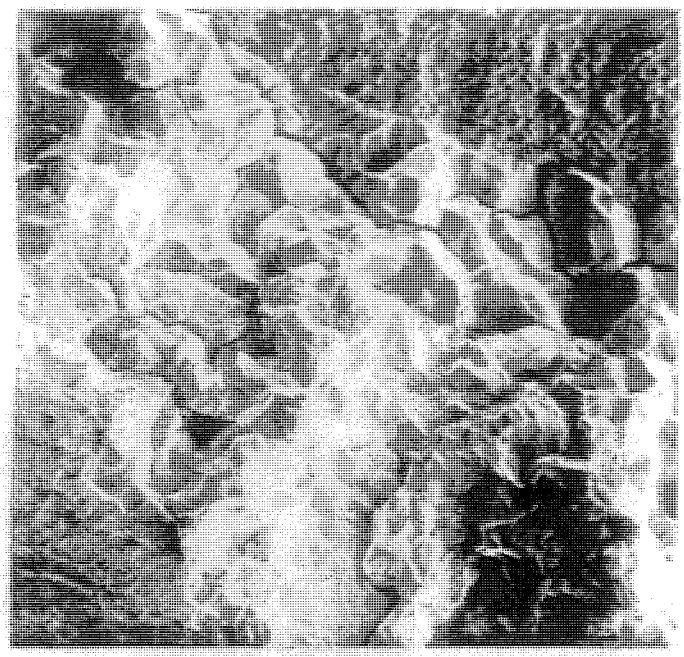

Micro graph 31 IGSCC crack surface from a CT-test specimen of austenitic stainless steel, type 304L, nuclear industry. Note the inter-granular crack growth.
Magnification 200 X.

IGSCC in nickel base alloy

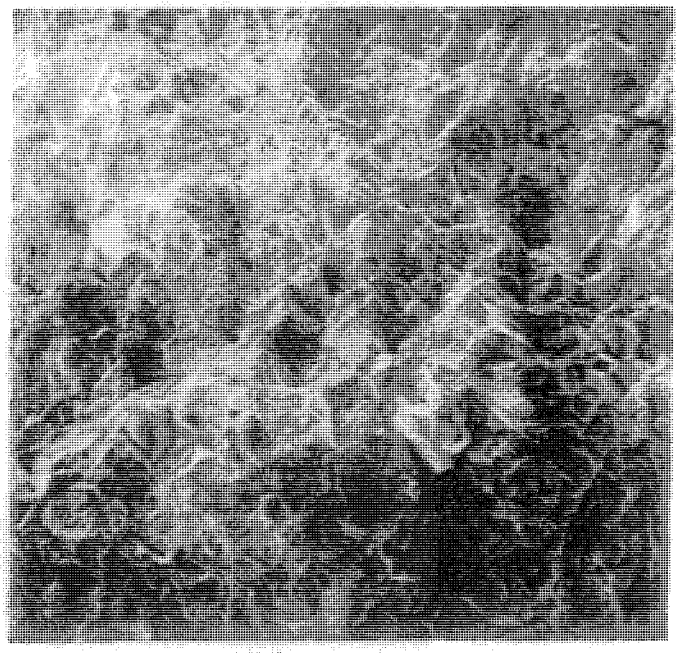

Micro graph 32 IGSCC crack surface from a CT-test specimen of nickel base alloy, Alloy 600, nuclear industry. Note, the intergranular crack growth.
Magnification 100 X.

TGSCC in stainless steel

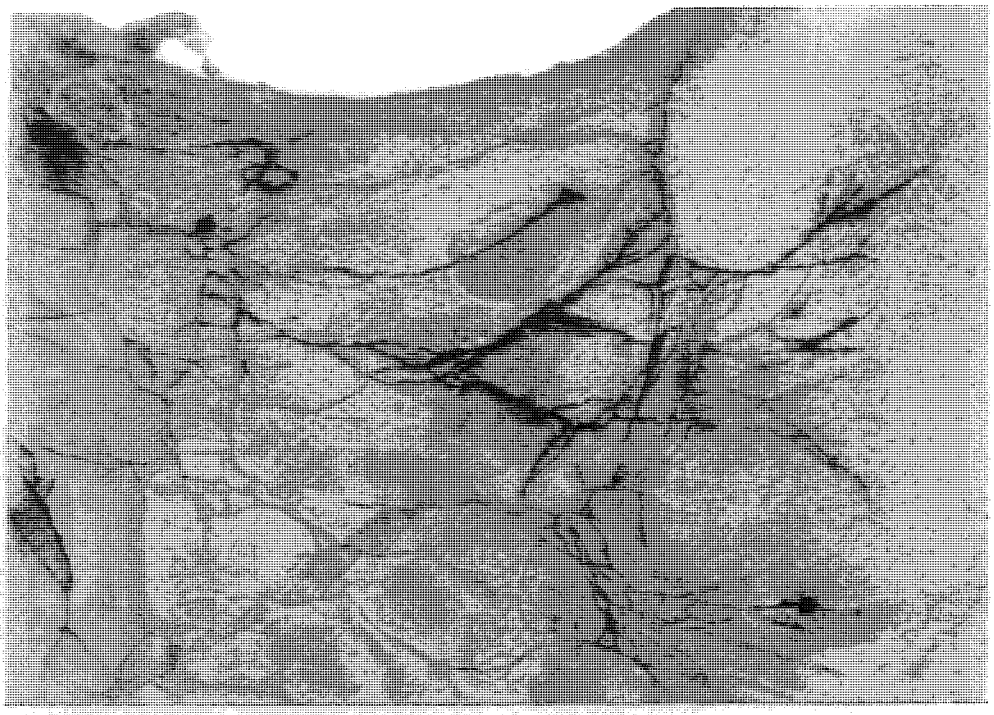

Micro graph 33 TGSCC in austenitic stainless steel plate parent metal, non-nuclear industry. Surface view. Note, the large number of cracks and the heavy macro branching.
Magnification 3 X.

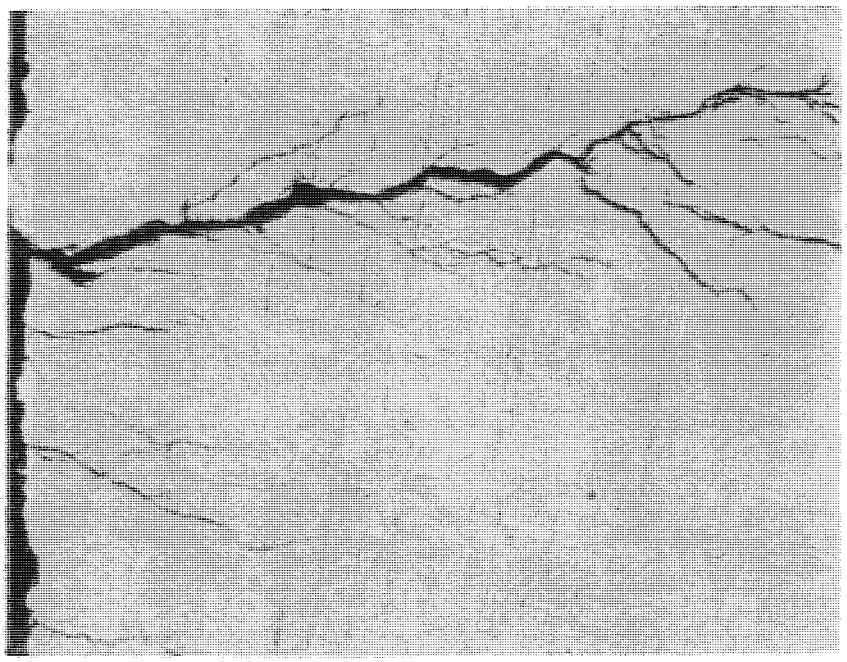

Micro graph 34 Longitudinal TGSCC in austenitic stainless steel pipe parent metal, non-nuclear industry. Cross section. Note, the large number of cracks and the heavy macro branching.
Magnification 100 X.

TGSCC in stainless steel

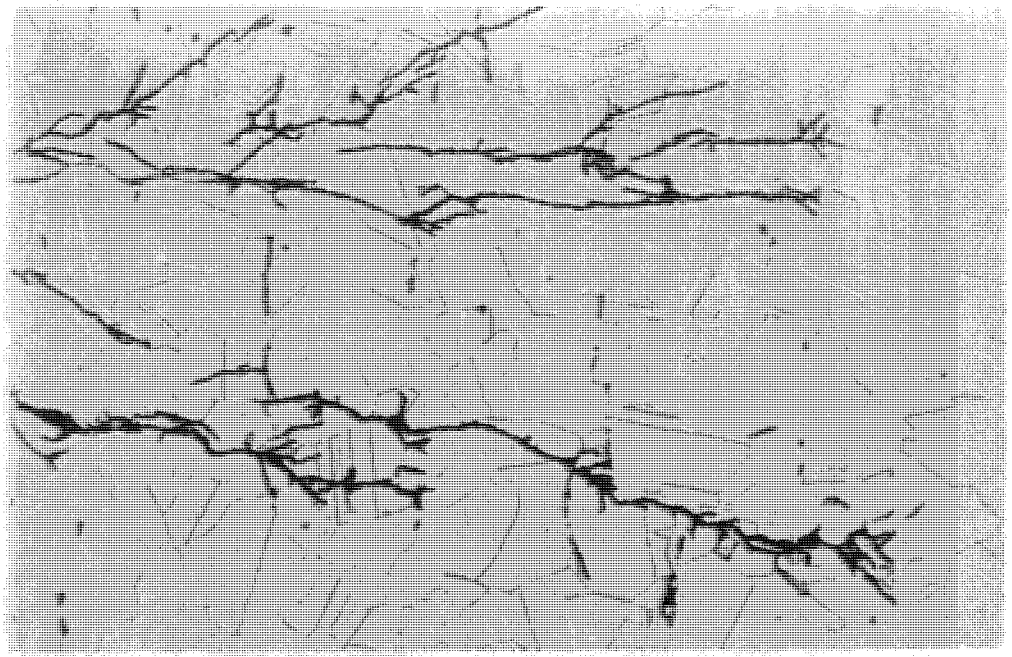

Micro graph 35 Crack tip region of TGSCC in austenitic stainless steel pipe parent metal, non-nuclear industry. Cross section. Note, the large number of cracks and the heavy branching.
Magnification 400 X.

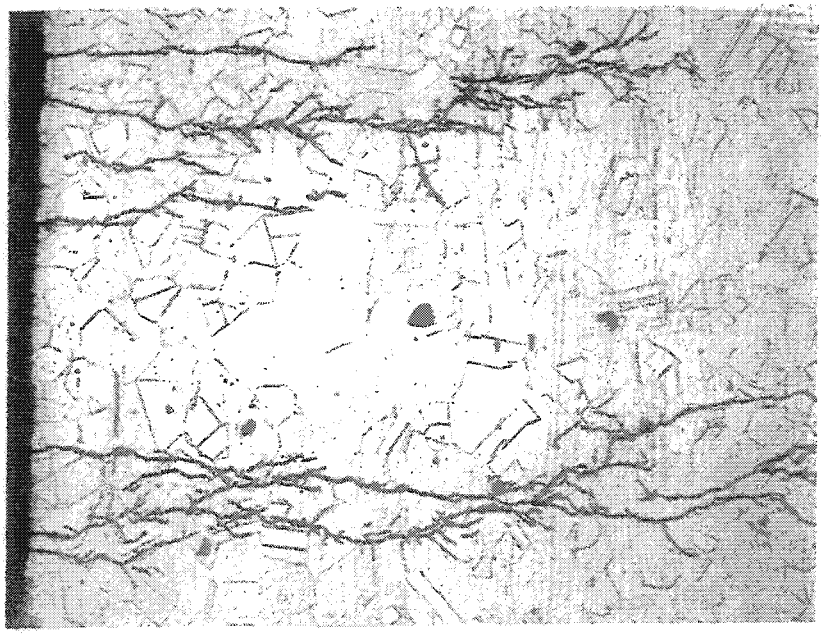

Micro graph 36 TGSCC in an austenitic stainless steel pipe, nuclear industry. Note, several transgranular cracks and a heavy branching.
Magnification 100 X.

TGSCC in stainless steel

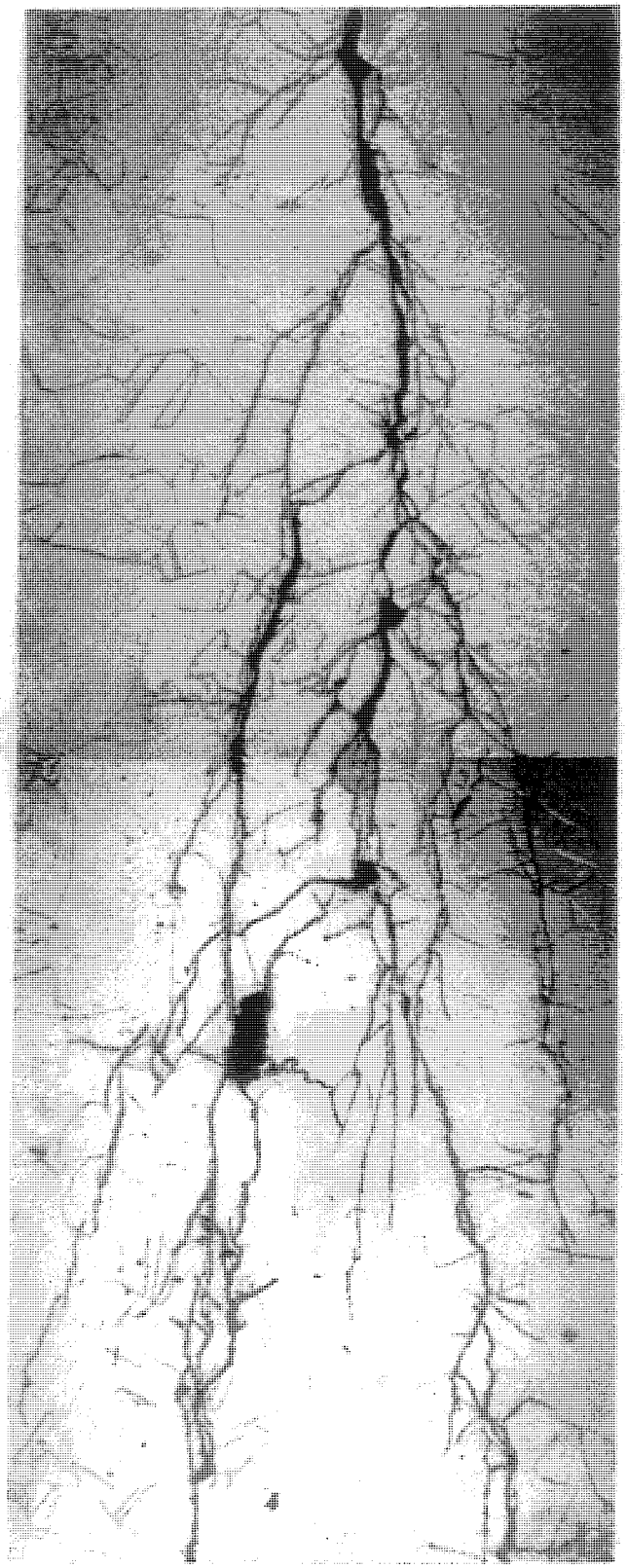

Micro graph 37 TGSCC in an internal part made of austenitic stainless steel, nuclear industry. Note, the transgranular crack growth and the heavy macro branching.
Magnification 100 X.

Mixed IGSCC and TGSCC in stainless steel

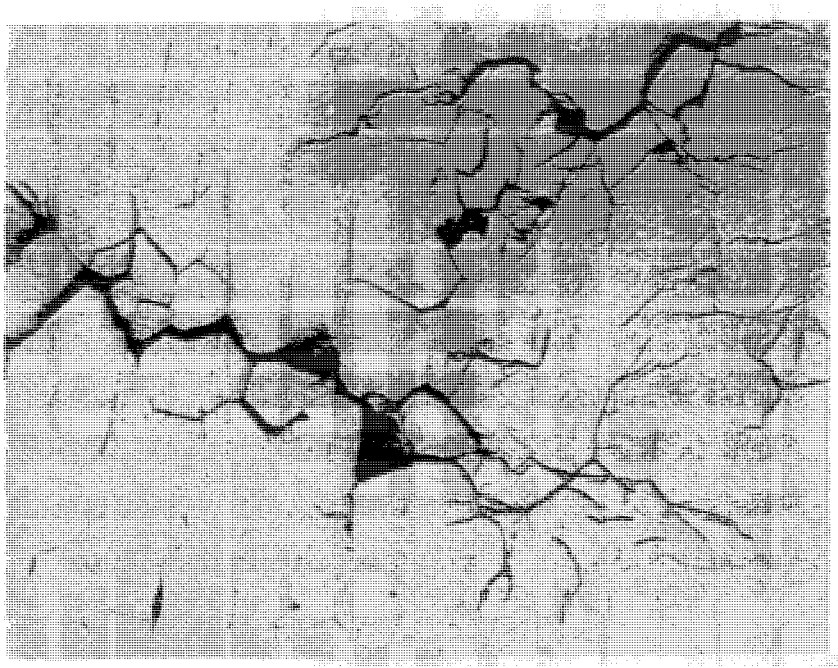

Micro graph 38 Mixed IGSCC and TGSCC in steam piping made of austenitic stainless steel, non-nuclear industry. Caustic environment service. Cross section at HAZ. Note, heavy micro crack branching. Magnification 200 X.

IDSCC in nickel base alloy

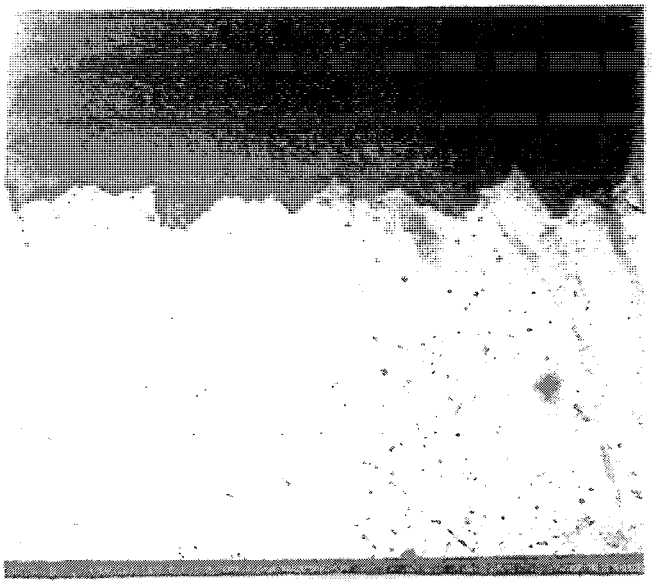

Micro graph 39 IDSCC crack in a CT-specimen of weld metal, Alloy 182, nuclear industry. Cross section perpendicular to the dendrites and to the crack propagation direction. Note, the rough crack surface. Magnification 20 X.

IDSCC in nickel base alloy

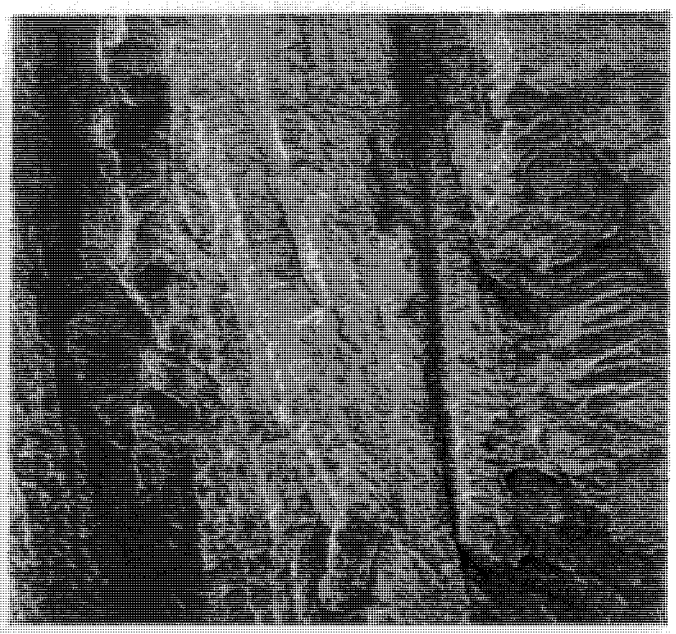

Micro graph 40 IDSCC crack surface from a CT-specimen of weld metal, Alloy 182, nuclear industry. Interdendritic crack growth. Magnification 100 X.

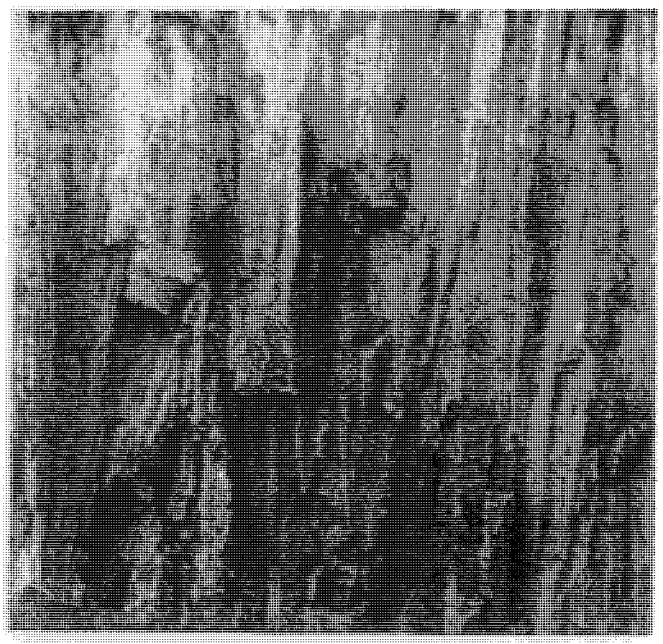

Micro graph 41 IDSCC crack surface from a CT-specimen of weld metal, Alloy 182, nuclear industry. Interdendritic crack growth. Magnification 20 X.

Weld defects

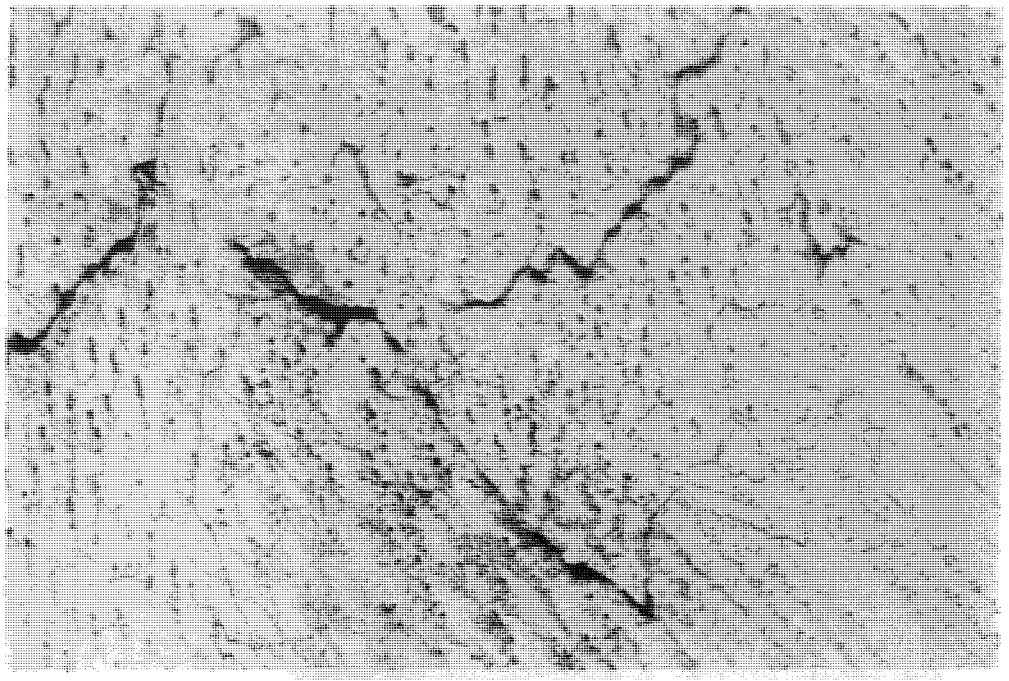

Micro graph 42 Hot cracks in austenitic stainless steel weld metal, non-nuclear industry. Cross section. Note, crack shape related to solidification pattern.
Magnification 100 X.

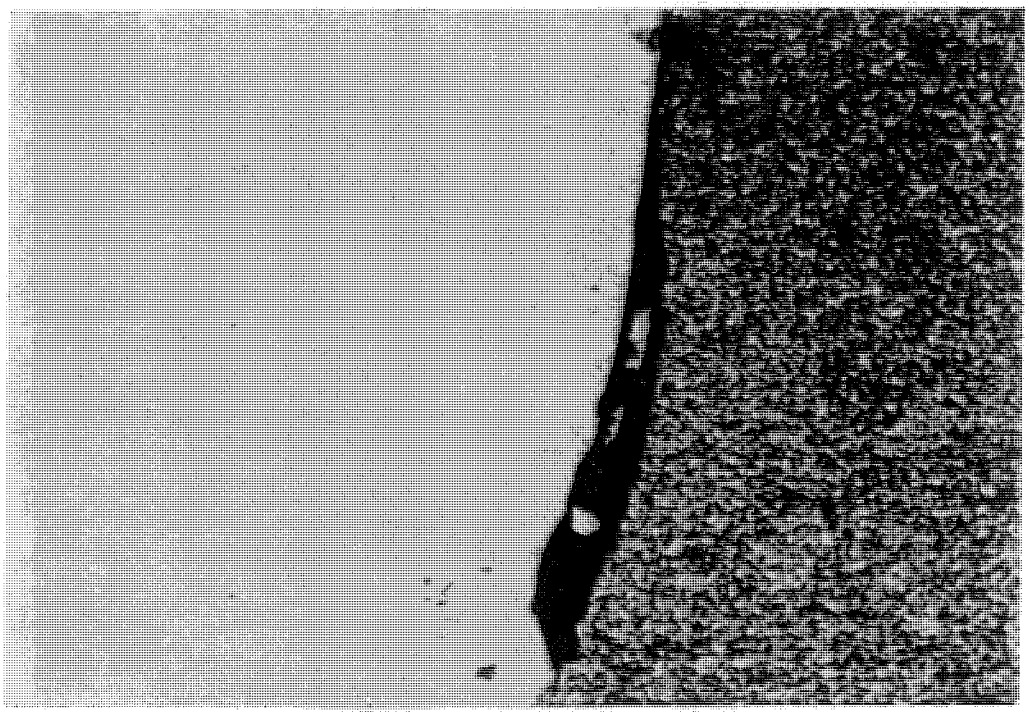

Micro graph 43 Lack of fusion flaw at fusion line, non-nuclear industry. Cross section. Stainless steel weld metal and carbon steel parent metal.
Magnification 50 X.

Weld defects

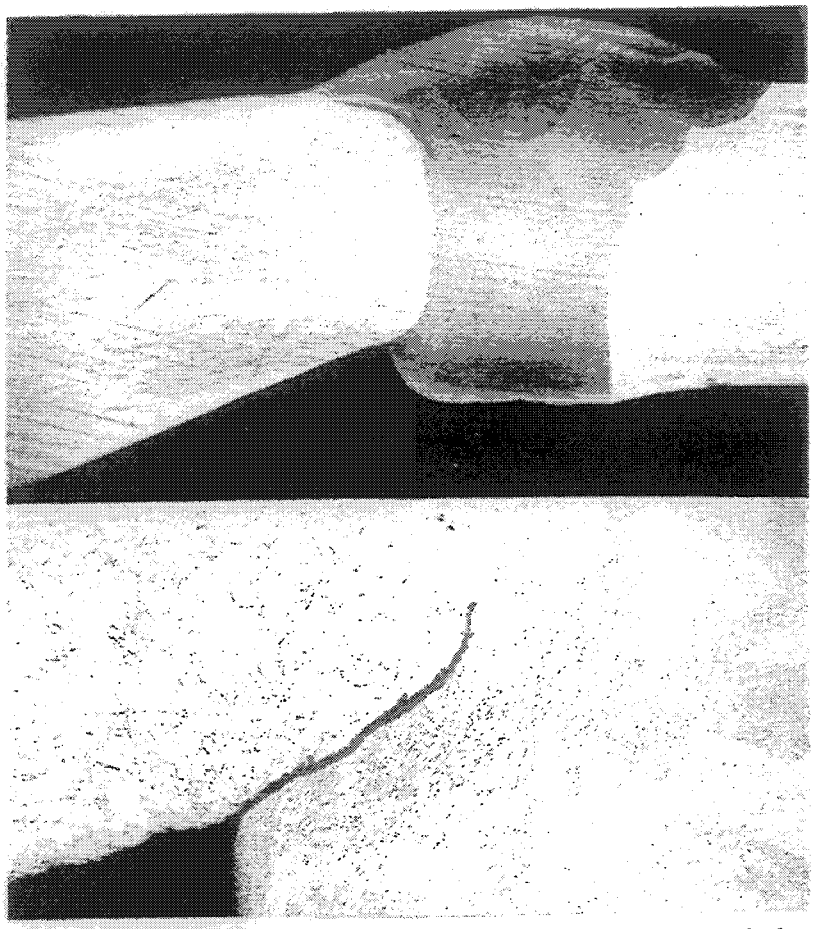

Micro graph 44 Lack of root fusion in a butt weld, nuclear industry. Note, the large difference in wall thickness between the two pipes.

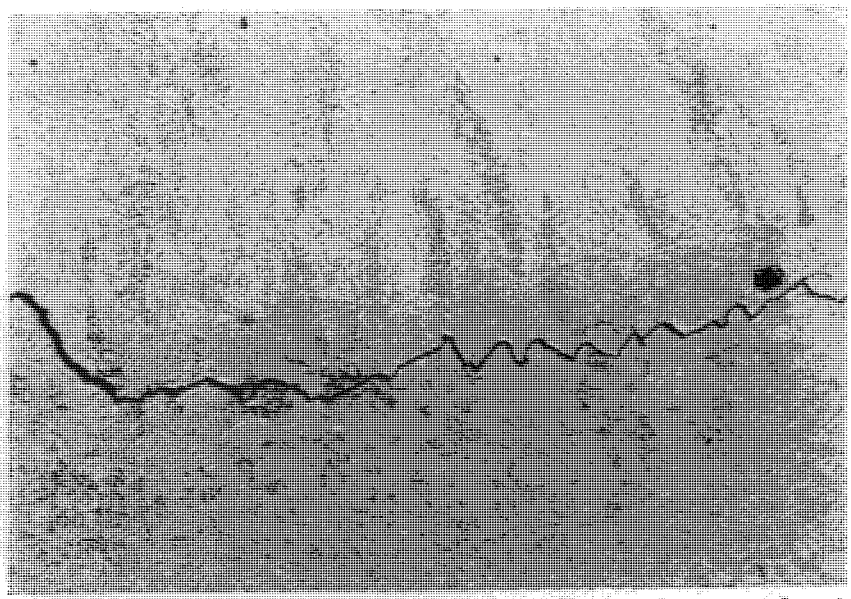

Micro graph 45 Cold crack in ferritic low alloy steel, non-nuclear industry. Cross section. Note, crack path along premature austenitic grain boundaries of the coarse grain HAZ.
Magnification 50 X.

www.ski.se

STATENS KÄRNKRAFTINSPEKTION
Swedish Nuclear Power Inspectorate

POST/POSTAL ADDRESS SE-106 58 Stockholm
BESÖK/OFFICE Klarabergsviadukten 90
TELEFON/TELEPHONE +46 (0)8 698 84 00
TELEFAX +46 (0)8 661 90 86
E-POST/E-MAIL ski@ski.se
WEBBPLATS/WEB SITE www.ski.se